ANTENNA SIDELOBE AND COUPLING REDUCTION BY MEANS OF REACTIVE LOADING OF THE GROUND PLANE

Constantine John Digenis

FOREWORD

ACKNOWLEDGEMENT

ABSTRACT

In this report the loading of the ground plane by a capacitive impedance is described as a method of reducing the sidelobes of one antenna and the coupling between adjacent antennas. Although in the analysis no restrictions are placed upon the frequency, practical considerations regarding the loading make this method particularly suitable for antennas operating in the microwave region of the spectrum.

Explicit expressions are derived for the directivity and radiation resistance of a monopole placed over an infinite sheet characterized by a capacitive surface impedance. Also the problem of a short monopole over an infinite screen which is perfectly conducting throughout except for an annulus of capacitive surface impedance is considered and closed form expressions are obtained for the far zone field by an approximate method. Numerical results show that there is an optimum position for an annulus of a given radial extent in order to achieve maximum antenna gain and minimum radiation along the ground plane. By using annular loading the radiation resistance of the monopole is not reduced considerably in contrast to the loading of the entire ground plane. Experiments conducted using corrugations to create a capacitive reactance show good agreement with theory. The monopole input impedance and near field coupling were also measured.

The study concludes with an experimental investigation of the radiation properties of the slot, horn and spiral antennas in the presence of the capacitive reactance loading. Sidelobe reduction of approximately 10dB and gain increase of up to 5dB have been measured over a 40 percent bandwidth using loading of approximately one wavelength radial extent.

TABLE OF CONTENTS

LIST OF ILLUSTRATIONS

LIST OF TABLES

x

INTRODUCTION

1.1 Statement of the Problem

Excessive electromagnetic interference or coupling is a problem often en-
countered in the operation of two or more antennas mounted on a common metal
surface such as the skin of an aircraft or a space vehicle. Excessive coupling
may exist between the antennas of either one or more systems. Given a pair
of antennas of which one transmits a (strong) signal and the second is meant to
receive the (weak) signal reflected from a scattering object, the signal directly
coupled from the transmitting to the receiving antenna interferes with the signal
reflected from the scatterer. This may cause significant errors in the operation
of a radar interferometer (Carl and Guccione, 1966). Mutual coupling between
the antenna elements of a phased array is also a problem since it causes the
array performance to vary with scan angle (Edelberg and Oliner, 1960; Allen,
1965; Lechtreck, 1968). To lessen these problems it is desirable to develop
methods by means of which the power normally coupled from one antenna to
another may be significantly reduced. The present study deals with one method
of coupling reduction — that of impedance or more specifically, reactive loading
of the ground plane.

The technique of reactive loading consists of modifying a part or the whole
of the surface of a conductor to create a surface reactance which is different
from zero. When the surface reactance is inductive the radiation along the sur-
face is increased compared to the radiation in the case of a perfectly conducting
surface. This has been explained physically by the introduction of the concept
of a surface wave. Inductive loading of the ground plane has been used to create
end-fire antennas. It was therefore envisioned that a capacitive surface reactance
would create the opposite effect, i.e. reduce the antenna radiation along the
ground plane thus decreasing the coupling between adjacent antennas mounted on
a common surface. In the case of antennas with their major lobe to the broad-
side of the ground plane, the reduction would be in the sidelobes. In the case

of the monopole the major lobe would be affected. The use of capacitive loading does not permit the propagation of surface waves and a new mathematical model is needed to obtain the antenna radiation pattern. Therefore formulation as a boundary value problem was chosen.

The study begins with an analytical investigation of the radiation properties of the short monopole as well as the quarter wavelength monopole placed over an infinite sheet characterized by a capacitive surface impedance. The monopole directivity, input resistance and direction of maximum radiation are calculated as functions of the surface impedance (Ch. II). This analysis yields a considerable amount of physical insight in a simple fashion and permits one to derive explicit analytical relations. Next a more practical case is considered, that of a short monopole over an infinite extent screen which is perfectly conducting throughout except for an annulus surrounding the monopole and characterized by a capacitive surface impedance (Ch. III). The monopole radiation pattern is obtained on the basis of an approximate analysis. Chapter IV includes the results of an experimental investigation of the same problem and a comparison between theory and experiment. The capacitive reactance annulus was realized by cutting circumferential corrugations in part of the ground plane. The term "isolated loading" is used to denote all cases where the impedance loading is restricted along one dimension of the surface (e.g. a single trench) while the term "continuous loading" is used in all cases where the loading extends over some area.

1.2 History

The theoretical formulation of the problem of a monopole or vertical electric dipole above an infinite sheet characterized by a non-zero surface impedance is very similar to that for the vertical dipole over an arbitrary earth characterized by finite conductivity, permittivity and permeability. The latter is a classical problem first solved by Sommerfeld (1909). Sommerfeld identified a part of his solution as a space wave and another part as a surface

wave. This problem has received a great deal of attention and papers with different or improved solutions were published by Weyl, Niessen, Van der Pol, Wise, Norton, Sommerfeld and Renner, Ott and Epstein (1947). Much of the work subsequent to Sommerfeld's first paper was concerned with the existence and the nature of a surface wave. A review of this work has been given by Bouwkamp (1950).

The formulation with a surface impedance boundary condition was used by Jones (1952), Fernando and Barlow (1956), Wait (1957) and Furutsu (1959). Jones and Fernando and Barlow examined the problem of launching and supporting a surface wave over a surface characterized by an inductive surface reactance created by corrugations. In their analysis only the fundamental mode of propagation along the corrugated surface was considered and a transmission line TEM mode within the trenches. Then the average impedance was matched at the common boundary to derive approximate expressions for the propagation constant as a function of the surface parameters. Based on this, the radiation field was obtained. Wait studied the problem more generally correlating the various forms of surface waves obtained by other authors . His solution, however, is valid only in the far field of the dipole. Furutsu derived the exact solution of the boundary value problem valid for any value of the surface impedance and throughout the half space above the impedance sheet, with no consideration as to how the surface impedance can be physically realized.

The properties of plane single-surface corrugated structures as transmission lines and radiators have been studied by Cutler (1944), Rotman (1951), Ehrlich and Newkirk (1953), Barlow and Cullen (1953), Cullen (1954), Elliott (1954), Hurd (1954), Watkins (1959) and Tseng (1967). The studies of Rotman, Ehrlich and Newkirk are chiefly experimental. In the studies of Cutler, Barlow and Cullen only the fundamental mode above the corrugations was considered. Elliott included higher order modes and found that the effect of these modes to the radiation pattern of an end-fire antenna is slight. He also concluded that when the number of corrugations per wavelength is large and the ratio of the tooth width to gap width

is small, the field distribution above the corrugations consists essentially of the fundamental mode. Hurd derived the exact solution for the amplitudes and phase velocities of the higher order modes for an infinite, source free, corrugated surface with vanishingly thin slot walls. Watkins obtained a determinantal equation for the surface wave cut-off frequency taking into account the finite width of the walls. Tseng formulated and solved the scattering problem for a source-free corrugated surface, focussing on the multi-mode aspects of the problem. The studies based on the existence of surface wave modes are applicable only when the surface parameters permit the propagation of such waves.

The scattering of a surface wave by a discontinuity in surface reactance has been solved by Kay (1959) for inductive reactances. His solution contains closed form expressions for the magnitude, but not the phase, of the reflected and transmitted surface waves as well as the radiation field. Thus this solution cannot be used to solve the discontinuity problem at the boundary lines of the surface impedance annulus because a) knowledge of the magnitude and phase of the fields near the discontinuity is necessary and b) capacitive rather than inductive reactances are used here. The radiation of an antenna in the presence of inductive surfaces is of interest in the analysis of surface wave antennas. This subject has been reviewed by Zucker (1961). Kane (1963) has given a nearly rigorous solution to the problem of a magnetic line source in a finite inductive surface. Andersen (1967) has given a simpler approximate solution based on the compensation theorem.

The use of a single trench to reduce surface currents has been reported by Saunders (1956). LaGrone and Roberts (1966) used a choke flange for reducing the sidelobes of a horn. For the same purpose corrugations have been placed along the flared walls of a horn (Kay, 1964; Lawrie et al, 1965). Experimental results have also been reported for the use of corrugations on ogives in order to reduce the back scattering (Lawrie and Peters, 1966). An obvious difficulty in the application of reactive loading by corrugations for backscattering reduction is the dependence of the loading characteristics upon the frequency and direction of the incident wave.

1.3 Remarks on Coupling

The coupling between two antennas is defined as the ratio of the power received by one antenna to the power transmitted by the other. It usually is expressed in dB. The term "isolation" defined as the inverse of coupling is sometimes used. When two antennas are in the far-field of each other the coupling is given by the Friis transmission formula as

$$C = (\frac{\lambda}{4\pi R})^2 D_t(\theta, \phi) D_r(\theta, \phi)\ p \tag{1.1}$$

where C is the coupling, λ the wavelength, R the antenna spacing, D the directivity function of each antenna and p the polarization mismatch factor. The antennas are assumed to be perfectly matched to their respective transmission lines. The coupling is related to the antenna mutual impedance Z_{12} by (Khan et al, 1964)

$$C = \frac{|Z_{12}|^2}{4R_{11}R_{22}} \tag{1.2}$$

where R_{11} and R_{22} are the resistances of the two antennas, provided that the mutual impedance is (absolutely) much less than the self impedance of either antenna.

Of prime interest in this work was the frequency range over which the coupling could be reduced by the reactive loading. Therefore, a swept frequency technique was adopted for most of the coupling measurements to show the dependence of coupling upon frequency with fixed antenna positions. With frequency sweeping the transmission lines cannot be optimally matched to the antennas for each frequency. Therefore, the measured coupling differs from that shown in Eqs. (1.1) and (1.2) by the impedance mismatch coefficients q_t and q_r between antenna and transmission line. The necessary correction can be made easily if the antenna input standing wave ratio is known. However, for the antenna types considered it was found that the absence of perfect matching did not affect the coupling data by more than 1 dB.

RADIATION FROM A MONOPOLE ANTENNA OVER AN INFINITE SCREEN WITH A CAPACITIVE SURFACE IMPEDANCE BOUNDARY CONDITION

2.1 Formulation of the Problem for a Short Electric Dipole

Consider a short electric dipole whose axis coincides with the z-axis of a cylindrical coordinate system. The plane z=0 represents the ground plane which exhibits a capacitive surface impedance. The dipole is located at a height h over the ground plane. The medium above the ground plane is assumed to be a loss-free dielectric. If the surface impedance is Z then the ratio of the tangential electric and magnetic fields is specified by (Fig. 2-1)

$$-\frac{E_r}{H_\phi}\bigg|_{z=0} = Z \ .$$

(2.1)
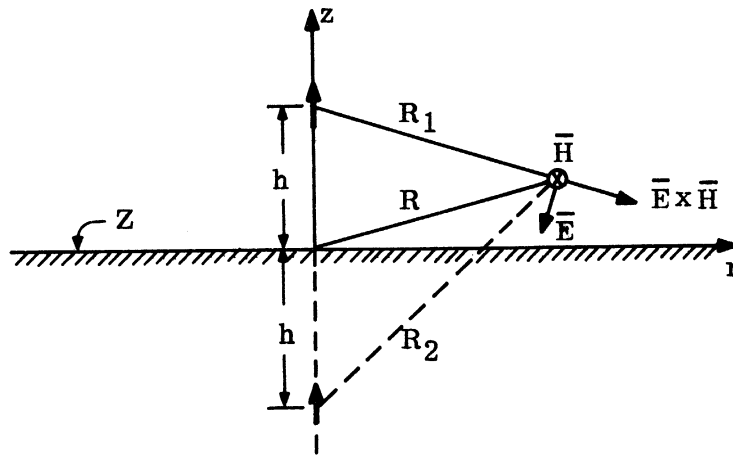
FIG. 2-1: PROBLEM GEOMETRY

The electric and magnetic field vectors outside the source can be derived from the Hertzian electric vector $\overline{\Pi}$ through

$$\overline{E} = \nabla\nabla\cdot\overline{\Pi} + k^2\overline{\Pi} = \nabla \times \nabla \times \overline{\Pi}$$
$$\overline{H} = j\omega\epsilon\,\nabla\times\overline{\Pi}$$

(2.2)

where k is the propagation coefficient of the medium. A harmonic time dependence expressed by the factor $e^{j\omega t}$ is understood and suppressed.

The field is cylindrically symmetrical about the z-axis . In the case of a short dipole in free space of length ℓ and uniform current peak value i, the Hertz potential is

$$\overline{\Pi}_o = A \cdot \frac{e^{-jkR_1}}{R_1}\,\hat{z}$$

(2.3)

where R_1 is the distance from the source to the observer (r, ϕ, z),

$$R_1 = \sqrt{r^2 + (z-h)^2}$$

(2.4)

and

$$A = \frac{i\ell}{j\omega 4\pi\epsilon}\ .$$

(2.5)

Following Sommerfeld's treatment of the problem of a vertical dipole over a plane, finitely conducting earth (Sommerfeld, 1949) one may write the Hertzian vector for the present problem as a sum of a "primary" contribution expressed by $\overline{\Pi}_o$ and a "secondary" or induced contribution $\overline{\Pi}_i$, representing the diffracted wave,

$$\overline{\Pi} = \overline{\Pi}_o + \overline{\Pi}_i = (\Pi_o + \Pi_i)\,\hat{z}\ .$$

(2.6)

Π_i must satisfy a) the wave equation, b) the radiation condition at infinity and c) together with $\overline{\Pi}_o$ the boundary condition at z=0. Since $\overline{\Pi}$ has only a z-component the non-vanishing components of the fields are derived from eq. (2.2) as

$$E_r = \frac{\partial^2 \Pi}{\partial r \partial z} \quad , \qquad\qquad \left.\rule{0pt}{9em}\right\}$$

$$E_z = \frac{\partial^2 \Pi}{\partial z^2} + k^2 \Pi \; ,$$

$$H_\phi = -j\omega\epsilon \; \frac{\partial \Pi}{\partial r} \qquad . \tag{2.7}$$

In view of eq. (2. 7) the boundary condition can be written as

$$\frac{\partial^2 \Pi}{\partial r \partial z} = j \, k \, \zeta \; \frac{\partial \Pi}{\partial r} \qquad\qquad (z=0) \tag{2.8}$$

where ζ is the normalized surface impedance

$$\zeta = Z \sqrt{\frac{\epsilon}{\mu}} \qquad . \tag{2.9}$$

Equation (2. 7) holds for all values of r and can, therefore, be integrated with respect to r. The functions and their derivatives must vanish as $r \rightarrow \infty$, therefore, the constant of integration is zero. Thus the boundary condition reduces to

$$\frac{\partial \Pi}{\partial z} = j k \zeta \Pi \; , \qquad\qquad (z=0) \; . \tag{2.10}$$

To find a function Π that satisfies this condition, both Π_0 and Π_i are expressed in terms of cylindrical wave functions of the type

$$\psi(r, z) = J_0(\lambda r) e^{-z \sqrt{\lambda^2 - k^2}} \; , \qquad (z > 0) \tag{2.11}$$

which satisfy the wave equation and the radiation condition. The real part of $\sqrt{\lambda^2 - k^2}$ is always chosen positive so that ψ vanishes as $z \rightarrow \infty$. (Here λ is a parameter and should not be confused with the wavelength.) The integral representation of the primary excitation in terms of the cylindrical wave functions is given by the following Fourier-Bessel integral

$$\frac{\Pi_0}{A} = \frac{e^{-jkR_1}}{R_1} = \int_0^\infty \frac{\lambda J_0(\lambda r)}{\sqrt{\lambda^2 - k^2}} \, e^{(z-h)\sqrt{\lambda^2 - k^2}} \, d\lambda \; , \quad (0 < z < h) \; . \tag{2.12}$$

The secondary excitation is also written in the form

$$\frac{\Pi_i}{A} = \int_0^\infty F(\lambda) J_0(\lambda r) e^{-z\sqrt{\lambda^2-k^2}} \, d\lambda \, , \qquad (z > 0) \qquad (2.13)$$

where $F(\lambda)d\lambda$ represents the arbitrary amplitude constant by which each eigen-function may be multiplied. The Hertzian vector of the resultant field is then

$$\Pi = A \int_0^\infty \left[\frac{\lambda}{\sqrt{\lambda^2-k^2}} e^{(z-h)\sqrt{\lambda^2-k^2}} + F(\lambda) e^{-z\sqrt{\lambda^2-k^2}} \right] J_0(\lambda r) d\lambda \, ,$$
$$(0 < z < h) \, . \qquad (2.14)$$

The function $F(\lambda)$ is then determined by the boundary condition. It is found that

$$F(\lambda) = \frac{\lambda}{\sqrt{\lambda^2-k^2}} \cdot \frac{\sqrt{\lambda^2-k^2}-jk\zeta}{\sqrt{\lambda^2-k^2}+jk\zeta} e^{-h\sqrt{\lambda^2-k^2}} \, , \qquad (z > 0) \qquad (2.15)$$

and therefore

$$\frac{\Pi}{A} = \frac{e^{-jkR_1}}{R_1} + \int_0^\infty \frac{\lambda J_0(\lambda r)}{\sqrt{\lambda^2-k^2}} \cdot \frac{\sqrt{\lambda^2-k^2}-jk\zeta}{\sqrt{\lambda^2-k^2}+jk\zeta} e^{-(z+h)\sqrt{\lambda^2-k^2}} \, d\lambda \, ,$$
$$(z > 0) \, . \qquad (2.16)$$

Noting that

$$\frac{\sqrt{\lambda^2-k^2}-jk\zeta}{\sqrt{\lambda^2-k^2}+jk\zeta} = 1 - j \frac{2k\zeta}{\sqrt{\lambda^2-k^2}+jk\zeta} \qquad (2.17)$$

and using eq. (2.12) one may also write

$$\frac{\Pi}{A} = \frac{e^{-jkR_1}}{R_1} + \frac{e^{-jkR_2}}{R_2} - 2jk\zeta \int_0^\infty \frac{\lambda J_0(\lambda r) e^{-(z+h)\sqrt{\lambda^2-k^2}}}{\sqrt{\lambda^2-k^2} (\sqrt{\lambda^2-k^2}+jk\zeta)} \, d\lambda \, ,$$
$$(z > 0) \qquad (2.18)$$

where

$$R_2 = \sqrt{r^2 + (z+h)^2} \, . \qquad (2.19)$$

Thus, the resultant field at the point of observation is composed of a) a direct contribution from the source, b) a contribution from its image at z=-h and c) an additional term accounting for the fact that the plane z=0 is not a perfect reflector. In the special case of a perfectly conducting plane ($\zeta=0$) eq. (2.18) reduces to the well known expression

$$\frac{\Pi}{A} = \frac{e^{-jkR_1}}{R_1} + \frac{e^{-jkR_2}}{R_2} \tag{2.20}$$

which is easily derived directly from Π_0 by the concept of images.

Instead of proceeding with the evaluation of the integral of eq. (2.18) one may obtain a simpler form by noting that

$$\frac{1}{\sqrt{\lambda^2-k^2}\ (\sqrt{\lambda^2-k^2}+jk\zeta)} = \frac{1}{jk\zeta}\left(\frac{1}{\sqrt{\lambda^2-k^2}} - \frac{1}{\sqrt{\lambda^2-k^2}+jk\zeta}\right). \tag{2.21}$$

Substituting in eq. (2.18) one obtains

$$\frac{\Pi}{A} = \frac{e^{-jkR_1}}{R_1} - \frac{e^{-jkR_2}}{R_2} + 2 I , \qquad (z>0) , \tag{2.22}$$

where

$$I = \int_0^\infty \frac{\lambda\ J_0(\lambda r)}{\sqrt{\lambda^2-k^2}+jk\zeta}\ e^{-(z+h)\sqrt{\lambda^2-k^2}}\ d\lambda\ ,\ (z>0) . \tag{2.23}$$

This integral has the drawback of extending from a fixed initial point ($\lambda=0$) to infinity. It is preferable to have an integration path extending to infinity at both ends. This can be achieved by using the relations

$$J_0(x) = \frac{1}{2}\left[H_0^{(1)}(x)+H_0^{(2)}(x)\right] \tag{2.24}$$

and

$$H_0^{(2)}(x) = -H_0^{(1)}(-x) \tag{2.25}$$

to write

$$\int_0^\infty J_0(x)f(x)dx = \frac{1}{2}\int_{-\infty}^\infty H_0^{(1)}(x)f(x)dx \tag{2.26}$$

where f(x) is any odd function of x . Applying this result to the integral I, one may write

$$I = \frac{1}{2}\int_{-\infty}^\infty \frac{\lambda H_0^{(1)}(\lambda r)}{\sqrt{\lambda^2-k^2}+jk\zeta}\, e^{-(z+h)\sqrt{\lambda^2-k^2}}\, d\lambda\,, \qquad (z>0)\ . \tag{2.27}$$

Introducing the integral representation for $H_0^{(1)}(x)$

$$H_0^{(1)}(x) = \frac{1}{\pi}\int_{W_1} e^{jx\cos w}\, dw\,, \tag{2.28}$$

where the path W_1 extends from $w_0 = a_1 + j\infty$ $(-\pi < a_1 < 0)$ to $w_1 = b_1 - j\infty$ $(0 < b_1 < \pi)$ and is only asymptotically restricted to the regions $[-\pi < \mathrm{Re}\,w < 0, 0 < \mathrm{Im}\,w < \infty]$ and $[0 < \mathrm{Re}\,w < \pi, -\infty < \mathrm{Im}\,w\,0]$ one may write

$$I = \frac{1}{2\pi}\int_{W_1} dw \int_{-\infty}^\infty d\lambda\, \frac{\lambda e^{-(z+h)\sqrt{\lambda^2-k^2}+j\lambda r\cos w}}{\sqrt{\lambda^2-k^2}+jk\,\zeta}\,. \tag{2.29}$$

Let

$$x = \frac{\lambda}{k} \tag{2.30}$$

$$r = R_2\sin\theta_2\,, \qquad z+h = R_2\cos\theta_2\,, \tag{2.31}$$

where θ_2 is the angle between the z-axis and the line connecting the source image at z= -h with the observation point. If $R_2 \gg h$ then $\theta_2 \cong \theta$ where θ is the usual spherical coordinate.

In view of eqs. (2.30) and (2.31) the integral I becomes

$$I = \frac{k}{2\pi} \int_{W_1} dw \int_{-\infty}^{\infty} dx \ \frac{xe^{kR_2\left(jx\cos w \cdot \sin\theta_2 - \cos\theta_2 \cdot \sqrt{x^2-1}\right)}}{\sqrt{x^2-1} + j\ \zeta} \ . \tag{2.32}$$

This integral can be evaluated asymptotically (for large kR_2) by the saddle point method of integration. Let k be a real, positive and large number and let the functions $g(z)$ and $f(z)$ be regular in a certain part of the complex plane. Then

$$\int_A^B g(z) \ e^{kf(z)} dz \cong g(z_0)e^{kf(z_0)} \sqrt{\frac{2\pi}{-kf''(z_0)}} \ , \quad (k \rightarrow \infty) \tag{2.33}$$

where z_0 is a saddle point of $f(z)$ through which one chooses to pass in order to go from A to B. If it is necessary to pass through two or more saddle points, then each one makes its contribution to the integral and a sum of terms like (2.33) is obtained.

Considering the integration with respect to x in eq. (2.32) a saddle point is found at

$$x_0 = \frac{\cos w \cdot \tan\theta_2}{\sqrt{1 + \cos^2 w \cdot \tan^2\theta_2}} \ . \tag{2.34}$$

For $w = 0$ one gets $x_0 = \sin\theta_2$ so that $0 < x_0 < 1$. The integration path through the saddle point is given by

$$\text{Im}\left[f(x)\right] = f(x_0) \tag{2.35}$$

and this replaces the original path extending from $-\infty$ to $+\infty$ along the real axis (Fig. 2-2). When ζ is capacitive the integrand has no poles and the term usually identified as a surface wave does not appear in the solution. The branch point at $x = 1$ (or $\lambda = k$) may be handled by a branch cut which may not intersect the path of integration.
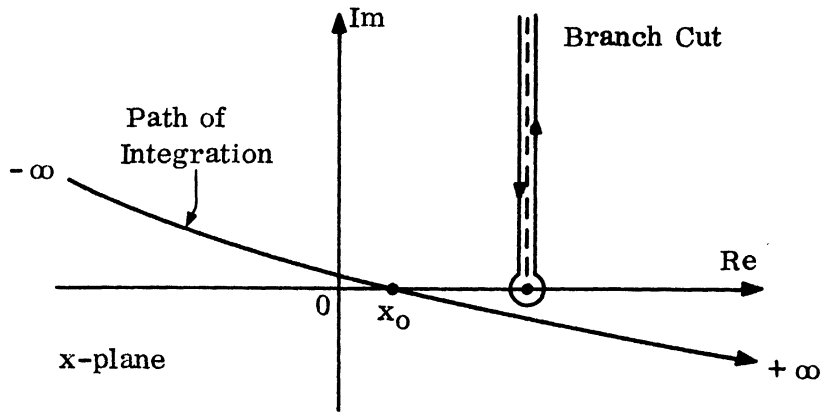
FIG. 2-2: DEFORMED PATH OF INTEGRATION

Carrying out the integration with respect to x, as described above, and then a similar integration with respect to w (the saddle point is w=0) one finds that

$$I = \frac{e^{-jkR_2}}{R_2} \cdot \frac{2 \cos \theta_2}{\cos\theta_2 + \zeta} .$$ (2.36)

Substituting in eq. (2.22) one obtains

$$\frac{\Pi}{A} = \frac{e^{-jkR_1}}{R_1} + \frac{e^{-jkR_2}}{R_2} \cdot \frac{\cos \theta_2 - \zeta}{\cos \theta_2 + \zeta} , \qquad (z > 0) .$$ (2.37)

The reflection coefficient of the infinite impedance screen is then

$$\rho = \frac{\cos \theta_2 - \zeta}{\cos \theta_2 + \zeta} .$$ (2.38)

The same ρ has been found in the solution of the two-dimensional problem of a line source above an impedance plane (Cullen, 1954; Keller and Karal, 1960).

The derivation of the electric and magnetic fields is straightforward. It is better to express the radiation fields in spherical rather than cylindrical coordinates. The only non-vanishing components in the far field (kR >> 1) are

$$H_{\phi} = B \cdot \frac{e^{-jkR}}{R} \left[e^{jkh\cos\theta} + e^{-jkh\cos\theta} \frac{\cos\theta - \zeta}{\cos\theta + \zeta} \right] \sin\theta \ , \quad (z > 0)$$

$$E_{\theta} = \eta \, H_{\phi}$$

(2.39)

where

$$\eta = \sqrt{\frac{\mu}{\epsilon}} \quad \text{and} \quad B = \frac{-i \, \ell \, k}{4\pi j} \ , \quad (k\ell \ll 1) \ .$$

(2.40)

2.2 Radiation from a Short Monopole

For a short monopole of height ℓ placed at z = 0 and having a uniform current distribution i, one obtains

$$H_{\phi} = B \frac{e^{-jkR}}{R} \frac{\sin (2\theta)}{\cos\theta + \zeta} \ , \qquad (z > 0 \ ) \ .$$

(2.41)

The mean power flow per unit area in a harmonic electromagnetic field is given by

$$\bar{S} = \frac{1}{2} \text{Re} [\bar{E} \times \bar{H}] \ .$$

(2.42)

When the surface impedance is created by corrugating a metal sheet, the resistance component is very small in comparison with the reactance. Therefore, one may write

$$\zeta = j \, X, \quad (X \leq 0 \ ) \ .$$

(2.43)

Then

$$\bar{S} = \frac{\eta |B|^2}{2R^2} \frac{\sin^2(2\theta)}{\cos^2\theta + X^2} \hat{R} \ , \qquad (z > 0 \ ).$$

(2.44)

The pattern of the radiated power appears independent of whether x is positive or negative (i.e. inductive or capacitive). However, it should be recalled that eq. (2.44) is valid only for X < 0. When X > 0 there is an additional term representing a surface wave which is predominant.

The radiation pattern has only one lobe with nulls along the monopole axis and the impedance plane and a maximum at

$$\theta = \text{arc cos} \sqrt{-X^2 - X \sqrt{X^2 + 1}} \quad , \quad (X \le 0) \tag{2.45}$$

given by

$$S_{max} = \frac{2\eta |H|^2}{R^2} (\sqrt{1 + X^2} + X)^2 \quad . \tag{2.46}$$

The total power radiated by the monopole is

$$W = \int_0^{2\pi} d\phi \int_0^{\pi/2} \sin\theta d\theta \cdot SR^2 = \frac{(ik\ell)^2}{4\pi} \eta \left\{ (1 + X^2) \left[1 - X\tan^{-1}(\frac{1}{X}) \right] - \frac{1}{3} \right\} . \tag{2.47}$$

The input resistance is equal to the radiation resistance since the maximum current along the monopole occurs at the input point. Therefore,

$$W = \frac{1}{2} i^2 R_{in} \tag{2.48}$$

and by comparison with eq. (2.47) one obtains

$$R_{in} = \frac{(k\ell)^2}{2\pi} \eta \left\{ (1 + X^2) \left[1 - X\tan^{-1}(\frac{1}{X}) \right] - \frac{1}{3} \right\} , \quad (X \le 0) \quad . \tag{2.49}$$

If the half space $z > 0$ is vacuum or air then $\eta = 120 \pi$ ohms. Furthermore, if X= 0, eq. (2.49) reduces to

$$R_{in} = 40 \, (k\ell)^2 \tag{2.50}$$

i. e. half the input resistance of a full dipole in free space, as expected.

The directivity with respect to an isotropic radiator is given by

$$D = \frac{4\pi \, U_{max}}{\int_0^{2\pi} \int_0^{\pi/2} U \sin\theta d\theta d\phi} \tag{2.51}$$

where

$$U = S R^2 \quad , \tag{2.52}$$

is the radiation intensity. It is found that

$$D = \frac{2\left(\sqrt{1+X^2}+X\right)^2}{(1+X^2)\left[1-X\tan^{-1}\left(\frac{1}{X}\right)\right]-\frac{1}{3}} \quad , (X \leq 0) \, . \tag{2.53}$$

Normalized radiation patterns computed from eqs. (2.44) to (2.46) for different values of X are presented in Fig. 2-3. As $|X|$ increases the pattern maximum shifts from along the ground plane towards the monopole axis approaching the limit of $\theta = \pi/4$ as $X \rightarrow -\infty$. The input resistance, however, decreases rapidly as X takes larger values approaching zero in the limit as $X \rightarrow -\infty$. A plot of a normalized input resistance, with respect to a monopole of the same height over a perfectly conducting infinite screen, is presented in Fig. 2-4 for different values of X. The variation of (maximum) directivity and position of the radiation pattern maximum (θ_{max}) are shown in the same figure. The directivity changes monotonically from $D_0=3$ (or 4. 77 dB) at X=0 to $D_{\infty}=3.75$ (5. 74 dB) at the limit as $X \rightarrow -\infty$. The upper limit for the directivity was derived from eq. (2.53) by expanding numerator and denominator in power series.

2. 3 Radiation from a Quarter-Wavelength Monopole

The radiation field due to the quarter-wavelength monopole is found by assuming a current distribution

$$i(h) = i_0 \cos(kh) \tag{2.54}$$

along the monopole and then integrating the contributions from elementary dipoles of length dh and current i(h) over the interval h=0 to $\lambda/4$. Thus

$$H_\phi = j i_0 k \cdot \frac{e^{-jkR}}{4\pi R} \sin\theta \int_0^{\lambda/4} \left(e^{jkh\cos\theta} + \frac{\cos\theta-\zeta}{\cos\theta+\zeta} e^{-jkh\cos\theta}\right) \cos(kh)dh \, , \tag{2.55}$$

which yields

FIG. 2-3: NORMALIZED RADIATION PATTERNS OF A SHORT MONOPOLE
OVER AN INFINITE SHEET OF CAPACITIVE REACTANCE.
Parameter: Normalized Reactance.

FIG. 2-4: POSITION OF MAXIMUM INPUT RESISTANCE AND DIRECTIVITY OF A SHORT MONOPOLE OVER AN INFINITE SHEET OF CAPACITIVE REACTANCE.

$$H_\phi = ji_o \frac{e^{-jkR}}{2\pi R} \left[\frac{\cos(\frac{\pi}{2}\cos\theta)}{\sin\theta} - \frac{\zeta}{\cos\theta+\zeta} \cdot \frac{\cos(\frac{\pi}{2}\cos\theta)+j\left[\cos\theta-\sin(\frac{\pi}{2}\cos\theta)\right]}{\sin\theta} \right] \cdot \tag{2.56}$$

Similarly,

$$E_\theta = \eta H_\phi \; . \tag{2.57}$$

For a purely reactive surface ζ is set equal to jX as before. The mean power flow per unit area is found by substituting H_ϕ and E_θ as given above into eq. (2.42). The result is (radial component only)

$$S = \frac{\eta i_o^2}{8\pi^2 R^2}\left[f_1(u)+f_2(u)\right] , \qquad (X \leq 0) \tag{2.58}$$

where
$$f_1(u) = \frac{\cos^2 v}{1-u^2} , \tag{2.59}$$

$$f_2(u) = \frac{X}{(1-u^2)(u^2+X^2)}\left\{ \left[(u-\sin v)^2-\cos^2 v\right]X+2u\cos v(u-\sin v)\right\} , \tag{2.60}$$

$$u = \cos\theta , \tag{2.61}$$

$$v = \frac{\pi}{2} u \; . \tag{2.62}$$

As in the case of the short monopole, the radiation pattern has only one lobe with nulls along the monopole axis and along the impedance screen. To find the maximum one sets

$$\frac{\partial S}{\partial \theta} = 0 \tag{2.63}$$

which results in

$$\frac{\pi}{2}(1-u^2)\sin(\pi u)+\frac{2Xu(1-2u^2-X^2)}{(u^2+X^2)^2}\left[X(u^2+\sin^2 v-2u\sin v-\cos^2 v)+2u\cos v(u-\sin v)\right]+$$

$$+\frac{X(1-u^2)}{u^2+X^2}\left[X(-2u-\pi\sin(\pi u)+2\sin v+\pi u\cos v)-2\cos v(u-\sin v)+2u\cos v(\frac{\pi}{2}\cos v-1)+\right.$$

$$+\pi u\sin v(u-\sin v)\Big] -2u\cos^2 v = 0 \; . \tag{2.64}$$

This equation is best solved numerically on an electronic computer. Anticipating a shift of the pattern maximum from a direction along the ground plane ($\theta = \pi/2$) at $X = 0$ towards the monopole axis ($\theta = 0$) as $X \to -\infty$, in analogy with the short monopole, it is interesting to examine the position of the maximum for $X \to -\infty$. From eq. (2.58), obtain

$$\lim_{X \to -\infty} S = \frac{\eta i_o^2}{8\pi^2 R^2} \cdot \frac{(u - \sin v)^2}{1 - u^2} \qquad (2.65)$$

which results in

$$(1 - u^2)\frac{\pi}{2} \cos v + u \sin v = 1 \qquad (2.66)$$

for θ_{max}. The answer, obtained numerically, is $\theta_{max} = 46.9^{\circ} (X \to -\infty)$.

The input resistance, being equal to the radiation resistance, is given by

$$R_{in} = \frac{2}{i_o^2} \int_0^{2\pi} \int_0^{\pi/2} SR^2 \sin\theta \, d\theta \, d\phi . \qquad (2.67)$$

Some of the integrals that result when the expression for S is substituted into (2.67) cannot be evaluated in closed form without expanding the terms in series. Instead of resorting to series expansions it is easier to evaluate the integral numerically. Some simplification is possible, resulting in

$$R_{in} = \frac{\eta}{2\pi} \left[\frac{\text{Cin}(2\pi)}{4} + A(X) \right] , \qquad (2.68)$$

where

$$\text{Cin}(x) = \int_0^x \frac{1 - \cos\theta}{\theta} \, d\theta , \qquad (2.69)$$

$$A(X) = \int_0^1 f_2(u) \, du . \qquad (2.70)$$

The directivity with respect to an isotropic radiator is

$$D(x) = \frac{8\left[f_1(u_o) + f_2(u_o)\right]}{Cin(2\pi) + 4A(X)} \quad , \qquad (X \leq 0) \tag{2.71}$$

where

$$u_o = cos(\theta_{max}) \; . \tag{2.72}$$

Normalized radiation patterns for different values of X are presented in Fig. 2-5 . The angle where the maximum of the radiation pattern occurs was obtained from eq. (2.64) and is presented in Fig. 2-6. This angle changes from 90° to 46.9^o as X is varied from 0 to $-\infty$. Eighty percent of this change takes place in the range $.01 < X < 1.5$. The monopole input resistance and directivity (over isotropic) are shown in the same figure[*]. The directivity increases slightly as $X \rightarrow -\infty$. The input resistance, however, decreases rapidly in-dicating that relatively small amounts of energy can be radiated when $|X|$ is large.

The physical explanation for the observed shift in the radiation pattern when the ground plane has a capacitive surface impedance can be better understood if one looks at the physical model. One method of creating a capacitive surface impedance is to cut corrugations in the surface of a metal plane. As described in more detail in Chapter IV in order for the corrugated surface to present a capacitive impedance it is sufficient that the depth of the corrugations be between $\lambda/4$ and $\lambda/2$, λ being the wavelength. Now consider a monopole over a corrugated surface with no current in the monopole. When the current is applied, waves are radiated which originally may be considered as following a normal radiation pattern, i.e. the large part of the energy flows along the ground plane. As the first wave passes over the corrugated surface, diffraction takes place at the tips of the walls of the corrugations and part of the energy is directed inside the trenches. Each trench looks like a shorted transmission line, so the diffracted waves are reflected at the bottom and return to the trench aperture where they

---

[*]The resistance values are based on the assumption that the medium above the impedance sheet is air or vacuum so that $\eta = 120 \; \pi$.
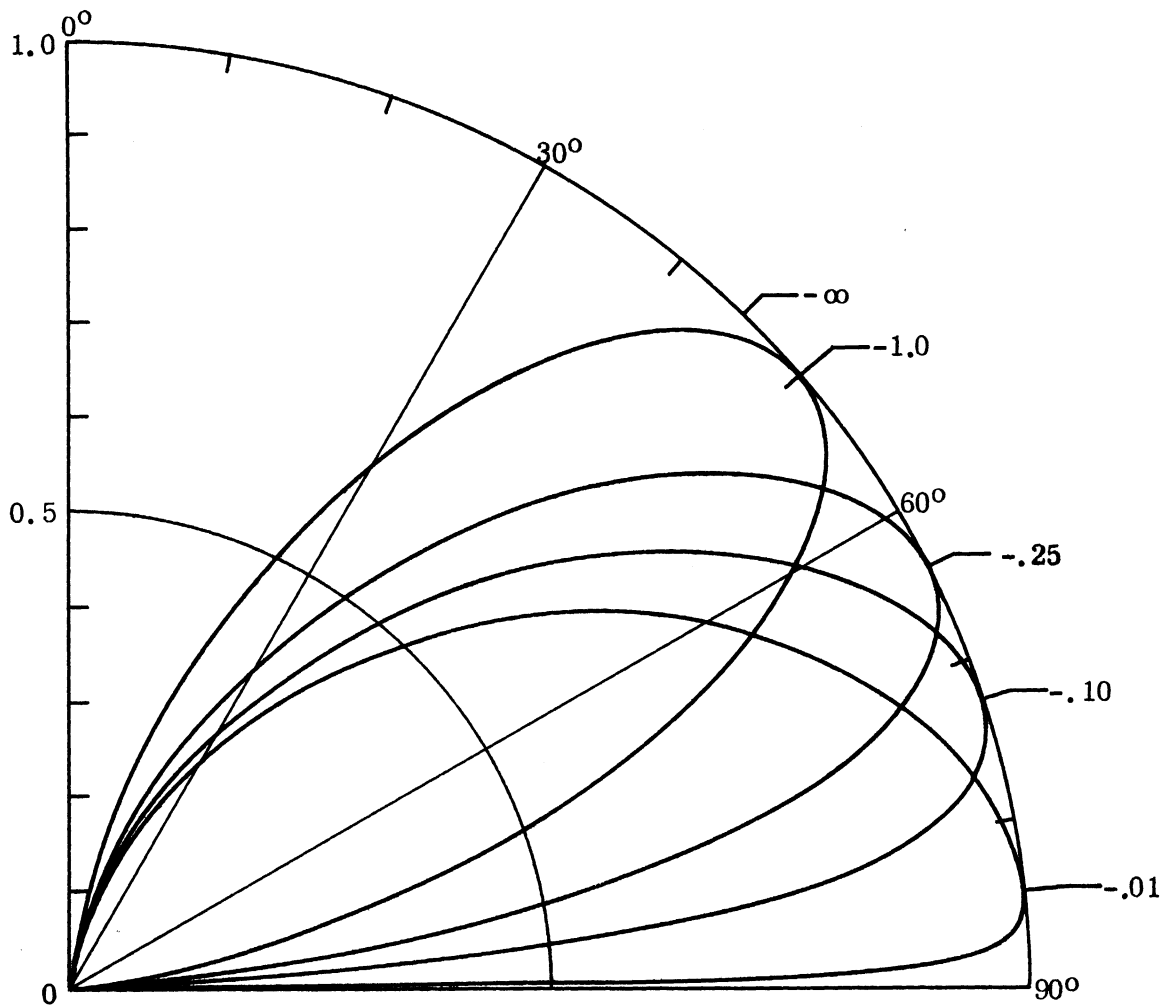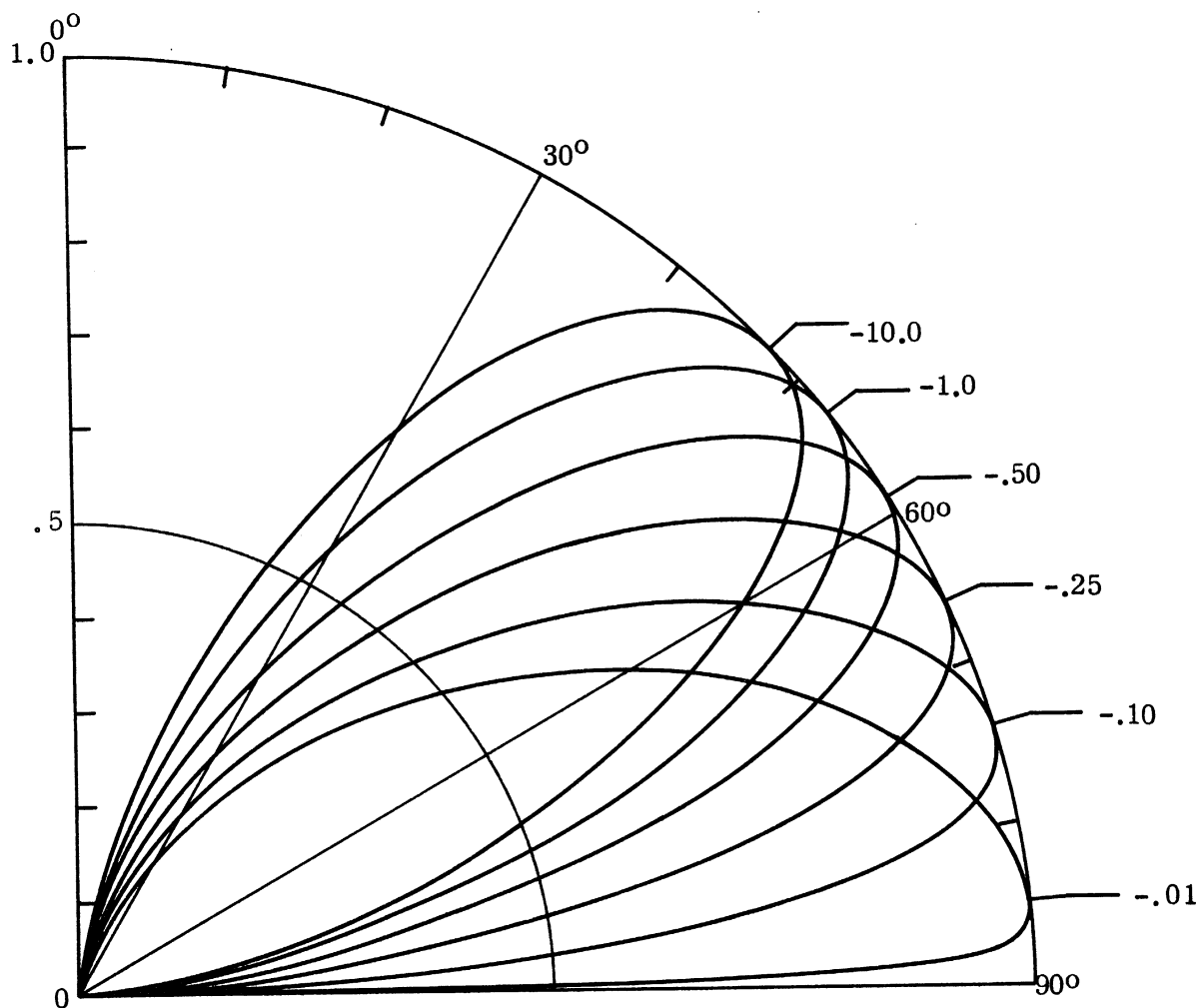
FIG. 2-5: NORMALIZED RADIATION PATTERNS OF A QUARTER-
WAVELENGTH MONOPOLE OVER AN INFINITE SHEET
OF CAPACITIVE REACTANCE.
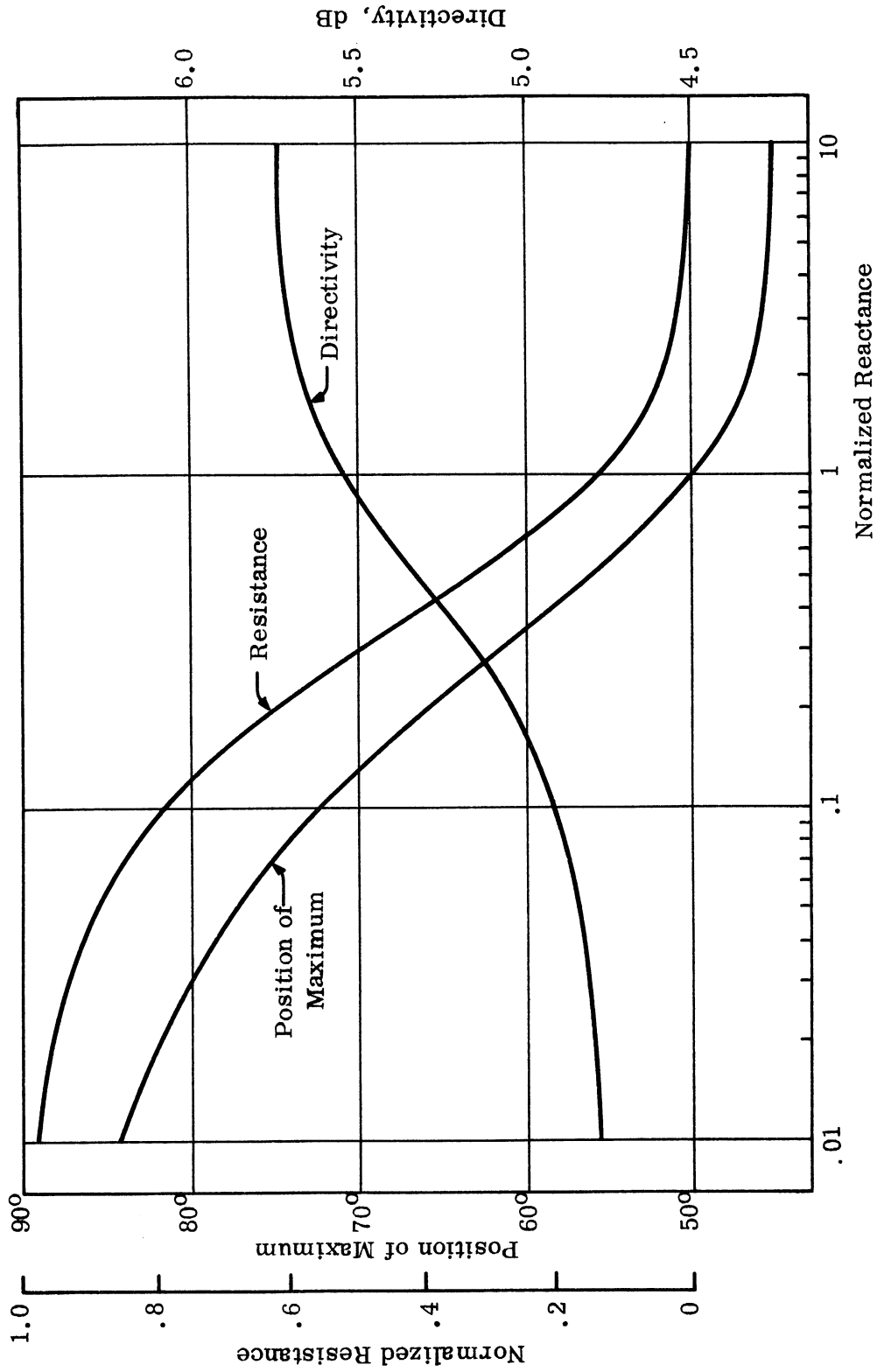Parameter: Normalized Reactance
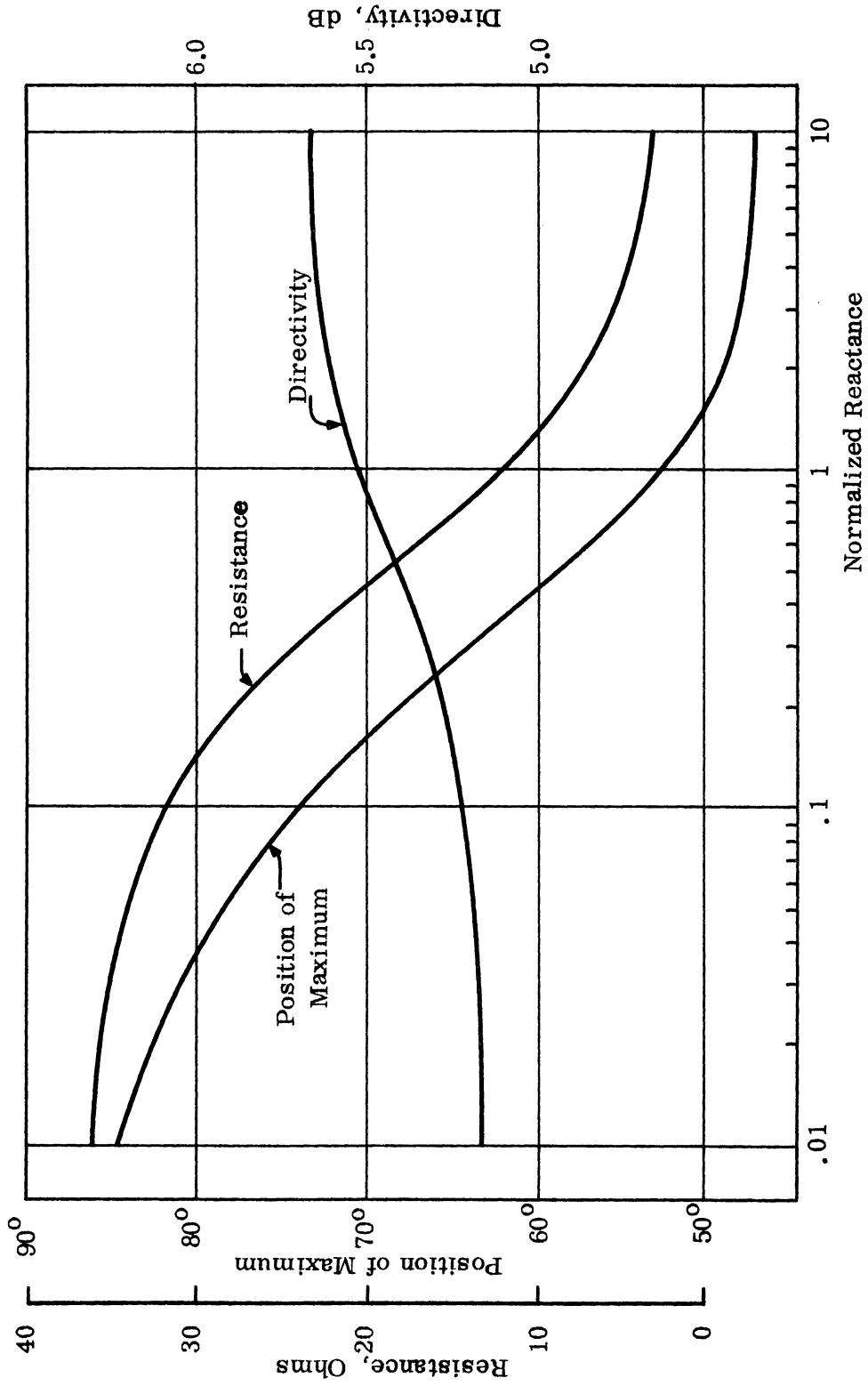
FIG. 2-6: POSITION OF MAXIMUM, INPUT RESISTANCE AND DIRECTIVITY OF A QUARTER-WAVELENGTH MONOPOLE OVER AN INFINITE SHEET OF CAPACITIVE REACTANCE.

are added to the waves traveling along the surface. Since the waves that are reflected at the trench bottom return to the surface with a phase difference corresponding to the path surface-trench bottom-surface, the field strength along the surface can be either enhanced or decreased. The former is true if the depth of the corrugations is such that an inductive surface impedance is created, the latter if the depth is adjusted to create a capacitive surface impedance. This is shown schematically in Fig. 2-7 where W_1 represents the wave originally radiated along the surface, W_2 is the wave diffracted at the corrugation tips and reflected at the trench bottom. Thus the corrugated surface is really acting as a secondary source of radiation, excited by the wave W_1 . The total field at any direction θ will be the sum of the direct wave in that direction, W_3 plus all the contributions of the waves W_2 from all the trenches.
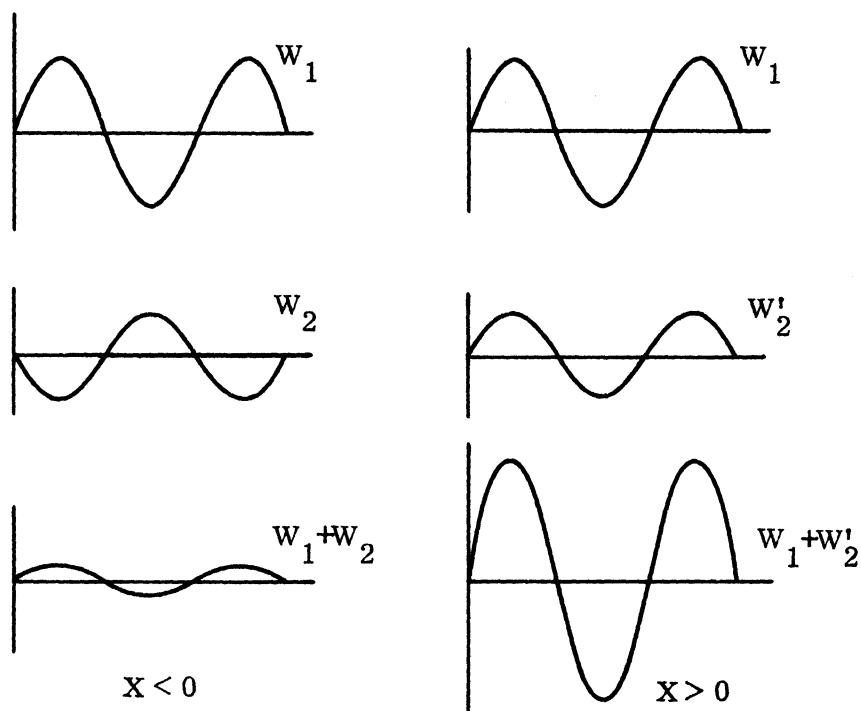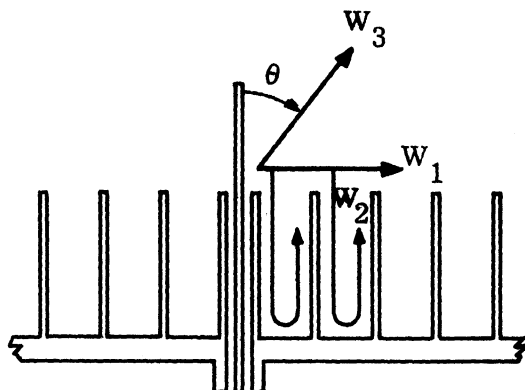
FIG.2-7: SIMPLIFIED MODEL FOR PHYSICAL
EXPLANATION.

RADIATION FROM A MONOPOLE ANTENNA OVER AN INFINITE SCREEN WITH AN ANNULUS OF CAPACITIVE SURFACE IMPEDANCE

3.1 Formulation of the Problem

It is practically impossible to realize an infinite screen with a capacitive surface impedance. If a method of corrugating a metal sheet is used for the creation of the appropriate boundary conditions, the radial extent of the corrugations is restricted by lower and upper limits imposed by the ability to cut a groove of very small or very large radius. The only possibility then is to create an annulus presenting a capacitive surface impedance in an otherwise smooth metal surface. Accordingly the following model is chosen.

Consider a short monopole antenna at the origin, along the z-axis of a cylindrical coordinate system and an infinite ground plane at z=0. The ground plane is assumed perfectly conducting in the vicinity of the antenna out to a radius a . This is followed by an area characterized by a boundary condition of a high capacitive surface impedance extending from radius a to b. The remaining area of the ground plane, outside radius b is again perfectly conducting (Fig. 3-1). The medium above the ground plane is assumed to be a loss-free dielectric, such as air.
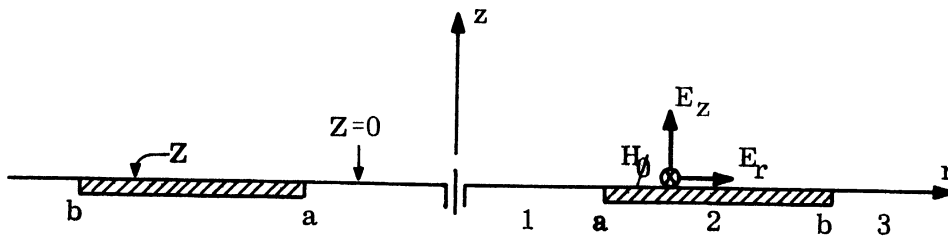
FIG. 3-1: PROBLEM GEOMETRY.

It is very difficult to obtain exact expressions for the electromagnetic field distribution in this case. An approximate method for determining the radiation field of the monopole starts with an assumed approximate form of current distribution on the plane z=0. It is known that the radiation pattern and the power radiated by the antenna are not very sensitive to errors in the assumed form of the current distribution and so the method is expected to give good results (Schelkunoff and Friis, 1952). Since the solution will not be exact, the order of magnitude of a and b is important to determine and justify the necessary approximations and the accuracy of the solution. Corresponding to what is considered of practical interest and the dimensions of an experimental model the domain of applicability of the solution should include the values ka= 4 and kb = 12 where k is the wave propagation number in free-space.

The current distribution in region 1 (0 < r < a) is assumed to be the same as if the whole plane z=0 were perfectly conducting. This means that the reflected waves from the surface discontinuity at r=a are neglected. However, as it is shown in the subsequent formulation,use of the current distribution in region 1 and any associated approximation errors can be avoided.

The current distribution in region 2 (a < r < b) is taken to be the same in form as that which would actually exist if the whole ground plane had the same impedance boundary condition. Here the known exact solution of the canonical problem (Furutsu, 1959) is multiplied by a complex factor α which accounts for the surface discontinuity at r=a. The value of α is determined later.

Lastly, the surface current in region 3 (b < r < ∞) is assumed to be of the same form as it would be if the ground plane were perfectly conducting throughout. A complex factor β is necessary to connect the surface current expressions in regions 2 and 3. However, in the case of an infinite screen knowledge of β is not necessary to derive the far-field pattern as it will be shown.

In the following, cylindrical coordinates (r, ϕ, z) will be used for the source point and spherical coordinates (R, θ, ϕ) for the field (observer) point. The time dependence of the source currents and fields is assumed to be expressed through a factor $e^{j\omega t}$ which will be understood and suppressed. MKS units are used throughout.

The free-space fields due to a short dipole at the origin, along the z-axis and of total length ℓ $(k\ell \ll 1)$ are obtained from those of an infinitesimal (Hertzian) dipole of moment p by letting

$$p = \frac{i\ell}{j\omega} \quad . \tag{3.1}$$

Thus there results

$$
\left.
\begin{aligned}
H_{\phi, 0} &= i\,\ell\,k\,\frac{e^{-jkR}}{4\pi R}\,(j+\frac{1}{kR})\,\sin\theta \quad , \\[2mm]
E_{r, 0} &= -ji\ell k\eta\,\frac{e^{-jkR}}{4\pi R}\,(-1+\frac{3j}{kR}+\frac{3}{k^2 R^2})\sin\theta\cos\theta \quad , \\[2mm]
E_{z, 0} &= -ji\ell k\eta\,\frac{e^{-jkR}}{4\pi R}\,\left[(-1+\frac{3j}{kR}+\frac{3}{k^2 R^2})\cos^2\theta+(1-\frac{j}{kR}-\frac{1}{k^2 R^2})\right] ,
\end{aligned}
\right\} \tag{3.2}
$$

where $\quad \eta = \sqrt{\frac{\mu}{\epsilon}} \quad .$ $\hspace{4cm}$ (3.3)

Equation (3.2) gives also the fields of a monopole of height $\ell/2$ over an infinite perfectly conducting plane at z=0. The fields of a monopole of height ℓ are then

$$
\left.
\begin{aligned}
H_{\phi, 1} &= 2H_{\phi, 0} = i\ell k\,\frac{e^{-jkr}}{2\pi r}\,(j+\frac{1}{kr}) , \\[2mm]
E_{z, 1} &= 2E_{z, 0}\Big|_{\theta=\frac{\pi}{2}} \quad , \\[2mm]
\end{aligned}
\right\} \tag{3.4}
$$

and $\qquad E_{r, 1} = 0 \quad .$

These are the assumed fields in region 1.

The exact fields of a short dipole located at the origin, along the z-axis, over an infinite screen with a surface impedance

$$Z = \zeta \eta \tag{3.5}$$

are given by (Furutsu, 1959)

$$H'_\phi = H_{\phi,0} + i\ell k \frac{e^{-jkR}}{4\pi R}\left[\frac{\sin\theta}{kR} + j\sin\theta \frac{\cos\theta - \zeta}{\cos\theta + \zeta} + 2j\frac{\zeta(1+\zeta\cos\theta)}{\sin\theta(\cos\theta+\zeta)} G(kR)\right],$$

$$E'_r = E_{r,0} - ji\ell k\eta \frac{e^{-jkR}}{4\pi R}\left[\frac{3\sin\theta\cos\theta}{k^2 R^2} + j\frac{3\cos\theta - 2\zeta}{kR}\sin\theta - \sin\theta\cdot\cos\theta\frac{\cos\theta-\zeta}{\cos\theta+\zeta} + \right.$$
$$\left. + \frac{2\zeta^2(1+\zeta\cdot\cos\theta)}{\sin\theta(\zeta+\cos\theta)} G(kR)\right], \qquad \left.\right\} \tag{3.6}$$

$$E'_z = E_{z,0} - ji\ell k\eta \frac{e^{-jkR}}{4\pi R}\left[\frac{3\cos^2\theta-1}{k^2 R^2} + j\frac{3\cos^2\theta-1-2\zeta\cos\theta}{kR} + \sin^2\theta\frac{\cos\theta-\zeta}{\cos\theta+\zeta} + \right.$$
$$\left. + 2\frac{\zeta(1-\zeta^2)}{\zeta+\cos\theta} F(kR)\right],$$

where

$$F(kR) = 1 + jkR(\cos\theta+\zeta)\left[j\frac{\pi}{2}e^{jkR(1+\zeta\cos\theta)} H_0^{(2)}(kR\sin\theta\sqrt{1-\zeta^2}) + \right.$$
$$\left. + \sum_{n=0}^{\infty}(jkR\sin\theta\sqrt{1-\zeta^2})^n f_n\right], \tag{3.7}$$

ith

$$f_0 = \psi_0,$$

$$f_1 = \psi_0\cosh\psi_0 - \sinh\psi_0,$$

$$\cdots\cdots$$

$$f_n = \frac{1}{n^2}\left[(2n-1)\cosh\psi_0 f_{n-1} - \sinh^2\psi_0 f_{n-2}\right], \tag{3.8}$$

$$\cosh\psi_0 = \frac{1+\zeta\cos\theta}{\sin\theta\sqrt{1-\zeta^2}} , \qquad \sinh\psi_0 = \frac{\cos\theta+\zeta}{\sin\theta\sqrt{1-\zeta^2}} , \tag{3.9}$$

$$\left|\arg\sqrt{1-\zeta^2}\right| < \frac{\pi}{2} , \tag{3.10}$$

and

$$G(kR) = 1 + jkR \sin\theta \sqrt{1-\zeta^2} \; \frac{\cos\theta + \zeta}{1 + \zeta\cos\theta} \left[\frac{\pi}{2} e^{jkR(1+\zeta\cos\theta)} H_1^{(2)}(kR\sin\theta \sqrt{1-\zeta^2}) + \right.$$
$$\left. + \sum_{n=0}^{\infty} (jkR\sin\theta \sqrt{1-\zeta^2})^n \, g_n \right], \qquad (3.11)$$

with $\qquad g_0 = \sinh\psi_0$, $\qquad\qquad\qquad\qquad\qquad\qquad$ (3.12)

$$g_1 = \frac{1}{2} \left[\cosh\psi_0 \, \sinh\psi_0 - \psi_0 \right], \qquad\qquad (3.13)$$

and

$$g_n = \frac{1}{n^2 - 1} \left[(2n-1)\cosh\psi_0 \, g_{n-1} - \sinh^2\psi_0 \, g_{n-2} \right]. \qquad (3.14)$$

On the ground plane ($\theta = \pi/2$) and with the help of eq. (3.2) one obtains from (3.6)

$$H'_\phi = i\ell k \, \frac{e^{-jkr}}{2\pi r} \left[\frac{1}{kr} + jG(kr) \right], \quad (z=0), \qquad (3.15)$$

where $G(kr)$ is obtained from eq. (3.11) by letting $\theta = \pi/2$.

The assumed fields in region 2 are then

$$H_{\phi,2} = \alpha i \ell k \, \frac{e^{-jkr}}{2\pi r} \left[\frac{1}{kr} + jG(kr) \right], \quad (z=0), \qquad (3.16)$$

and $\qquad E_{r,2} = -\zeta \eta H_{\phi,2}$. $\qquad\qquad\qquad\qquad\qquad$ (3.17)

For large kr the infinite series in eq. (3.11) converges very slowly. In such a case it is better to use the asymptotic expansion of $G(kr)$ which in the case of capacitive surface impedance is

$$G(kr) \cong - \sum_{n=1}^{\infty} \cdot \frac{g'_n}{(-jkr)^n}, \qquad\qquad (3.18)$$

where

$$g'_n = (-1)^n (n+1)! \; \zeta^2 \sum_{\ell=0}^{n+1} \frac{\binom{1/2}{\ell}\binom{1/2}{n-\ell+1}}{(1-\sqrt{1-\zeta^2})^\ell (1+\sqrt{1-\zeta^2})^{n-\ell+1}} \; , \; (\theta = \pi/2) \; , \qquad (3.19)$$

and
$$\binom{\lambda}{n} = \frac{1}{n!} \; \lambda(\lambda-1)\ldots(\lambda-n+1) \; , \qquad (3.20)$$

$$\binom{\lambda}{0} = 1 \; . \qquad (3.21)$$

Finally, the magnetic field in region 3 is

$$H_{\phi,3} = \beta i \ell k \; \frac{e^{-jkr}}{2\pi r} \; (j + \frac{1}{kr}) \; , \; (z=0). \qquad (3.22)$$

3.2 The Radiation Field

Consider a volume V enclosed by a surface S over which the values of the fields are specified. Also consider a closed contour C lying on S and dividing the surface S into two zones S_1 and S_2 . The vectors $\overline{E}$ and $\overline{H}$ and their first derivatives must be continuous over each one of the regions S_1 and S_2 and satisfy Maxwell's equations there. However, it is permissible for the tangential components of $\overline{E}$ and $\overline{H}$ to undergo a discontinuous change in passing across the contour C. Such discontinuities can be reconciled with the field equations by the introduction of a line distribution of sources (charges or currents) along the contour C. Under the above conditions the fields at any point inside the volume V can be obtained from the specified fields on the boundary S. Several formulae exist for obtaining the fields inside V. They can generally be classified into two categories, those using the classical approach with the Green's function being a scalar, a vector or a dyadic (Kottler 1923, Schelkunoff 1939, Stratton and Chu 1939, Levine and Schwinger 1950, Toraldo di Francia 1953) and those using the Fourier transform method (Borgiotti 1963, Rhodes 1964, Tai 1967).

In the problem at hand the volume V encompasses the half-space above the ground plane into which the monopole radiates. Thus the surface S consists of the plane z=0 and a hemispherical surface at infinity where the fields vanish. The assumed field expressions in regions 1, 2, and 3 of the plane z=0 satisfy Maxwell's equations there. There are two contours where the tangential components of the fields are discontinuous, a circumference C_1 of radius a separating regions 1 and 2 and a circumference C_2 of radius b separating regions 2 and 3. In the case where S consists of a plane (closed at infinity) which is perfectly conducting everywhere except for one or more finite regions, the most suitable of the expressions based on a vector Green's function is the one given by Toraldo di Francia. Let the primed coordinates indicate the source point and the unprimed the field point. Then the fields at any point inside V due to the fields on the boundary are:

$$\bar{E}_i(\bar{R}) = \iint_{S'} \nabla \times \left[G_1 \, \hat{z} \times \bar{E}(\bar{R}') \right] \, dS' \tag{3.23}$$

$$\bar{H}_i(\bar{R}) = \frac{-1}{j\omega\mu} \iint_{S'} \nabla \times \nabla \times \left[G_1 \, \hat{z} \times \bar{E}(\bar{R}') \right] \, dS' \tag{3.24}$$

where

$$G_1(\bar{R}, \bar{R}') = \frac{e^{-jk|\bar{R}-\bar{R}'|}}{2\pi |\bar{R}-\bar{R}'|} \quad . \tag{3.25}$$

In the formal derivation of these relations it is shown that the contribution from the hemispherical surface at infinity to the surface integral is zero. Therefore the surface integral extends only over region 2 of the z=0 plane where $\hat{z} \times \bar{E}$ is different than zero. So,

$$\hat{z} \times \bar{E}(\bar{R}') = \hat{\phi}' \, E_r(r') \quad , \quad (z=0) \; . \tag{3.26}$$

Taking E_r outside the curl operators which apply only to the unprimed coordinates one obtains

$$\nabla \times \nabla \times \left[G_1 \hat{\phi}' \right] = -\hat{\phi}' \, \nabla^2 G_1 + (\hat{\phi}' \cdot \nabla) \, \nabla G_1 \; . \tag{3.27}$$

Noting that

$$\hat{\phi}' = \hat{\phi}\cos(\phi'-\phi)-\hat{r}\sin(\phi'-\phi) \tag{3.28}$$

$$\nabla = \hat{r}\,\frac{\partial}{\partial r}+\hat{\phi}\,\frac{1}{r}\,\frac{\partial}{\partial\phi}+\hat{z}\,\frac{\partial}{\partial z} \tag{3.29}$$

it is easily shown that the contribution of the second term of eq. (3.27) to the surface integral of (3.24) is zero. So,

$$\overline{H}_i(\overline{R})=\frac{1}{j\omega\mu}\iint\limits_{S'}E_r(r')\hat{\phi}'\,\nabla^2 G_1 dS' \;. \tag{3.30}$$

The function G_1 satisfies the equation

$$(\nabla^2+k^2)G_1(\overline{R},\overline{R}')= -\,\delta\,(\overline{R},\overline{R}') \tag{3.31}$$

where $\delta(\overline{R},\overline{R}')$ is the delta function. Therefore for $\overline{R}\neq\overline{R}'$ the following is true

$$\iint\limits_{S'}E_r(\nabla^2+k^2)G_1(\overline{R},\overline{R}')dS'=0 \tag{3.32}$$

and eq. (3.30) may be written

$$\overline{H}_i(\overline{R})=j\omega\epsilon\int_0^{2\pi}d\phi'\int_a^b dr'\,r'E_r G_1(\overline{R},\overline{r}')\hat{\phi}' \;. \tag{3.33}$$

By considering pairs of surface elements symmetrically located with respect to r and analyzing $\hat{\phi}'$ in components along $\hat{\phi}$ and $\hat{r}$ it can be readily seen that the r-components cancel out. Retaining only the ϕ-component one may then replace $\hat{\phi}'$ by $\hat{\phi}\cos(\phi'-\phi)$ in the integrand.

In the far field $(R\gg R')$ one may use the approximations

$$\frac{1}{|\overline{R}-\overline{R}'|}\cong\frac{1}{R} \tag{3.34}$$

and

$$\exp\left\{|\overline{R}-\overline{R}'|\right\}\cong\exp\left\{R-r'\sin\theta\cos(\phi-\phi')\right\} \tag{3.35}$$

to write eq. (2.33) in the simplified form

$$H_{\phi,i}(\overline{R})=j\omega\epsilon\,\frac{e^{-jkR}}{2\pi R}\int_0^{2\pi}d\phi'\int_a^b dr'\,r'E_r e^{+jkr'\sin\theta\cos(\phi-\phi')}\cos(\phi-\phi') \;. \tag{3.36}$$

Recognizing part of the integrand as the integral representation of the Bessel function

$$J_1(z) = \frac{1}{2\pi j} \int_0^{2\pi} e^{jz\cos\phi}\cos\phi\,d\phi \ ,\tag{3.37}$$

one may write eq. (3.36) as

$$H_{\phi,i}(\overline{R}) = -\omega\epsilon\,\frac{e^{-jkR}}{R}\int_a^b E_r J_1(kr\sin\theta)r\,dr \ .\tag{3.38}$$

Substituting $E_{r,2}$ from eq. (3.14) into (3.38) one obtains

$$H_{\phi,i}(\overline{R}) = \alpha\,\zeta\,A\int_{ka}^{kb} e^{-jkr}\left[\frac{1}{kr}+j\,G(kr)\right]J_1(kr\sin\theta)d(kr)\tag{3.39}$$

where

$$A = i\,\ell\,k\,\frac{e^{-jkR}}{2\pi R} \ .\tag{3.40}$$

Equation (3.39) gives the induced field at a distant point due to the fields on the boundary z'=0 . To find the total field at any point inside V one must add to the induced field the field radiated directly by the monopole itself which, because of the choice of Green's function is $2\overline{H}_0$, i.e. identical with the field of the monopole in the presence of an infinite, perfectly conducting ground plane. Thus, the total field is

$$H_\phi = 2\,H_{\phi,0} + H_{\phi,i} \ .\tag{3.41}$$

In the case of a perfectly conducting, infinite ground plane, it is evident from eq. (3.39) that $H_{\phi,i} = 0$ and then $H_\phi = 2H_{\phi,0}$ as expected.

It is necessary to evaluate the integral

$$I = \int_{ka}^{kb} e^{-jx}\left[\frac{1}{x}+j\,G(x)\right]J_1(x\sin\theta)\,dx \ .\tag{3.42}$$

First a general expression will be obtained, valid for all values of x but of practical use for numerical computation only for small x (e. g. x < 5). Then a second expression will be obtained valid only for large values of $x\sin\theta$ (e. g. $x \sin \theta > 5$) employing the asymptotic expansion for $G(x)$. Details as to the accuracy of these expressions are given in the section with the numerical results.

3. 2. 1 Calculation of Integral I in the General Case

Substituting $G(x)$ from eq. (3. 11), with $\theta = \pi/2$, into (3. 42) and letting

$$x = kr \tag{3.43}$$

one obtains

$$I = \int_{ka}^{kb} e^{-jx} \left[\frac{1}{x} + j - x \ \zeta\sqrt{1-\zeta^2} \left\{ \frac{\pi}{2} e^{jx} H_1^{(2)}(x\sqrt{1-\zeta^2}) + \sum_{n=o}^{\infty} (jx\sqrt{1-\zeta^2})^n g_n \right\} \right] \cdot$$
$$\cdot J_1(x\sin\theta)dx . \tag{3.44}$$

The integrals that appear are

$$I_{-1} = \int \frac{e^{-jx}}{x} J_1(x\sin\theta)dx , \tag{3.45}$$

$$I_0 = \int e^{-jx} J_1(x\sin\theta)dx , \tag{3.46}$$

$$I_{n+1} = \int e^{-jx} x^{n+1} J_1(x\sin\theta)dx, \ n=0, 1, 2, 3 \ldots , \tag{3.47}$$

and

$$K = \int x \ H_1^{(2)}(x\sqrt{1-\zeta^2}) J_1(x\sin\theta)dx . \tag{3.48}$$

First the integral I_{n+1} will be evaluated from which I_{-1} and I_0 will be obtained as special cases. The power series expansions, about x=0, of the terms appearing in the integrand of I_{n+1} are

$$e^{-jx} = \sum_{m=o}^{\infty} \frac{(-j)^m}{m!} x^m \tag{3.49}$$

and $\qquad J_1(x\sin\theta) = \dfrac{x\sin\theta}{2} \displaystyle\sum_{m=0}^{\infty} \dfrac{1}{m!\,(m+1)!} \left(\dfrac{j\sin\theta}{2}\right)^{2m} x^{2m}$. $\qquad$ (3.50)

The Cauchy product of two power series in the special case where one series has only even terms is given by

$$\left(\sum_{m=0}^{\infty} a_m x^{2m}\right)\left(\sum_{m=0}^{\infty} b_m x^m\right) = \sum_{m=0}^{\infty} x^m \sum_{\ell=0}^{[m/2]} a_\ell b_{m-2\ell} \qquad (3.51)$$

where $[m/2]$ denotes the greatest integer which is less than or equal to $m/2$. Using eqs. (3.49) to (3.51) to express the integrand and then integrating term by term one obtains (the integration constant being understood and suppressed)

$$I_{n+1} = -jx^n \sum_{m=0}^{\infty} \dfrac{(-jx)^{m+3}}{n+m+3} \sum_{\ell=0}^{[m/2]} \dfrac{1}{\ell!\,(\ell+1)!\,(m-2\ell)!} \left(\dfrac{\sin\theta}{2}\right)^{2\ell+1} ,$$

$$(n \geqq -2) \ . \ (3.52)$$

Although the values of index n in I_{n+1} were such that I_{-1} and I_0 did not appear as special cases, the result expressed by eq. (3.52) is general enough to include I_{-1} and I_0 . Instead of writing two infinite power series one for each of I_{-1}, I_0 some simplication can be achieved by expressing I_{-1} in terms of I_0 . Starting with I_0 and integrating by parts one obtains

$$I_{-1} = -j\cos^2\theta I_0 + \left[j\sin\theta J_0(x\sin\theta) - J_1(x\sin\theta)\right] e^{-jx} . \qquad (3.53)$$

where

$$I_0 = I_{n+1}\Big|_{n=-1} . \qquad (3.53')$$

The evaluation of K is straightforward resulting in

$$K = \dfrac{x}{\cos^2\theta - \zeta^2} \left[\sin\theta J_0(x\sin\theta) H_1^{(2)}(x\sqrt{1-\zeta^2}) - \sqrt{1-\zeta^2} J_1(x\sin\theta) H_0^{(2)}(x\sqrt{1-\zeta^2})\right].$$

$$(3.54)$$

Collecting terms and substituting into eq. (3.39) one obtains

$$H_{\emptyset,i}(\overline{R}) = \alpha\,\zeta\,A\left[\Phi(kb) - \Phi(ka)\right] , \qquad (3.55)$$

where

$$\Phi(x) = -j\sin^2\theta \sum_{m=o}^{\infty} \frac{(-jx)^{m+2}}{m+2} \sum_{\ell=o}^{[m/2]} \frac{1}{\ell!\,(\ell+1)!\,(m-2\ell)!} \left(\frac{\sin\theta}{2}\right)^{2\ell+1}$$

$$+e^{-jx}\left[j\sin\theta J_0(x\sin\theta) - J_1(x\sin\theta)\right]$$

$$-\frac{\frac{\pi}{2}\zeta\sqrt{1-\zeta^2}}{\cos^2\theta-\zeta^2} \times \left[\sin\theta J_0(x\sin\theta)H_1^{(2)}(x\sqrt{1-\zeta^2}) - \sqrt{1-\zeta^2}\,J_1(x\sin\theta)H_0^{(2)}(x\sqrt{1-\zeta^2})\right]$$

$$+j\,\zeta\sqrt{1-\zeta^2} \sum_{n=o}^{\infty} (jx\sqrt{1-\zeta^2})^n g_n \sum_{m=o}^{\infty} \frac{(-jx)^{m+3}}{n+m+3} \sum_{\ell=o}^{[m/2]} \frac{1}{\ell!\,(\ell+1)!\,(m-2\ell)!} \cdot$$

$$\cdot \left(\frac{\sin\theta}{2}\right)^{2\ell+1} \,. \tag{3.56}$$

Combining eq. (3.55) with (3.2) the distant magnetic field of the short monopole is obtained as

$$H_\phi(\bar{R}) = A\left\{j\sin\theta + \alpha\,\zeta\left[\Phi(kb) - \Phi(ka)\right]\right\} \,. \tag{3.57}$$

It is possible to avoid the two infinite series in the last term of $\Phi(x)$ (eq. 3.56) by deriving the integral I_n through a recurrence relation. This will be particularly useful when the product $x\sin\theta$ is small (e. g. $x\cdot\sin\theta < 4$) while x is not small enough for the series to converge rapidly.

Let I_n be given by eq. (3.47) and

$$I_n^o = \int e^{-jx}\, x^n J_0(x\sin\theta)\, dx \,. \tag{3.58}$$

Then, the following pair of recurrence relations is derived

$$\cos^2\theta\cdot I_n = x^n\, e^{-jx}\left[\sin\theta\cdot J_0(x\sin\theta) + jJ_1(x\sin\theta)\right] -j(n-1)I_{n-1} -n\sin\theta\, I_{n-1}^o \,, \tag{3.59}$$

and

$$\cos^2\theta\cdot I_n^o = x^n e^{-jx}\left[-\sin\theta J_1(x\sin\theta) + jJ_0(x\sin\theta)\right] +\sin\theta(n-1)I_{n-1} -jn\, I_{n-1}^o \,. \tag{3.60}$$

For $\theta = \pi/2$ these relations break down but this is not a serious problem since the above relations are intended to be used only for small values of the angle θ .

It is noted that instead of one, two recurrence relations are necessary. Thus in order to obtain I_n one starts with the pair (I_0, I_0^o) from which the pair (I_1, I_1^o) is obtained and so on through the pair (I_{n-1}, I_{n-1}^o) from which I_n can be obtained. Two basic integrals are necessary. Of these I_0 has been derived earlier (eq. 3.53). The second integral, I_0^o, can be similarly obtained with the use of eq. (3.49) and

$$J_0(x\sin\theta) = \sum_{m=0}^{\infty} \frac{(-1)^m}{m!\,m!} (\frac{\sin\theta}{2})^{2m} x^{2m} . \tag{3.61}$$

The result is (the integration constant being understood and suppressed)

$$I_0^o = j \sum_{m=0}^{\infty} \frac{(-jx)^{m+1}}{m+1} \sum_{\ell=0}^{[m/2]} \frac{1}{(\ell!)^2 (m-2\ell)!} (\frac{\sin\theta}{2})^{2\ell} . \tag{3.62}$$

Thus the last term of $\Phi(x)$ (eq. 3.56) can be replaced by

$$-\zeta \sqrt{1-\zeta^2} \sum_{n=0}^{\infty} (j\sqrt{1-\zeta^2})^n \cdot g_n \cdot I_{n+1} . \tag{3.63}$$

3.2.2 Calculation of Integral I in the Case of Large (ka $\sin\theta$) .

In this section the integral of (3.42) will be evaluated using the Hankel asymptotic expansion for the Bessel function $J_1(x)$, eq. (3.74), through the x^{-3} term to guarantee adequate accuracy even when ka is not very large. The incorporation of even higher order terms if needed to improve the accuracy is also straightforward. Also the asymptotic expansion for the quantity $G(x)$ given by eqs. (3.15) through (3.17) will be used. This is generally a divergent infinite series whose terms at first decrease rapidly but later they start increasing again. Such divergent asymptotic series occur frequently in the solution of diffraction problems. In such cases it is common practice to consider as the "sum" of the series the quantity obtained by keeping only a few terms by truncating the series at or before the point where terms start increasing. The truncation of the series determines a limit to the accuracy of this "sum" beyond which it is impossible

to penetrate (Erdélyi, 1956) . Furutsu (loc. cit) has also obtained a convergent asymptotic series for G(x) in which the terms include the incomplete gamma function. However, although this is of great analytical importance, it turns out that it is of little value for the numerical computations. Therefore the ordinary asymptotic expansion which has a somewhat simpler form is considered more suitable for the present treatment.

Substituting G(x) from eq. (3.15) into (3.42) one obtains

$$I = \int_{ka}^{kb} e^{-jx} \left[\frac{1}{x} + j \sum_{n=1}^{n_o} \frac{g'_n}{(-jx)^n} \right] J_1(x\sin\theta) \, dx \ . \tag{3.64}$$

The integrals that appear are of the general form

$$I_n = \int \frac{e^{-jx}}{x^n} J_1(x\sin\theta) \, dx \ , \quad n=1,2,3,\ldots \ . \tag{3.65}$$

First a recurrence relation will be developed and then the basic types will be evaluated. Note that

$$\frac{J_1(x)}{x} = J_0(x) - \frac{dJ_1(x)}{dx} \ , \tag{3.66}$$

and substitute in the integrand and then integrate by parts. The following relation is obtained (the integration constants being understood and suppressed)

$$I_n = \frac{1}{n} \left[-j\,I_{n-1} + \sin\theta\,I^o_{n-1} - \frac{e^{-jx}}{x^{n-1}} J_1(x\sin\theta) \right] \tag{3.67}$$

where I^o_n is defined as

$$I^o_n = \int \frac{e^{-jx}}{x^n} J_0(x\sin\theta) \, dx \ . \tag{3.68}$$

It is noted that I_n and I_n^o as defined here are different from those of the previous section. To determine I_n one must know both I_{n-1} and I_{n-1}^o. One more relation is required which is given by

$$I_n^o = \frac{1}{n-1} \left[-\sin\theta\, I_{n-1} - j\, I_{n-1}^o - \frac{e^{-jx}}{x^{n-1}} J_0(x\sin\theta) \right] , \quad n \geq 2 . \tag{3.69}$$

The basic integrals for the pair of recurrence relations given by eqs. (3.67) and (3.69) are

$$I_1 = \int \frac{e^{-jx}}{x} J_1(x\sin\theta)\, dx , \tag{3.70}$$

and

$$I_1^o = \int \frac{e^{-jx}}{x} J_0(x\sin\theta)\, dx , \tag{3.71}$$

which will be determined next. Given the pair (I_1, I_1^o) one obtains the pair (I_2, I_2^o), then (I_3, I_3^o) and so forth.

For large arguments, $J_1(x)$ can be represented by the Hankel asymptotic expansion. By substituting the asymptotic expansion of $J_1(x)$ into I_1 a number of integrals result of the general type

$$\int \frac{e^{-jx}}{x^{p/2}} dx . \tag{3.72}$$

Recurrence relations can be established by successive integrations by parts, expressing these integrals in terms of

$$\int \frac{e^{-jx}}{x} dx \tag{3.73}$$

which in turn can be expressed through an error function with complex argument or through the Fresnel integrals.

The Hankel asymptotic expansion for $J_1(x)$ for large x, is (Magnus et al, 1966)

$$J_1(x) = \sqrt{\frac{2}{\pi x}} \left[P(1,x)\cos y - Q(1,x)\sin y \right] , \quad |x| \to \infty , \tag{3.74}$$

where

$$P(1,x) \cong \sum_{k=0}^{\infty} (-1)^k \frac{(1,2k)}{(2x)^{2k}} = 1 + \frac{\alpha_2}{x^2} - \dots ,$$ (3.75)

$$Q(1,x) \cong \sum_{k=0}^{\infty} (-1)^k \frac{(1,2k+1)}{(2x)^{2k+1}} = \frac{\alpha_1}{x} - \frac{\alpha_2}{x^3} + \dots ,$$ (3.76)

$$(n,k) = \frac{\Gamma(\frac{1}{2}+n+k)}{k! \, \Gamma(\frac{1}{2}+n-k)} ,$$ (3.77)

and

$$y = x - \frac{3}{4}\pi .$$ (3.78)

It is found that

$$\alpha_1 = \frac{3}{8} , \quad \alpha_2 = \frac{15}{128} \text{ and } \alpha_3 = \frac{105}{1024} .$$ (3.79)

With the help of eq (3.74) the integrand of I_1 is written as

$$dI_1 \cong \frac{1}{\sqrt{2\pi \sin\theta}} \cdot \frac{1}{x^{3/2}} \left\{ \left[(1+\frac{\beta_2}{x^2})+j(\frac{\beta_1}{x} - \frac{\beta_3}{x^3}) \right] e^{-jx(1-\sin\theta)-j3\pi/4} \right.$$

$$\left. + \left[(1+\frac{\beta_2}{x^2})-j(\frac{\beta_1}{x} - \frac{\beta_3}{x^3}) \right] e^{-jx(1+\sin\theta)+j3\pi/4} \right\} dx$$ (3.80)

where

$$\beta_k = \frac{a_k}{\sin^k\theta} \text{ and } k = 1,2,3 .$$ (3.81)

Consider the first part of dI_1

$$dI_{11} = \frac{1}{\sqrt{2\pi \sin\theta}} \cdot \frac{1}{x^{3/2}} \left[(1+\frac{\beta_2}{x^2})+j(\frac{\beta_1}{x} - \frac{\beta_3}{x^3}) \right] e^{-jx(1-\sin\theta)-j3\pi/4} dx.$$ (3.82)

To treat the general case $(\sin\theta \neq 1)$ let

$$u = x(1-\sin\theta), \quad (\sin\theta \neq 1)$$ (3.83)

$$\gamma_k = \alpha_k \left(\frac{1-\sin\theta}{\sin\theta}\right)^k \quad \text{for } k = 1, 2, 3 \tag{3.84}$$

and

$$A_{11} = e^{-j3\pi/4} \left(\frac{1-\sin\theta}{2\pi\sin\theta}\right)^{1/2} . \tag{3.85}$$

Then eq. (3.82) can be written

$$dI_{11} = A_{11} \frac{e^{-ju}}{u^{3/2}} \left[(1 + \frac{\gamma_2}{u^2}) + j(\frac{\gamma_1}{u} - \frac{\gamma_3}{u^3})\right] du, \quad (\sin\theta \neq 1) . \tag{3.86}$$

In integrating it is advantageous to consider the definite integral extending from u to infinity, noting that the integrals of the terms of eq. (3.86) can all be expressed in terms of

$$B = \int_u^\infty \frac{e^{-ju}}{\sqrt{u}} du . \tag{3.87}$$

By means of the substitution

$$u = -jt^2 , \tag{3.88}$$

B can be expressed by means of the complement of the error function, namely

$$B = \sqrt{\frac{\pi}{2}} (1-j) \operatorname{erfc}\left(e^{j\frac{\pi}{4}} \sqrt{u}\right) \tag{3.89}$$

where

$$\operatorname{erfc}(t) = \frac{2}{\sqrt{\pi}} \int_t^\infty e^{-t^2} dt = 1 - \operatorname{erf}(t) . \tag{3.90}$$

An alternate expression for B is

$$B = \sqrt{2\pi} \int_{\sqrt{2u/\pi}}^\infty e^{-j\frac{\pi}{2}t^2} dt$$

$$= \sqrt{2\pi} \left\{ \left[\frac{1}{2} - C\left(\sqrt{\frac{2u}{\pi}}\right)\right] - j \left[\frac{1}{2} - S\left(\sqrt{\frac{2u}{\pi}}\right)\right] \right\}, \tag{3.91}$$

where $C(x)$ and $S(x)$ are the Fresnel integrals

$$C(x) = \int_0^x \cos(\frac{\pi}{2} t^2) dt$$

and

$$S(x) = \int_0^x \sin(\frac{\pi}{2} t^2) \, dt \; . \tag{3.92}$$

After expressing the integrals resulting from eq. (3.86) in terms of B and collecting terms together one obtains

$$\int_u^\infty dI_{11} = A_{11} \frac{2e^{-ju}}{\sqrt{u}} \left[(1 + \frac{2}{3}\gamma_1 - \frac{4}{15}\gamma_2 + \frac{8}{105}\gamma_3) + j\frac{1}{u}(\frac{1}{3}\gamma_1 - \frac{2}{15}\gamma_2 + \frac{4}{105}\gamma_3) \right.$$

$$\left. + \frac{1}{u^2}(\frac{1}{5}\gamma_2 - \frac{2}{35}\gamma_3) - j\frac{1}{u^3}\frac{1}{7}\gamma_3 \right] - jB(1 + \frac{2}{3}\gamma_1 - \frac{4}{15}\gamma_2 + \frac{8}{105}\gamma_3) \; . \tag{3.93}$$

Although in this derivation it was assumed that $\sin\theta \neq 1$, the result is valid also for $\sin\theta = 1$ as can be seen by integrating directly eq. (3.82) and comparing with (3.93). The singularities created by the presence of u in the denominator of eq. (3.93) are canceled out by corresponding terms in the numerator (A_{11} and γ_k's). This will appear more clearly in the final result expressed in terms of the original variable x.

The second part of dI_1 can be treated in a similar way. By collecting all terms going back to the original variable and substituting for all coefficients their numerical values the result can be written in the final form. Let

$$\psi_1(x) = -\int_x^\infty \frac{e^{-jx}}{x} J_1(x\sin\theta) \, dx \; , \tag{3.94}$$

then

$$\mathcal{\psi}_1(x) \cong \frac{+(1+j)}{\sqrt{\sin\theta}} \left\{ \frac{e^{-jx(1-\sin\theta)}}{\sqrt{\pi x}} \left[(1 + \frac{1-\sin\theta}{4\sin\theta} - \frac{(1-\sin\theta)^2}{32\sin^2\theta} + \frac{(1-\sin\theta)^3}{128\sin^3\theta}) + \right. \right.$$

$$+j\frac{1}{x}(\frac{1}{8\sin\theta} - \frac{1-\sin\theta}{64\sin^2\theta} + \frac{(1-\sin\theta)^2}{256\sin^3\theta}) +$$

$$\left. +\frac{1}{x^2}(\frac{3}{128\sin^2\theta} - \frac{3(1-\sin\theta)}{512\sin^3\theta}) - j\frac{1}{x^3}\frac{15}{1024\sin^3\theta} \right]$$

$$- \sqrt{2(1-\sin\theta)} \left[\left\{ \frac{1}{2} - S\left(\sqrt{\frac{2x(1-\sin\theta)}{\pi}}\right) \right\} + j\left\{ \frac{1}{2} - C\left(\sqrt{\frac{2x(1-\sin\theta)}{\pi}}\right) \right\} \right] \cdot$$

$$\left. \cdot \left[1 + \frac{1-\sin\theta}{4\sin\theta} - \frac{(1-\sin\theta)^2}{32\sin^2\theta} + \frac{(1-\sin\theta)^3}{128\sin^3\theta} \right] \right\}$$

$$+\frac{(1-j)}{\sqrt{\sin\theta}} \left\{ \frac{e^{-jx(1+\sin\theta)}}{\sqrt{\pi x}} \left[(1 - \frac{1+\sin\theta}{4\sin\theta} - \frac{(1+\sin\theta)^2}{32\sin^2\theta} - \frac{(1+\sin\theta)^3}{128\sin^3\theta}) \right. \right.$$

$$-j\frac{1}{x}(\frac{1}{8\sin\theta} + \frac{1+\sin\theta}{64\sin^2\theta} + \frac{(1+\sin\theta)^2}{256\sin^3\theta}$$

$$\left. +\frac{1}{x^2}(\frac{3}{128\sin^2\theta} + \frac{3(1+\sin\theta)}{512\sin^3\theta}) + j\frac{1}{x^3}\frac{15}{1024\sin^3\theta} \right]$$

$$- \sqrt{2(1+\sin\theta)} \left[\left\{ \frac{1}{2} - S\left(\sqrt{\frac{2x(1+\sin\theta)}{\pi}}\right) \right\} + j\left\{ \frac{1}{2} - C\left(\sqrt{\frac{2x(1+\sin\theta)}{\pi}}\right) \right\} \right] \cdot$$

$$\left. \cdot \left[1 - \frac{1+\sin\theta}{4\sin\theta} - \frac{(1+\sin\theta)^2}{32\sin^2\theta} - \frac{(1+\sin\theta)^3}{128\sin^3\theta} \right] \right\} , \quad |x\sin\theta| \to \infty .$$

$$(3.95)$$

It should be noted at this point that an exact and much simpler expression exists for the special case where $\sin\theta=1$, namely

$$I_1 = e^{-jx} \left[-J_1(x) + j J_0(x) \right] + C , \tag{3.96}$$

which yields

$$\mathcal{\psi}_1(x) = - \int_x^\infty \frac{e^{-jx}}{x} J_1(x)dx = +e^{-jx}\left[-J_1(x) + j J_0(x) \right] . \tag{3.97}$$

By introducing the asymptotic expansions for $J_1(x)$ and $J_0(x)$ into eq. (3.97) it can easily be verified that it is identical with eq. (3.95) when in the latter one sets $\sin\theta$ equal to one. The function $\bar{\psi}_1(x)$ has been introduced to replace I_1 since it was found advantageous to work with the definite rather than the indefinite integral. In general let

$$\bar{\psi}_n(x) = -\int_x^\infty \frac{e^{-jx}}{x^n} J_1(x\sin\theta)dx = -I_n\Big|_x^\infty \qquad (3.98)$$

and

$$\bar{\psi}_n^o(x) = -\int_x^\infty \frac{e^{-jx}}{x^n} J_0(x\sin\theta)dx = -I_n^o\Big|_x^\infty \, . \qquad (3.99)$$

The recurrence relations (3.67) and (3.69) which were derived for I_n and I_n^o apply equally well to $\bar{\psi}_n$ and $\bar{\psi}_n^o$ as they are.

The function $\bar{\psi}_1^o$ can be obtained in an analogous manner. The Hankel asymptotic expansion of $J_0(x)$ for large x is given by

$$J_0(x) = \sqrt{\frac{2}{\pi z}}\left[P(0,x)\cos y - Q(0,x)\sin y\right] , \quad |x| \to \infty \qquad (3.100)$$

where

$$P(0,x) \approx 1 - \frac{\alpha'_2}{x^2} + \frac{\alpha'_4}{x^4} - \ldots , \qquad (3.101)$$

$$Q(0,x) \approx \frac{-\alpha'_1}{x} + \frac{\alpha'_3}{x^3} - \ldots , \qquad (3.102)$$

$$y = x - \frac{\pi}{4} , \qquad (3.103)$$

with $\quad \alpha'_1 = \frac{1}{8} , \quad \alpha'_2 = \frac{9}{128} , \quad \alpha'_3 = \frac{75}{1024} \quad$ and $\quad \alpha'_4 = \frac{3675}{32768}$. $\qquad (3.104)$

Inserting the above expression for $J_0(x)$ in eq. (3.71) one obtains the following result

$$\Psi_1^o(x) = -\int_x^\infty \frac{e^{-jx}}{x} J_0(x\sin\theta)dx \cong$$

$$\cong \frac{-(1-j)}{\sqrt{\sin\theta}} \left\{ \frac{e^{-jx(1-\sin\theta)}}{\sqrt{\pi x}} \left[(1- \frac{1-\sin\theta}{12\sin\theta} + \frac{3(1-\sin\theta)^2}{160\sin^2\theta} - \frac{5(1-\sin\theta)^3}{896\sin^3\theta}) \right. \right.$$

$$-j\frac{1}{x}(\frac{1}{24\sin\theta} - \frac{3(1-\sin\theta)}{320\sin^2\theta} + \frac{5(1-\sin\theta)^2}{1792\sin^3\theta})$$

$$\left. - \frac{1}{x^2}(\frac{9}{640\sin^2\theta} - \frac{15(1-\sin\theta)}{3584\sin^3\theta}) + j\frac{1}{x^3}\frac{75}{7168\sin^3\theta} \right]$$

$$- \sqrt{2(1-\sin\theta)} \left[\left\{\frac{1}{2} -S(\sqrt{\frac{2x(1-\sin\theta)}{\pi}})\right\} +j \left\{ \frac{1}{2} -C(\sqrt{\frac{2x(1-\sin\theta)}{\pi}})\right\} \right] \cdot$$

$$\left. \cdot \left[1- \frac{1-\sin\theta}{12\sin\theta} + \frac{3(1-\sin\theta)^2}{160\sin^2\theta} - \frac{5(1-\sin\theta)^3}{896\sin^3\theta} \right] \right\}$$

$$- \frac{(1+j)}{\sqrt{\sin\theta}} \left\{ \frac{e^{-jx(1+\sin\theta)}}{\sqrt{\pi x}} \left[(1+ \frac{1+\sin\theta}{12\sin\theta} + \frac{3(1+\sin\theta)^2}{160\sin^2\theta} + \frac{5(1+\sin\theta)^3}{896\sin^3\theta}) \right. \right.$$

$$+j\frac{1}{x}(\frac{1}{24\sin\theta} + \frac{3(1+\sin\theta)}{320\sin^2\theta} + \frac{5(1+\sin\theta)^2}{1792\sin^3\theta})$$

$$\left. - \frac{1}{x^2}(\frac{9}{640\sin^2\theta} + \frac{15(1+\sin\theta)}{3584\sin^3\theta}) - j\frac{1}{x^3}\frac{75}{7168\sin^3\theta} \right]$$

$$- \sqrt{2(1+\sin\theta)} \left[\left\{\frac{1}{2} -S(\sqrt{\frac{2x(1+\sin\theta)}{\pi}})\right\} + j \left\{ \frac{1}{2} -C(\sqrt{\frac{2x(1+\sin\theta)}{\pi}})\right\} \right] \cdot$$

$$\left. \cdot \left[1+ \frac{1+\sin\theta}{12\sin\theta} + \frac{3(1+\sin\theta)^2}{160\sin^2\theta} + \frac{5(1+\sin\theta)^3}{896\sin^3\theta} \right] \right\} , \quad |x\sin\theta| \to \infty . \tag{3.105}$$

No exact expression has been derived for I_1^o in the case where $\sin\theta= 1$.

With all the terms calculated one may now go back to integral I of eq. (3. 64).

Let

$$\Psi(x) = -\int_x^\infty e^{-jx} \left[\frac{1}{x} -j \sum_{n=1}^{n_0} \frac{g_n'}{(-jx)^n} \right] J_1(x\sin\theta)dx . \tag{3.106}$$

Then I is given by

$$I = \tilde{\psi}(kb) - \tilde{\psi}(ka) , \qquad |x\sin\theta| \to \infty \qquad (3.107)$$

and consequently

$$H_{\phi,i}(\bar{R}) = \alpha \ \zeta \ A\left[\tilde{\psi}(kb) - \tilde{\psi}(ka)\right] , \qquad |x\sin\theta| \to \infty . \qquad (3.108)$$

The function $\tilde{\psi}(x)$ can be readily written down with the help of $\tilde{\psi}_n(x)$ as

$$\tilde{\psi}(x) = \tilde{\psi}_1(x) - j \sum_{n=1}^{n_0} g'_n \ j^n \ \tilde{\psi}_n(x) \qquad (3.109)$$

where $\tilde{\psi}_n(x)$ is obtained from $\tilde{\psi}_1(x)$ and $\tilde{\psi}_1^0(x)$ from the recurrence relations (3. 67) and (3. 69)

3. 2. 3 The Radiation Field in the Case of Small ka and Large kb

In the previous sections two different expressions have been derived for the radiation field. The first is generally valid but practically useful only for small arguments (kr) while the second is valid only for large arguments (krsinθ). An obvious difficulty occurs when kr is large while sinθ is small. At the limit θ=0, corresponding to the monopole axis, the magnetic field is obviously zero but its value for θ near zero cannot be readily obtained. The most suitable expression for this case is the general solution as modified by eq. (3. 63). Still, the most important range is near the value $\theta = \pi/2$ and near the maximum of the radiation pattern and in this range the derived expressions do apply.

In the case where ka is small but kbsinθ large the two expressions are combined by writing eq. (3. 42) in the form

$$I = \int_0^\infty L(x)dx - \int_0^{ka} L(x)dx - \int_{kb}^\infty L(x)dx \qquad (3.110)$$

where the common integrand in the above integrals is

$$L(x) = e^{-jx} \left[\frac{1}{x} + jG(x)\right] J_1(x\sin\theta) . \qquad (3.111)$$

Using the functions $\Phi(x)$ and $\Psi(x)$ (see eqs. (3.56) and (3.109)) one may write

$$I = \int_0^\infty L(x)dx - \left[\Phi(ka) - \Phi(0)\right] + \Psi(kb) \ . \qquad (3.112)$$

Since a direct substitution of x=0 into $\Phi(x)$ yields some terms with undetermined forms, $\Phi(0)$ will be evaluated as

$$\Phi(0) = \lim_{x \to 0} \Phi(x) \ . \qquad (3.113)$$

Using the limiting forms of the Bessel functions for small arguments

$$\left.\begin{array}{l} J_0(x) \sim 1 \\ J_1(x) \sim \dfrac{1}{2} x \\ jH_0^{(2)}(x) \sim \dfrac{2}{\pi} \ell n \ x \\ jH_1^{(2)}(x) \sim -\dfrac{1}{\pi} \dfrac{2}{x} \end{array}\right\} \quad x \to 0 \qquad (3.114)$$

it is found that

$$\Phi(0) = j\sin\theta(1 - \frac{\zeta}{\cos^2\theta - \zeta^2}) \ . \qquad (3.115)$$

Furthermore, have

$$\int_0^\infty L(x)dx = \int_0^\infty \frac{e^{-jx}}{x} J_1(x\sin\theta)dx + j\int_0^\infty e^{-jx}G(x)J_1(x\sin\theta)dx \ . \qquad (3.116)$$

The first of the two integrals is given by

$$\int_0^\infty \frac{e^{-jx}}{x} J_1(x\sin\theta)dx = -j \frac{1-\cos\theta}{\sin\theta} \ . \qquad (3.117)$$

To calculate the second, use is made of the integral representation of G(x) which is (Furutsu, 1959)

$$G(x) = 1 - j \ xe^{jx} \ \zeta \sqrt{1-\zeta^2} \int_{\psi_0}^{\infty - j\frac{\pi}{2}} \cosh\psi \ e^{-jx\sqrt{1-\zeta^2} \cosh\psi} d\psi \qquad (3.118)$$

where

$$\cosh \psi_0 = \frac{1}{\sqrt{1-\zeta^2}} \quad \text{and} \quad \sinh \psi_0 = \frac{\zeta}{\sqrt{1-\zeta^2}} \ . \tag{3.119}$$

Inserting (3.118) into the second integral of (3.116) one may write

$$\int_0^\infty e^{-jx} G(x) J_1(x\sin\theta) dx = \int_0^\infty e^{-jx} J_1(x\sin\theta) dx$$
$$-j\zeta \sqrt{1-\zeta^2} \int_0^\infty x J_1(x\sin\theta) \int_{\psi_0}^{\infty-j\frac{\pi}{2}} \cosh\psi \ e^{-jx\sqrt{1-\zeta^2}\cosh\psi} \ d\psi dx \ . \tag{3.120}$$

For the first term in the right hand side of (3.120) one obtains

$$\int_0^\infty e^{-jx} J_1(x\sin\theta) dx = -\frac{1-\cos\theta}{\sin\theta\cos\theta} \ . \tag{3.121}$$

The second term denoted below by K, is calculated by interchanging the order of integration,[*] integrating first with respect to x using the relation

$$\int_0^\infty e^{-\alpha t} J_1(\beta t) t \, dt = \frac{\beta}{(\alpha^2+\beta^2)^{3/2}} \ , \quad (\text{Re } \alpha > |\text{Im}\beta|) \tag{3.122}$$

and then with respect to ψ, to find

$$K = \frac{\zeta \sin\theta}{\cos\theta(\cos\theta+\zeta)} \ . \tag{3.123}$$

Substituting (3.121) and (3.123) into (3.120) one obtains

$$\int_0^\infty e^{-jx} G(x) J_1(x\sin\theta) dx = \frac{(\zeta-1)(1-\cos\theta)}{\sin\theta(\zeta+\cos\theta)} \ . \tag{3.124}$$

Substituting (3.124) and (3.117) into (3.116) one finds that

$$\int_0^\infty L(x) dx = -j\frac{\sin\theta}{\zeta+\cos\theta} \ . \tag{3.125}$$

[*]See footnote at end of Chapter.

With the help of eqs. (3. 125) and (3. 115), eq. (3. 110) becomes

$$I = \psi \ (kb) - \Phi(ka) + j\sin\theta \ (1 - \frac{\cos\theta}{\cos^2\theta - \zeta^2})$$

(3. 126)

and the far-zone magnetic field is therefore

$$H_\phi(\bar{R}) = A \left\{ j\sin\theta + \alpha \ \zeta \ \left[\psi \ (kb) - \Phi(ka) + j\sin\theta \ (1 - \frac{\cos\theta}{\cos^2\theta - \zeta^2}) \right] \right\}.$$

(3. 127)

There remains the determination of the complex coefficient α . This is accomplished on the basis of the following physical argument. It is known (see Ch. II) that in the case of an infinite sheet with capacitive surface impedance the radiation pattern has a null along the ground plane. Therefore by letting kb $\rightarrow\infty$, in which case ψ (kb) $\rightarrow 0$, and $\theta = \pi/2$, the magnetic field given by eq. (3. 127) should be zero. This leads to an equation which can be solved for α. The result is

$$\alpha = \frac{-1}{\zeta \left[1 + j \ \Phi \ (ka) \right]} \quad , \quad (\theta = \pi/2) \ .$$

(3. 128)

In the case of large ka a simpler expression is derived from eq. (3. 98) namely,

$$\alpha = \frac{-1}{j \ \zeta \ \psi \ (ka)} \quad , \quad (ka = large) \ .$$

(3. 129)

As seen, the factor α depends upon ka. This was expected since the magnitude and phase of the field induced from the impedance annulus, which is controlled by α, depends upon how far the primary source, i. e. the monopole, is situated.

For ka = 0 one finds from eqs. (3. 128) and (3. 115) that

$$\alpha = 1 \ , \qquad (ka = 0 \ ) \ .$$

(3. 130)

This result again is according to expectations since when the impedance boundary extends all the way to the source, the assumed surface field should be identical with the exact solution. It is interesting to note that although α was determined solely on the basis of what should happen when kb $\rightarrow \infty$ (with ka arbitrary), it automatically satisfies the other limiting condition, i. e. ka=0

with kb arbitrary.

Numerical values of the magnitude and phase of α computed from (3.128) and (3.129) for different values of a purely reactive surface impedance (ζ=jX, X< 0) are plotted in Fig. 3-2 versus ka.

For finite kb the ratio of the field intensity along the ground plane to the value that would exist in the absence of the impedance annulus is given by

$$\Gamma = \left| \frac{H_\phi\left(\frac{\pi}{2}\right)}{H_{\phi,1}\left(\frac{\pi}{2}\right)} \right| = \left| \frac{\psi\,(kb)}{\Phi\,(ka)-j} \right| \quad \text{for ka = small}$$

$$= \left| \frac{\psi\,(kb)}{\psi\,(ka)} \right| \quad \text{for ka = large} .$$

(3.131)

The ratio in the radiated power in the same two cases is Γ^2 .

The radiation field has been calculated using Eqs. (3.56) and (3.127) for different values of ka, kb and X assuming that the real part of the surface impedance is zero. Typical radiation patterns are shown in Fig.3-3. All patterns were normalized with respect to the maximum intensity in the case of an infinite, perfectly conducting screen which is taken as one. For a given pair of ka and kb four patterns were calculated for different values of X and are shown grouped together. When -0.1 < X < 0 the patterns tend to be very similar to the pattern obtained with X=0. When -∞ <X<-2.5 and $\alpha \geq \lambda$ (λ is the wavelength) the pattern changes very little (cf. with Ch. II). The values of ka and kb were chosen so that the radial extent of the reactive annulus in the different cases would be equal to either $\lambda/2$ or λ.

Optimum selection of ka, kb and X is possible with respect to various objectives. By comparing the pattern corresponding to the same value of X and radial extent of the reactance annulus but different ka (Fig 3-3, a, c, e, g, h) an optimum value of ka can be chosen so that the ratio of $H_\phi(90°)$ to the maximum value of $H_\phi(\theta)$ would be minimized (ka=π or α=λ). If the objective is maximum beamwidth, Fig. 3-3g shows that when ka = $3\pi/2$, kb= $5\pi/2$ and X= -2.5 the field intensity does not vary more than 9 percent over a 73° beamwidth.

FIG. 3-2: FACTOR α. Parameter: Normalized Reactance

a) Magnitude
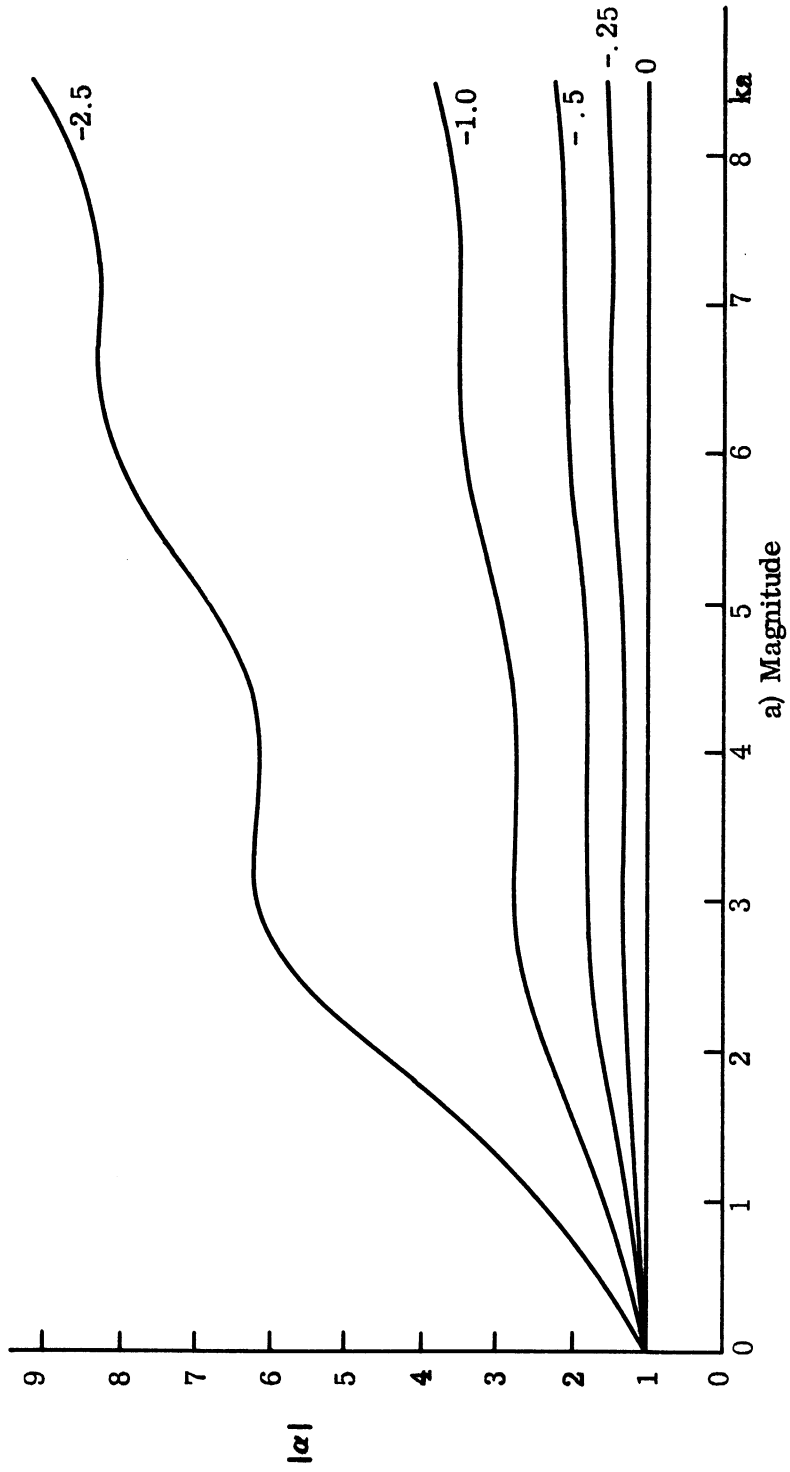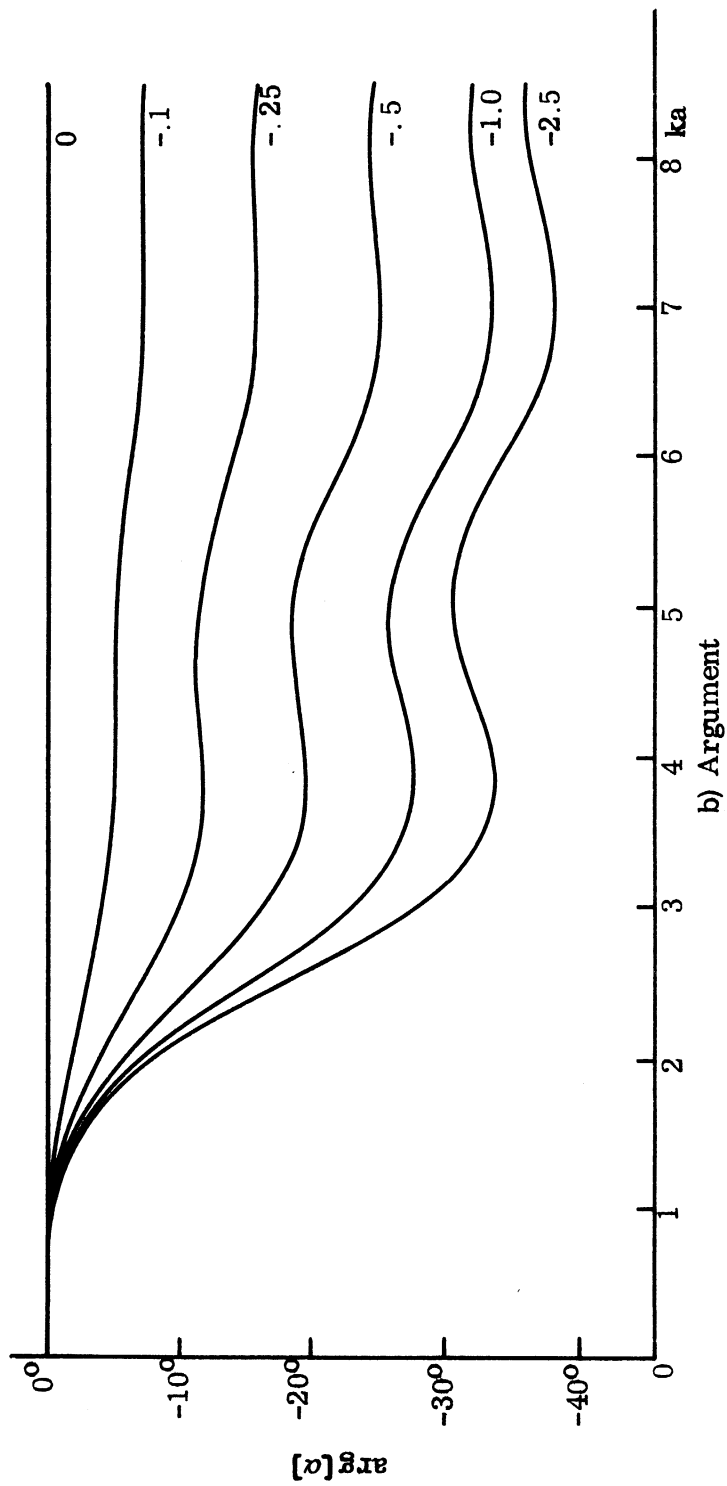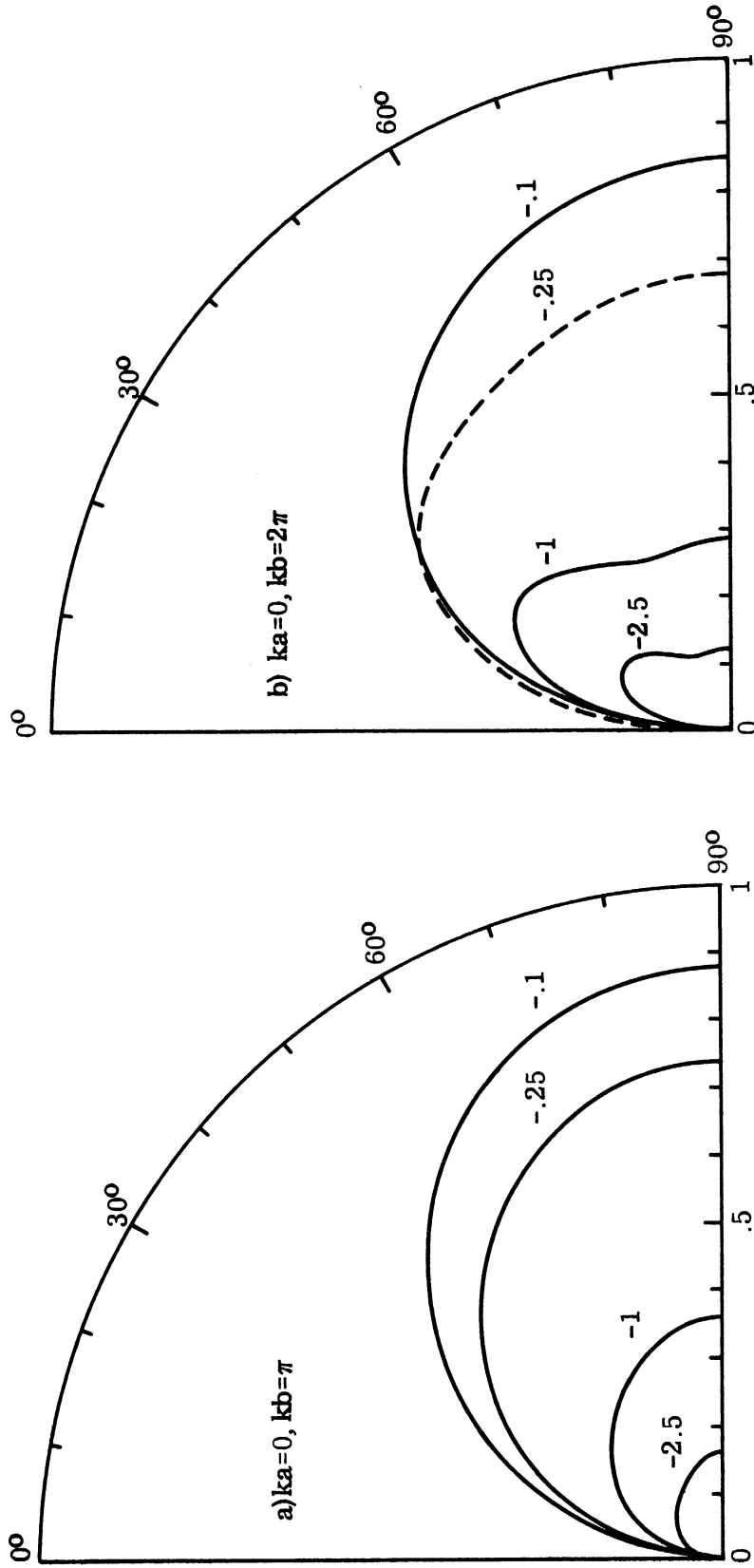
FIG. 3-2: Continued.

FIG. 3-3: RADIATION FIELD PATTERNS OF A MONOPOLE OVER AN INFINITE SCREEN WITH AN ANNULUS OF CAPACITIVE SURFACE REACTANCE. Parameter: Normalized Reactance.

d) ka $= \dfrac{\pi}{2}$, kb $= \dfrac{5\pi}{2}$

c) ka $= \dfrac{\pi}{2}$, kb $= \dfrac{3\pi}{2}$

FIG. 3-3: Continued

f) ka=π , kb= 3π

e) ka=π , kb= 2π

FIG. 3-3: Continued

h) ka=2π, kb=3π

g) ka=3π/2, kb=5π/2
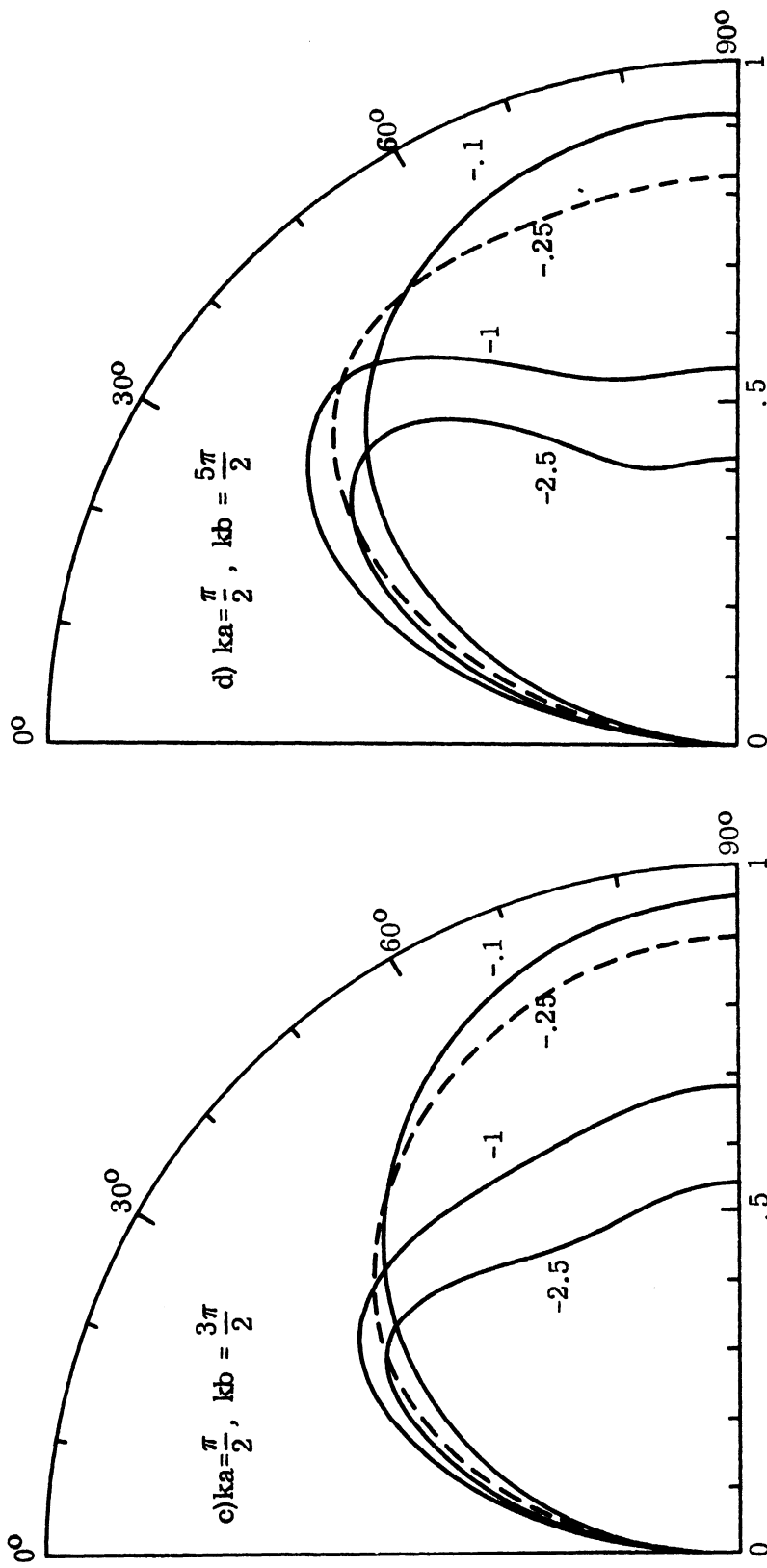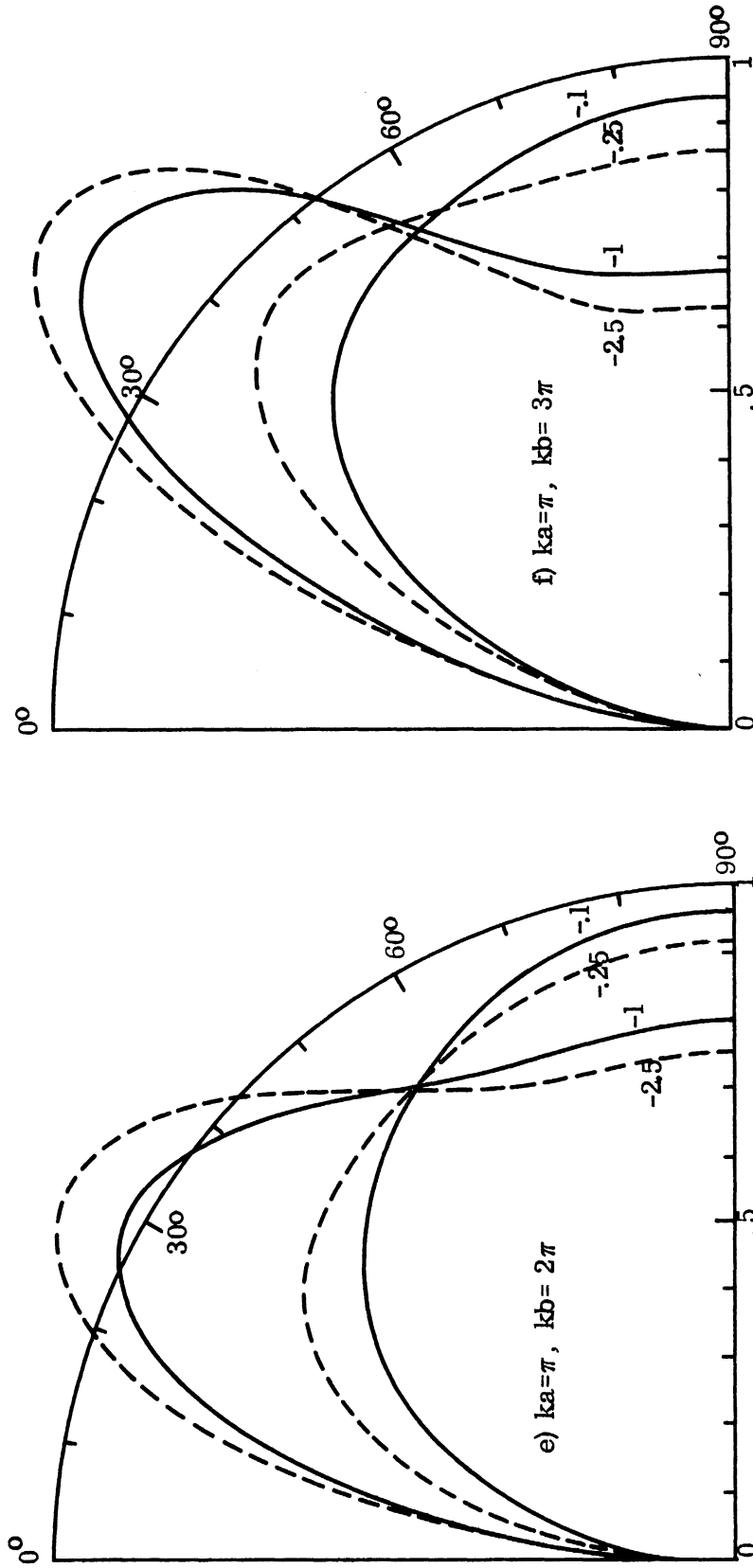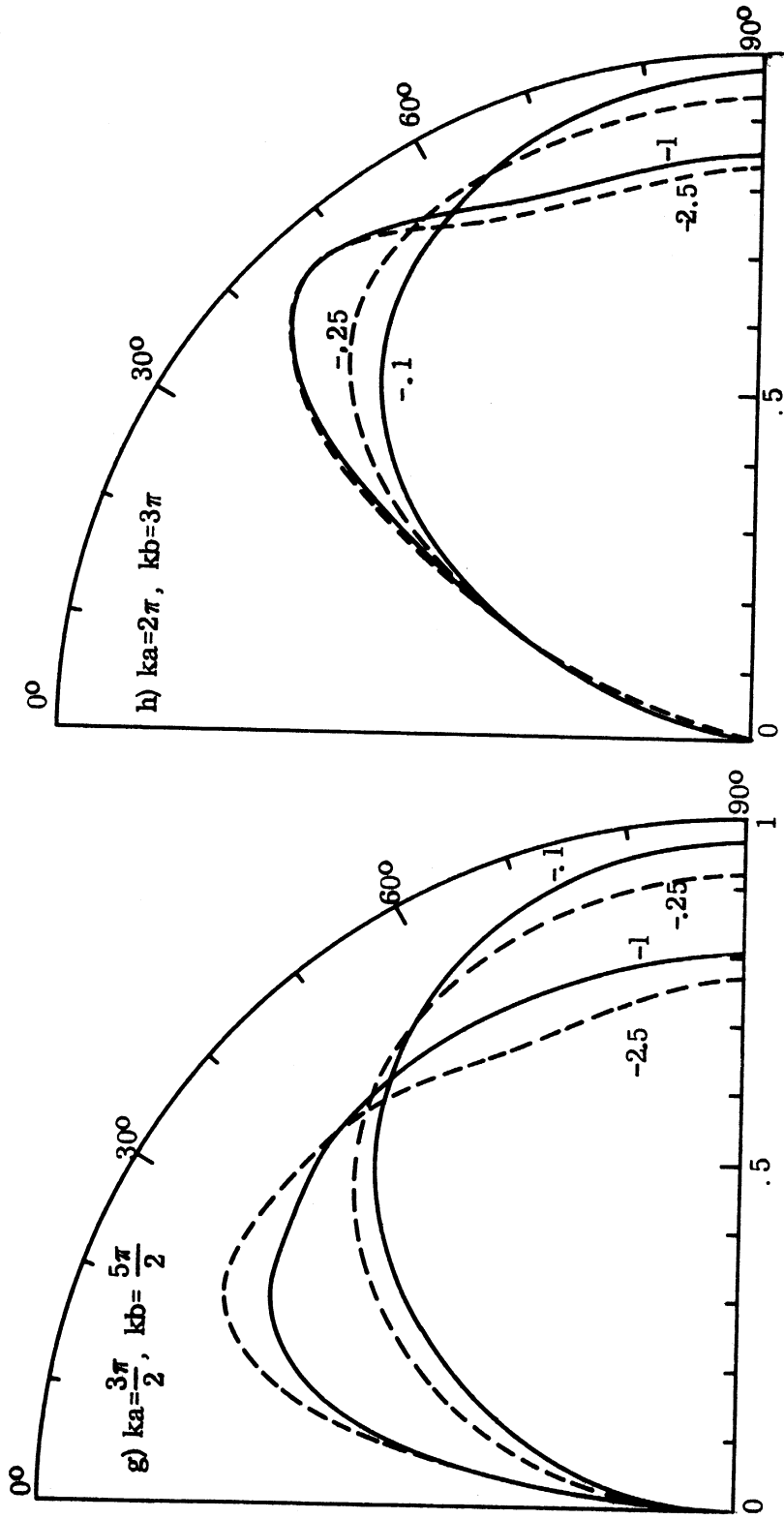
FIG. 3-3: Concluded.

3. 3   Comparison with the Exact Solution in Limiting Cases

There are two limiting cases for the problem treated in this chapter for which the exact solution is known. One is when the surface impedance of the annulus $a < r < b$ is equal to zero in which case the problem reduces to the well known case of a monopole over an infinite, perfectly conducting ground plane. This limiting case can also be reached by letting $ka = kb$. In either case it is obvious from the beginning of the solution (eqs. 3. 39 and 3. 41) that there is agreement with the exact solution.

The second limiting case is obtained by letting $ka \rightarrow 0$ and $kb \rightarrow \infty$. Then the problem reduces to that of a monopole over an infinite sheet with surface impedance ζ . Substituting in eq. (3. 127) with

$$\Phi (0) = \lim_{ka \rightarrow o} \Phi (ka) = j\sin\theta \left(1 - \frac{\zeta}{\cos^2\theta - \zeta^2}\right)$$

(3. 132)

$$\Psi (\infty) = \lim_{kb \rightarrow \infty} \Psi(kb) = 0$$

(3. 133)

it is found that

$$H_\phi(\overline{R}) = ji \, \ell \, k \, \frac{e^{-jkR}}{2\pi R} \cdot \frac{\sin\theta\cos\theta}{\cos\theta + \zeta}$$

(3. 134)

which is identical with the first term (radiation field) of the exact solution, eq. (3. 6). This term has also been derived directly in Ch. II, eq. (2. 41).

*In the absence of a rigorous proof, it is noted that the inversion of the order of integration is consistent with numerical results which show that the resulting value for I, given by eq. (3.126), is identical with the alternate form

$$I = \Psi (kb) - \Psi (kc) + \Phi (kc) - \Phi (ka), \quad a < c < b .$$

IV

THE MONOPOLE ANTENNA OVER A SCREEN
WITH AN ANNULUS OF CAPACITIVE SURFACE REACTANCE:
EXPERIMENTAL INVESTIGATION

4.1 Facilities

The experiments reported here were conducted in two anechoic chambers. The dimensions of the first chamber are 50' x 30' x 15' with a 12' square aluminum ground plane mounted in the center of one end wall. The ground plane consists of nine 4' x 4' individual sections joined by 2" aluminum tape. The ceiling and floor are covered by four-inch thick hairflex microwave absorber while the rear and side walls are covered with 26- and 18-inch absorber pyramids, respectively. The chamber is lined with interlocking aluminum foil sheets to provide a known uniform termination for the absorbing material and to shield the room from external signals. These sheets provide also an electric continuation to the ground plane (Lyon et al, 1966). Measurements of radiation patterns, coupling and impedance have been performed in this chamber.

The second chamber consists of a rectangular portion with dimensions 11' x 12' x 10' and a tapered portion 33' long. This chamber has been designed primarily for surface field measurements and was used for this purpose (Knott, 1965). The walls of the test area consisting of the rectangular portion of the chamber are covered with absorber pyramids while the tapered section is covered by hairflex absorber. The antenna under test is placed on a styrofoam support column. The field probe is supported by a balsa wood structure and can be moved anywhere near the test antenna by the positioning servomechanism located above the chamber.

4.2 Experimental Models

4.2.1 Creation of a High Surface Impedance

At microwave frequencies the surface of a perfectly conducting body can be modified into a surface with an impedance different from zero either by coating the body with dielectric or ferrite materials, or by creating corrugations

59

in the metal surface (Rotman, 1951; Barlow and Cullen, 1953). In the former case
the impedance is generally complex. In the latter case the resistance is either
zero, for a perfectly conducting body, or very small, for a metal of finite con-
ductivity and can be neglected in comparison with the much larger reactive
part.

A non-perfect conductor has generally a small surface impedance given by

$$Z = (1+j) \frac{\omega \mu \delta}{2} \quad , \tag{4.1}$$

where δ is the skin depth, μ the permeability and ω the angular frequency. By
corrugating the metal surface with parallel-wall grooves a high surface reac-
tance can be created.

Each trench of a corrugated structure with parallel walls may be considered
as a uniform transmission line of length d (the depth of the groove) terminated
by a short (trench bottom). If the trenches are narrow enough, so that only a
TEM-mode propagates in them, the impedance as seen at the trench aperture
is

$$Z = j \eta \tan (kd) \quad , \tag{4.2}$$

where k is the propagation coefficient in free space and η is the free space
characteristic resistance. It is assumed that there are at least three corru-
gations per wavelength. The resistive component of the surface impedance
has been neglected as being very small compared to the reactive component.

Because of the finite thickness of the wall separating two adjacent slots, the
surface impedance of the corrugated structure is not uniform but varies from
zero, over the wall, to Z over the slot. A first order approximation is to con-
sider an average, uniform, surface impedance, i.e.

$$Z = j \frac{w}{s} \eta \tan (kd) \quad , \tag{4.3}$$

where w is the slot width and s is the center-to-center spacing of two adjacent
slots.

It is obvious that the surface impedance of a corrugated sheet is anisotropic. For Eq. (4. 2) to be valid it is necessary that the components of the magnetic and electric field along the surface be parallel and perpendicular to the corrugations, respectively. Thus in the case of a monopole, the surface reactance can be created by cutting concentric grooves in the ground plane. If in any cross section through the monopole axis the trench walls are parallel, these corrugations would still be considered having parallel walls. In the case of an infinite magnetic line source, which may represent a very long thin slot, the grooves should be parallel to the line source.

Using Eq. (4. 2) one may determine, for a given depth d, the range of frequencies over which Z is inductive or capacitive. To reduce the radiation along the ground plane it is desired that Z be capacitive. An inductive impedance may support a surface wave and therefore result in increased power flow along the ground plane. Thus, there is a pass-band for a surface wave for $0 < kd < \frac{\pi}{2}$, or $0 < d < \frac{\lambda}{4}$ (λ being the wavelength), a stop band for $\frac{\lambda}{4} < d < \frac{\lambda}{2}$ and so forth. A more accurate analysis shows that the stop band actually extends over a wider range of frequencies when $w \neq 0$. A brief outline of this analysis is given below.

A two-dimensional, periodic, corrugated surface is considered. A TM-mode is assumed above the corrugations. By using Floquet's theorem for periodic structures and considering an infinite number of space-harmonics above the surface in order to satisfy the non-uniform boundary condition one obtains a determinental equation from which the phase constants of the space harmonics can be determined. At the frequency where the cut-off of the first pass-band occurs this equation is simplified to the following form (Watkins, 1958)

$$\frac{1}{kd\tan(kd)} = \frac{2s}{\pi^2 d} \sum_n \frac{1}{|1+2n|} \cdot \frac{\sin\left[(1+2n)\frac{\pi w}{2s}\right]}{(1+2n)}, n=0, \pm 1, \pm 2, \ldots \quad (4.4)$$

This equation can be solved by graphical methods or by trial and error. For a desired cut-off frequency the propagation coefficient k is specified and then there are three parameters (d, w, s) to be chosen to satisfy Eq. (4. 4). The most

critical parameter is d. As a starting point for a trial and error solution d may be chosen slightly less than $\lambda_0/4$ where λ_0 is the free space wavelength at the desired cut-off frequency.

It is known that a greater surface impedance results in greater reduction of the radiation along the ground plane. Therefore, and in view of Eq. (4.3), it is desirable to make the ratio w/s as great as possible, the upper limit being one. Considering s as constant for the moment, it follows that the wall thickness t should become as small as possible. Here a limit is imposed by consideration of the metal properties and the construction method that will be used.

A consideration of the ω-β diagram for the corrugated sheet (Watkins, 1958) shows that the larger the ratio s/d, the more the cut-off frequency deviates from the value for which $d = \dfrac{\lambda_0}{4}$ causing the stop band to increase, which is desirable in broadband applications of the method. For this reason one would wish to make s and therefore w (since t is fixed) as great as possible. On the other hand w is constrained by an upper limit imposed by the conditions under which Eq. (4.4) was derived namely that the trenches are narrow enough so that only a TEM-mode propagates inside. In order to obtain reasonably accurate results from (4.4) and to avoid spurious harmonics one would have to limit w to approximately one-tenth of a wavelength. However, values of $w = \lambda/3$ have also been used with good agreement with (4.4). (See Ch. V, Section 5.3.1.)

4.2.2 Antenna Models

Following the above outlined procedure, sets of circumferential corrugations have been designed and built for use with a monopole antenna. Each set of circumferential corrugations had an opening at the center where a monopole with a small metal disk or some other antenna could be mounted. Then the whole structure with the antenna at the center surrounded by the corrugated zone forming a reactance annulus was either mounted in the 12' square ground plane or used alone in a free space environment. Two sets of parallel wall circumferential corrugations have been designed for operation at S-band (2.7 to 4.0 GHz) and X-band (8.2 to 12.4 GHz).

The monopoles used at X-band were one quarter of a wavelength long and they were cut from copper wire. Irises of different diameters were used at the monopole base to improve the matching to the coaxial line feeding the monopole. However, a poor repeatability was detected in some measurements due to the strict mechanical tolerances required at X-band. Therefore, these results are not shown here.

Three cylindrical monopoles were used at S-band. Two of these were one quarter of a wavelength long (at 3.07 GHz) and they were machined from brass. The third was a short monopole and was cut from copper wire. The dimensions of these monopoles are shown in Table IV-1.

TABLE IV-1: DIMENSIONS OF MONOPOLES

Monopole	Height, h	Diameter, d	h/d
A	2.44 cm (.960 in)	0.11 cm (.045 in)	21.3
B	2.44 cm (.960 in)	0.16 cm (.062 in)	15.5
C	0.81 cm (.320 in)	0.08 cm (.032 in)	10.0

The monopole mount that was used consisted of a type-N connector attached to a tapered coaxial section acting as an impedance transformer. The input and output characteristic impedances of this mount are 51 Ω and 55 Ω respectively, calculated from

$$Z_o = \frac{1}{2\pi} \sqrt{\frac{\mu}{\epsilon}} \ \ln \left(\frac{r_o}{r_i} \right) ,$$

(4.5)

where r_i and r_o are the inner and outer radii of the coaxial line respectively. The dimensions of this mount are shown in Fig. 4-1. Monopoles A and C were used with this mount as transmitting antennas. Monopoles B and C were used with a slightly different mount as receiving antennas in the coupling measurements.

The mount was terminated to a small flat disk which would be mounted at the center of a set of circumferentual corrugations. The corrugations, designed for operation at S-band (hereafter referred to as corrugations S) had the following dimensions

d = 2.41 cm (.950 in),
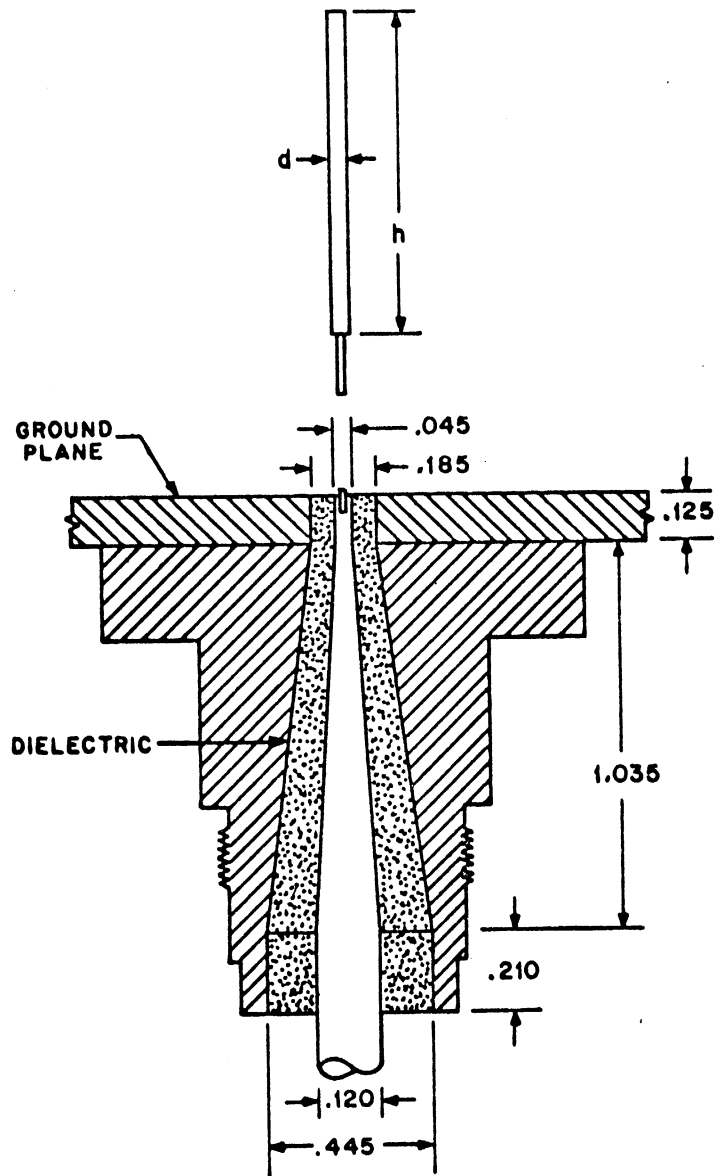w = .81 cm (.320 in),
s = .89 cm (.350 in) .

FIG. 4-1: MONOPOLE MOUNT (Dim. in Inches).

When the monopole with the small disk was mounted at the center, the corrugated area extended from an inner radius of 5. 73 cm out to a radius of 16. 32 creating an annulus extending radially for 1. 2 λ at 3. 4 GHz. The corrugations were milled in a solid piece of brass. They are shown in Fig. 5-10 with a broadband S-band slot mounted at the center instead of the monopole.

Using Eq. (4. 4) which is strictly applicable only to infinite extent corrugated surfaces one finds that for corrugations with the above dimensions the cut-off frequency for the first pass band is 2. 74 GHz and for the second pass bend 8. 31 GHz. Thus the corrugations should reduce the antenna radiation along the ground plane at both S- and X-bands.

4. 3 Impedance Measurements

The monopole standing wave ratio and input impedance were measured with the antenna mounted in the 12' square aluminum ground plane facing the anechoic chamber. Two sets of readings were taken, one with a flat ground plane to establish a reference, and one with the corrugated disk surrounding the monopole. In the latter case the tips of the corrugations were flush with the rest of the ground plane.

In the experimental set-up a coaxial slotted line having a residual standing wave ratio less than 1. 06 was connected directly to the antenna. A broadband crystal detector was used and the signal amplitude read on a standing-wave-ratio meter. The frequency was read on a resonant cavity frequency meter with error less than 0. 1 percent. For the impedance measurements a thumbtack short was placed at the termination of the coaxial line at the ground plane, re-placing the monopole. A standing-wave-ratio of at least 30 dB was then observed.

The variation of the standing wave ratio of monopole A is shown in Fig. 4-2. The two cases, with and without the corrugations, are presented in the same figure for comparison. Rectangular plots of the resistive and reactive parts of the input impedance constructed by reading off values from the Smith chart are shown in Figs. 4-3 and 4-4.
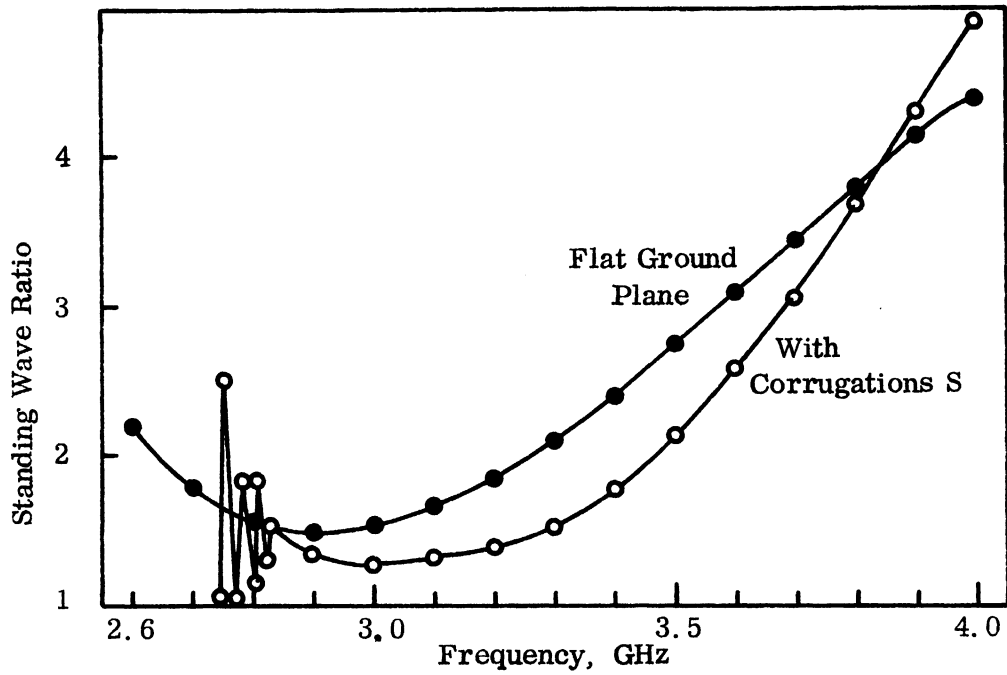
FIG. 4-2: STANDING WAVE RATIO FOR CYLINDRICAL MONOPOLE
FED BY 55 Ω COAXIAL LINE (h=2. 44 cm, d=0. 11 cm).
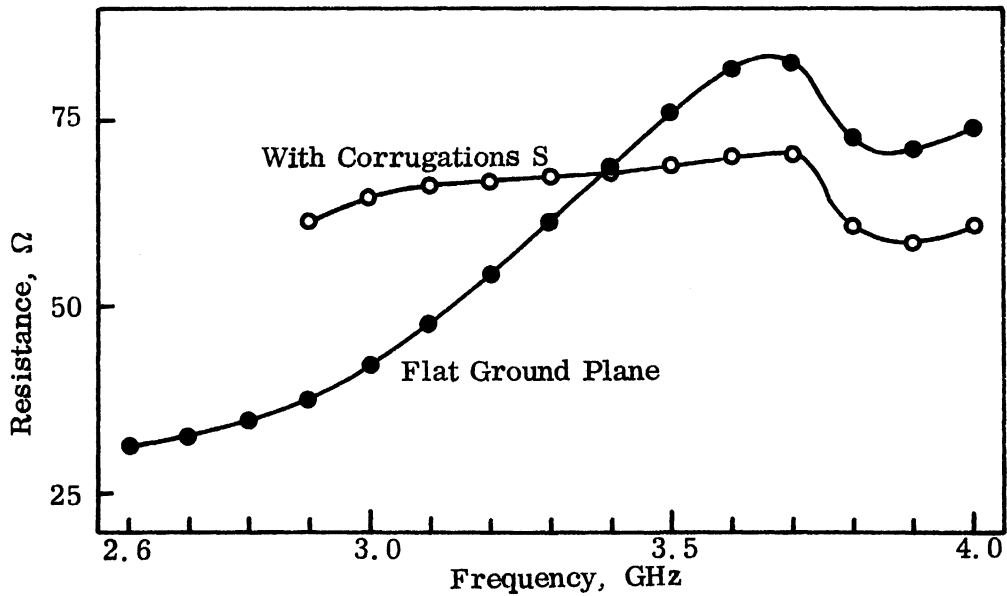

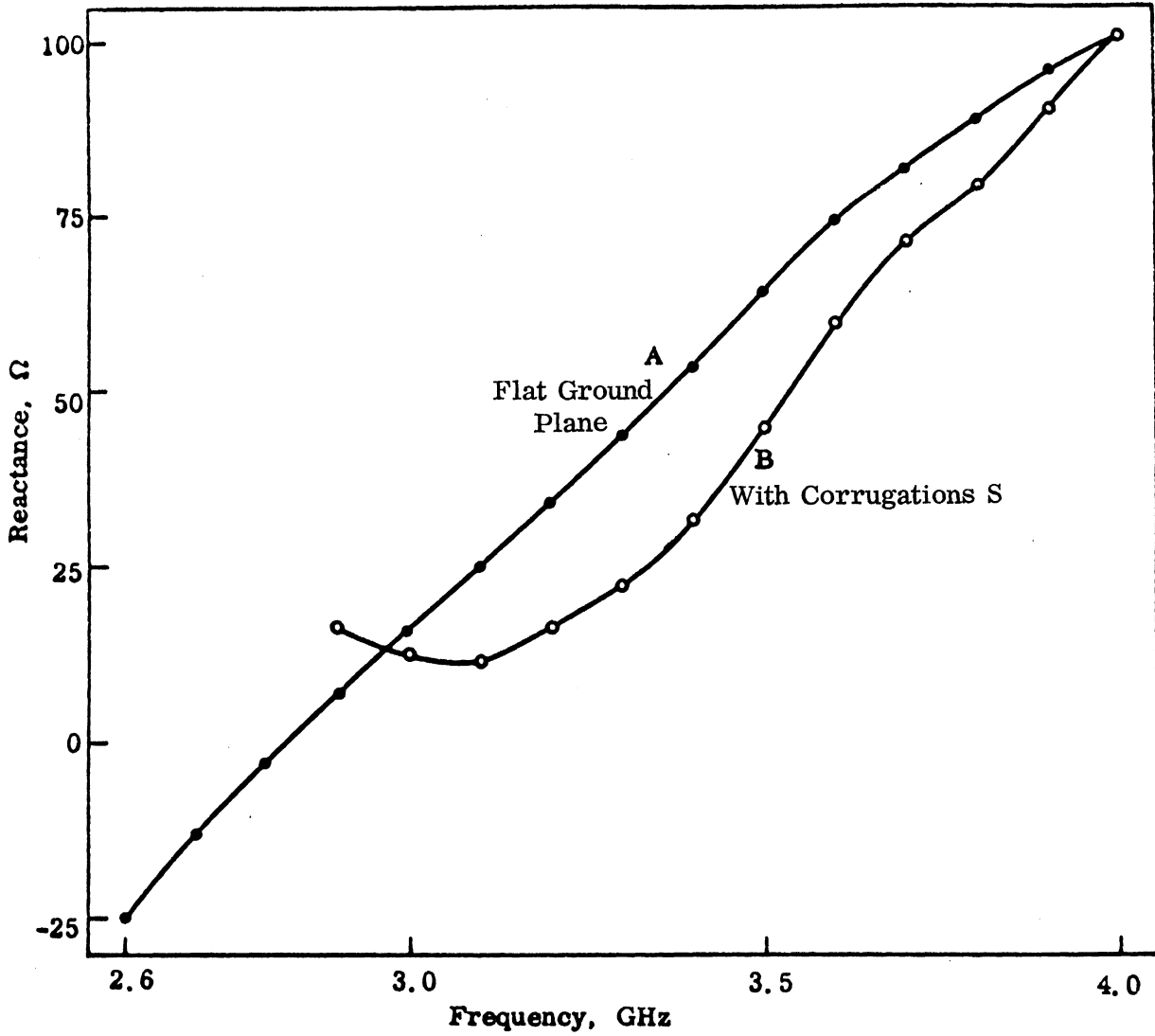FIG. 4-3: INPUT RESISTANCE OF CYLINDRICAL MONOPOLE
(h=2. 44 cm, d= 0.11 cm).

FIG. 4-4:INPUT REACTANCE OF CYLINDRICAL MONOPOLE
(h= 2. 44 cm, d=0. 11 cm).

These measurements show that in the presence of the capacitive impedance annulus the input resistance of the antenna remains nearly constant over a considerable frequency range, thus permitting a better matching to the transmission line. The antenna input reactance, however, follows the same general trend as when a flat ground plane is used. In conclusion, the presence of the corrugations has a beneficial rather than adverse effect on the monopole input impedance. This is in direct contrast to the case where the capacitive surface extends all the way to the monopole base when the monopole input resistance becomes very small (see Ch. II, Fig. 2-6).

4. 4 Near Field Measurements

The near field of the monopole in the presence of the capacitive surface reactance was measured in the smaller anechoic chamber described earlier. An unbalanced, shielded loop probe was used for measurement of the magnetic field near the surface of the ground plane. The probe was made of semi-rigid coaxial line with an outer diameter of 0. 9 mm. The inner diameter of the loop was 1. 5 mm which is equal to 0. 015 λ at 3 GHz. The outer conductor had a very thin gap of approximately 0. 2 mm to expose the inner conductor. A tiny drop of epoxy resin applied to the region of the gap served to electrically insulate the probe from the surface and to strengthen the loop (Knott, 1965).

Whiteside (1962) shows that such a loop measures magnetic fields accurately when its diameter is very small compared to a wavelength, as in the present case. The output voltage of the probe is a measure of the average magnetic field through the loop. The signal from the loop was fed into a wide range receiver where it was amplified and then read on a standing wave meter. The system was checked for square-law response with the help of a precision attenuator set.

In all the near field measurements reported here, the probe was parallel to the monopole. In this case a source of error is the disturbance of the original field distribution due to the presence of the probe when the probe is very close to the monopole. Another source of error is the sensitivity of the probe to electric fields . The electric sensitivity of the probe can be determined by

rotating the probe about its axis and noting the change in the output signal strength. The probe that was used exhibited a signal variation upon rotation of 0.2 dB. A practical way to test the overall system accuracy is to measure the magnetic field in a case where the exact field distribution is known and then compare theory and experiment. To obtain such a comparison, monopole A was mounted at the center of a 3' x 2' aluminum ground plane. It was assumed that the field distribution near the monopole and far from the edges of the ground plane was essentially the same with that which would be observed if the ground plane were of infinite extent. The exact magnetic field in the latter case is

$$H_\phi = \frac{j\,I_m}{4\pi r} \left(e^{-jkR_1} + e^{-jkR_2} - 2\cos(kh)e^{-jkR} \right) \tag{4.6}$$

where I_m is the maximum current along the monopole and the other symbols are as defined in Chapter III. The magnetic field was measured near the ground plane at 3.0, 3.2, 3.6 and 4.0 GHz with the probe moving along the longest axis of the ground plane at a distance of 0.3" to 9" from the monopole. Then the experimental data were compared with the theoretical data derived from Eq. (4.6). The agreement was excellent for spacings greater than 1.5" but significant differences (up to 0.75 dB) appeared at closer spacings. The differences between theoretical and experimental values that were observed at close spacings with a flat ground plane, were tabulated for the above four frequencies and used as correction constants in the subsequent measurements.

Next, a zone of the ground plane in the form of an annulus was replaced by the set of corrugations S and the surface magnetic field was measured at the same four frequencies. The results are shown in Fig. 4-5 after the near field correction. The theoretically derived magnetic field in the case of a perfectly conducting, infinite ground plane is shown superimposed for comparison. The two curves on each plot, whose overall levels are arbitrary, were positioned with respect to each other on the basis of a near field coupling measurement, at a spacing of 9.0", which is described in detail in Section 4.6. The two arrows along the axis of abscissas in Fig. 4-5 indicate the extent of the
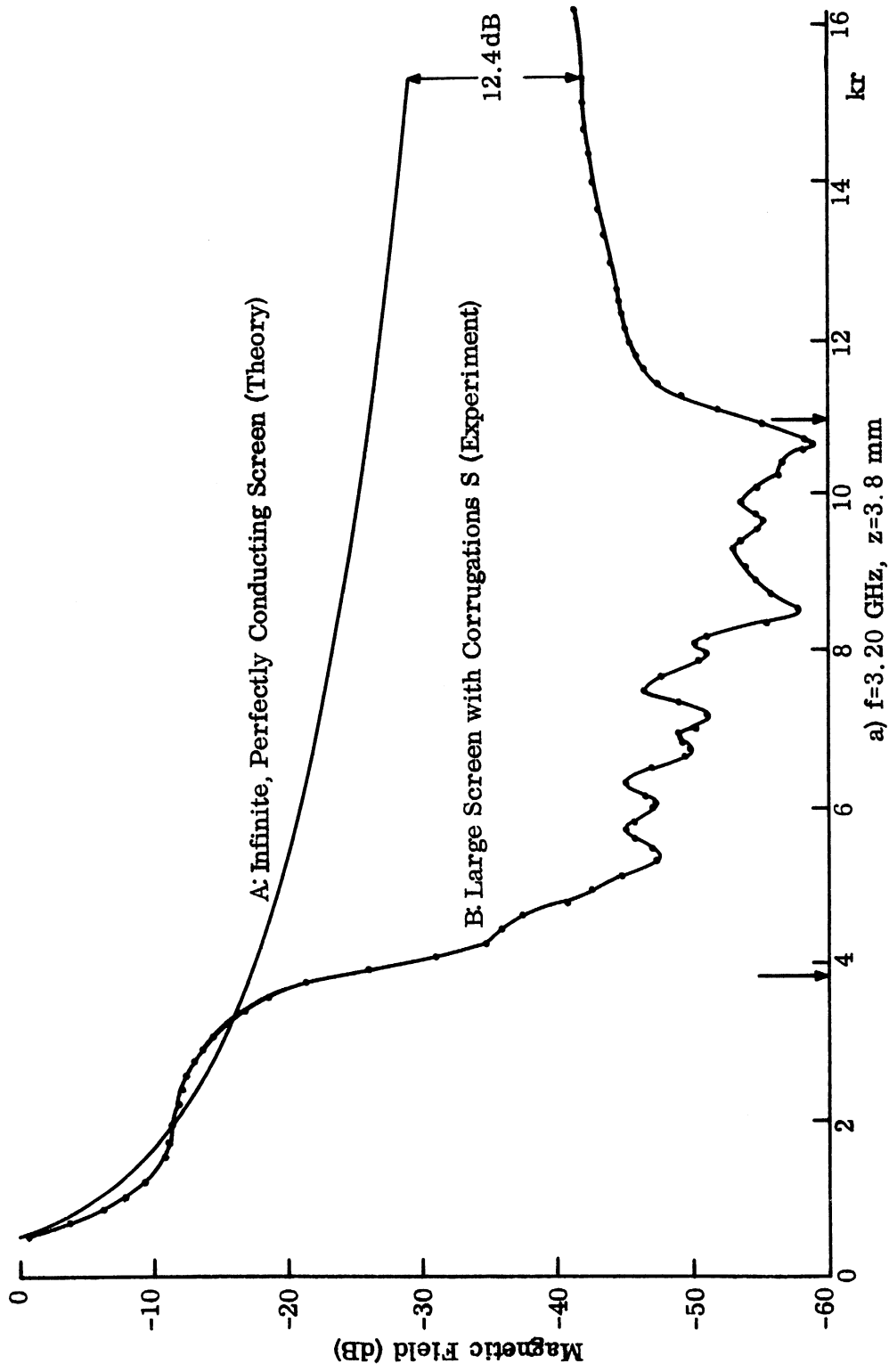
FIG. 4-5: MAGNETIC FIELD OF MONOPOLE OVER SCREEN WITH CAPACITIVE REACTANCE ANNULUS.

a) f=3.20 GHz, z=3.8 mm

A: Infinite, Perfectly Conducting Screen (Theory)
B: Large Screen with Corrugations S (Experiment)
C: Infinite Screen with Capacitive Reactance Annulus. X=-3.58 (Theory)
D: Infinite Screen with Capacitive Reactance Annulus. X= -2.5 (Theory)

b) f = 3.60 GHz, z = 3.3 mm.

FIG. 4-5: Continued

72

A: Infinite, Perfectly Conducting Screen (Theory).
B: Large Screen with Corrugations S (Experiment).
C: Infinite Screen with Capacitive Reactance Annulus. X=-1.89 (Theory).

c) f = 4.0 GHz, z = 3.0 mm

FIG. 4-5: Concluded

corrugated area. Parameter z indicates the height of the magnetic field probe center above the ground plane. The different probe heights shown were chosen so that they would correspond to the same fraction of the free space wavelength at every frequency ($.04 \lambda_0$). The theoretically obtained magnetic field above the reactively loaded area of the ground plane is shown at two frequencies for comparison.

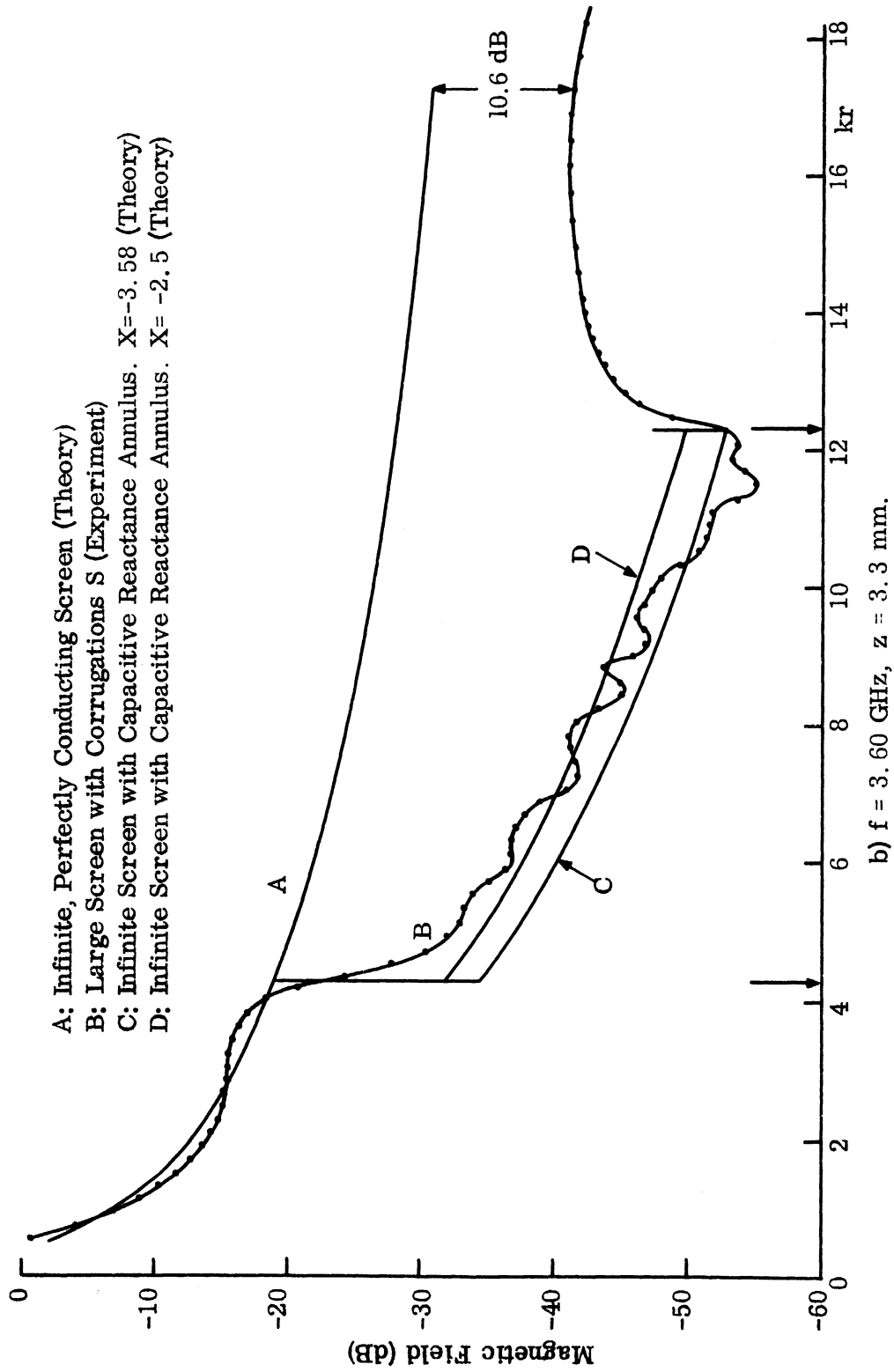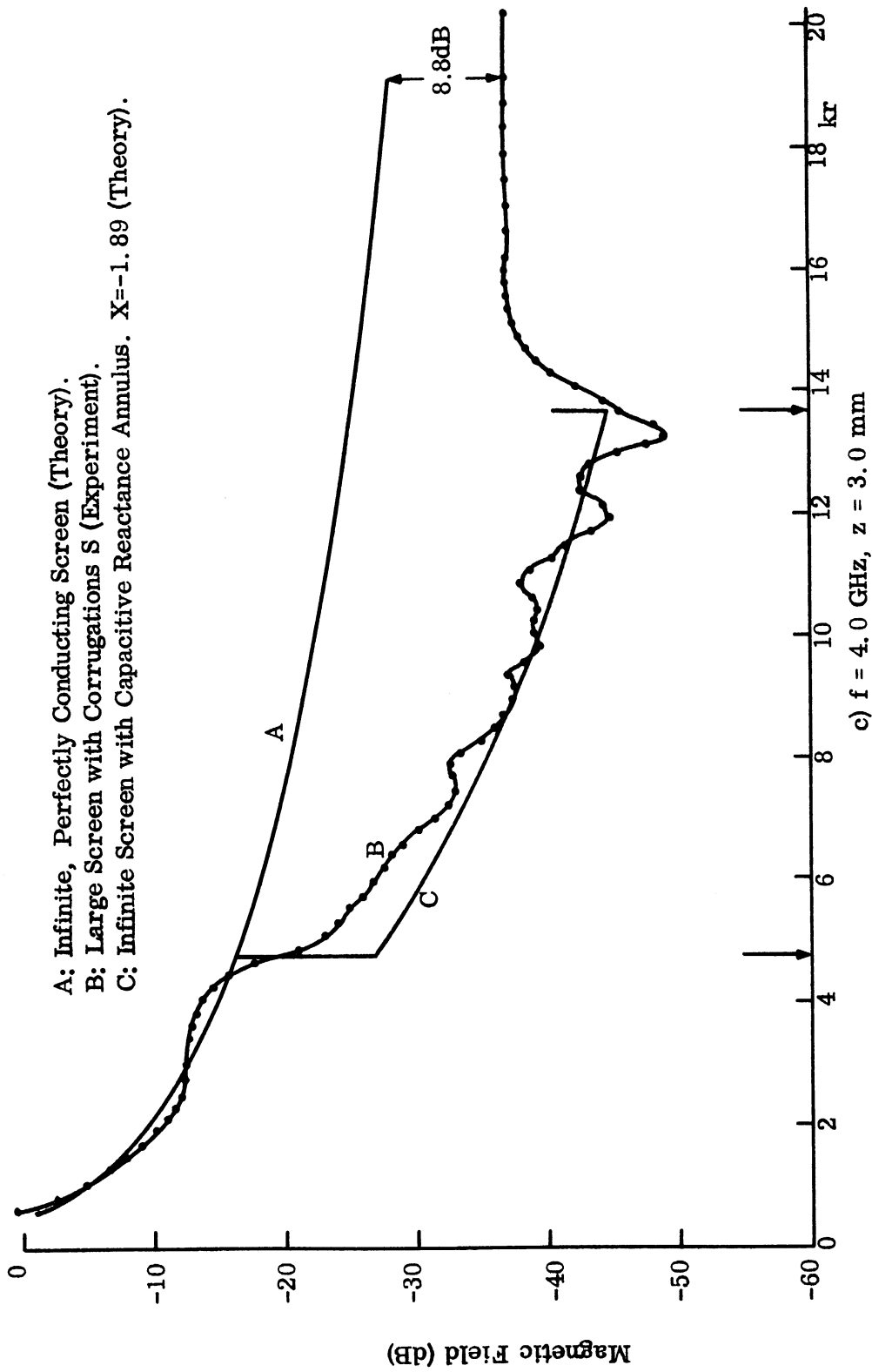The many undulations present in the experimental curves are caused by the non-uniform surface of the physical model. The field is stronger above the wall separating two trenches and weaker over the trench. This effect is more pronounced at the lower frequencies, near the surface wave cut-off frequency. By increasing the probe elevation slightly one may obtain a smooth curve as shown in Fig. 4-6. When this is done, however, the overall level of the measured surface field is a little higher, as shown. That is the reason why the theoretically obtained surface field for X = -3.58 (see Fig. 4-5b) appears lower than the measured field. Using a different value for the surface reactance (X= -2.5) the theoretically obtained surface field appears to agree better with the experiment. However, the resulting radiation field pattern (using X= -2.5) is slightly farther away from the measured pattern than the pattern obtained using X= -3.58 which is the value obtained from Eq. (4.3).

The surface field distributions shown in Fig. 4-6 were obtained with the ground plane terminated at the end of the corrugated area. A comparison of Fig. 4-6 with Fig. 4-5c, shows that the surface field above the corrugations may be considered to a first order approximation as independent of the existence of a ground plane beyond the corrugations. The reason is that the reflected waves arising from the discontinuity at the end of the corrugations are quickly attenuated traveling over a high capacitive reactance.

4.5 Radiation Field Patterns

The radiation field patterns of the monopole mounted on the 12' square ground plane were measured using a pyramidal log-periodic antenna with a gain of 7 to 9 dB as receiving antenna. The receiving antenna was rotated in the polar
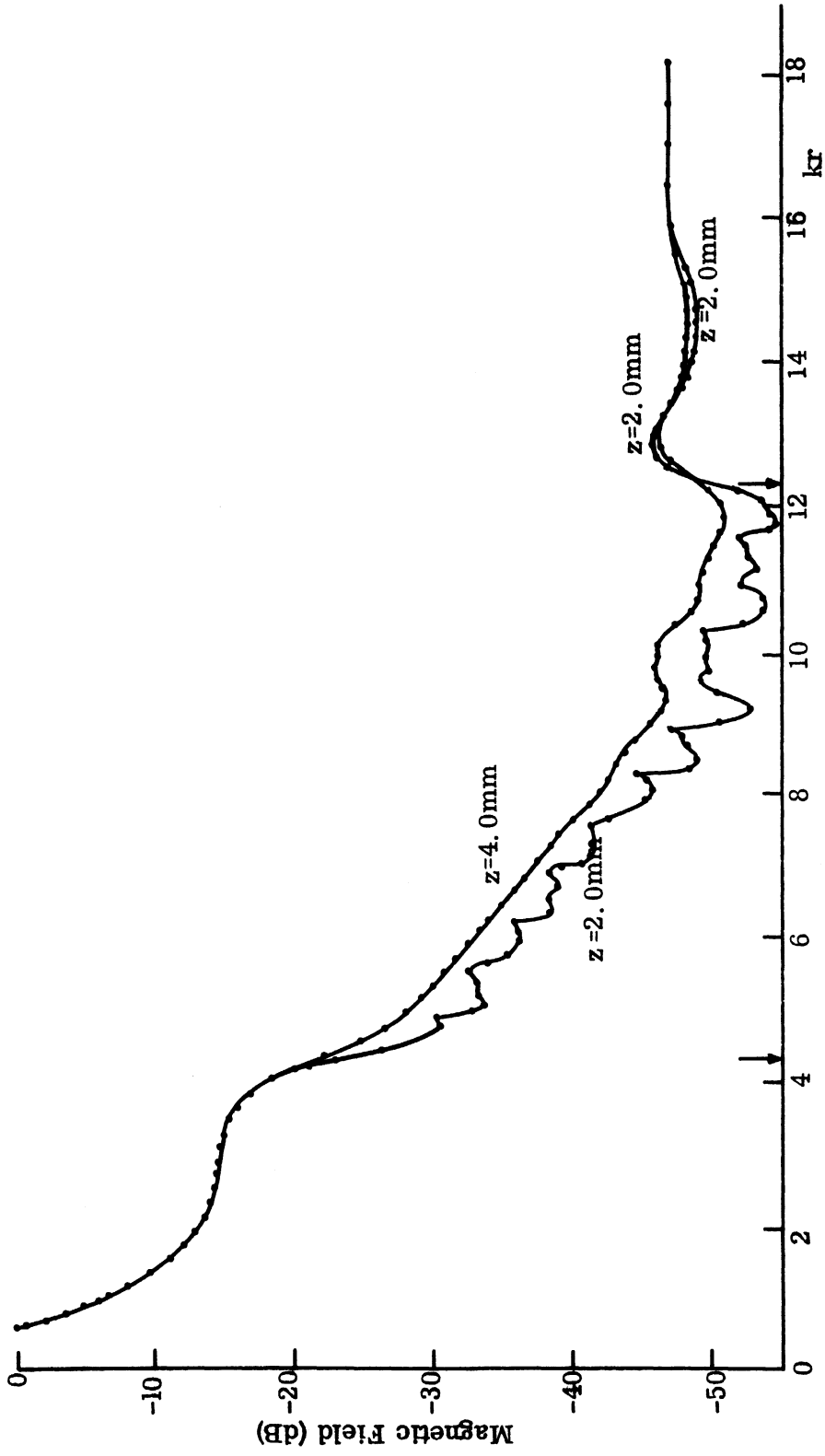
FIG. 4-6: MEASURED MAGNETIC FIELD OF MONOPOLE OVER CIRCULAR SCREEN WITH CORRUGATIONS S AT 3. 60 GHz.

plane of the monopole with its apex at a radius of 1.83 m (18 λ_0 at 3 GHz). At the position closest to the ground plane the axis of the log-periodic array was at an angle of $\theta=86°$ from the monopole axis. The reactive loading was accomplished by using the corrugated disk S around the monopole with the tips of the corrugations flush with the surrounding ground plane. Three cases of reactive loading were considered. In the first, corrugations S were completely exposed; in the second, only the inner half of the corrugated area was exposed, the other half being covered by aluminum foil; in the third, only the outer half was exposed. A variety of radiation patterns was thus obtained providing suitable tests for the theory developed in Ch. III. A comparison of experiment and theory is provided in Fig. 4-7 where experimental results for the three different extents of reactive loading and two different frequencies are shown together with the theoretically derived far field patterns. In these figures the amplitude is normalized, with the maximum in the case of an infinite perfectly conducting ground plane taken as unity. The agreement between theory and experiment is better at 4.0 GHz than at 3.6 GHz. The main reason is believed to be that the mathematical model of a uniform surface reactance used in the theoretical derivation and Eq. (4.3) used to derive the equivalent surface reactance of the parallel wall corrugations represent better the physical model at frequencies further away from the surface wave cut-off frequency. Some comments on the numerical computations are given in Appendix A.

The monopole surrounded by the reactively loaded ground plane is still omnidirectional in the azimuth direction, however, the direction of the maximum shifts much closer to the monopole axis. For large absolute values of the surface reactance such as $X < -2.5$, the radiation pattern depends little upon the precise values of X and more on ka and kb which determine the position of the corrugations relative to the monopole. With the capacitive reactive loading the radiation along the ground plane is reduced and thereby the unwanted coupling to adjacent antennas is reduced. Also there is some increase in antenna gain and some control over the position of the maximum in the radiation pattern.

a) 4.0 GHz, ka=4.80, kb=9.24, X=-1.89
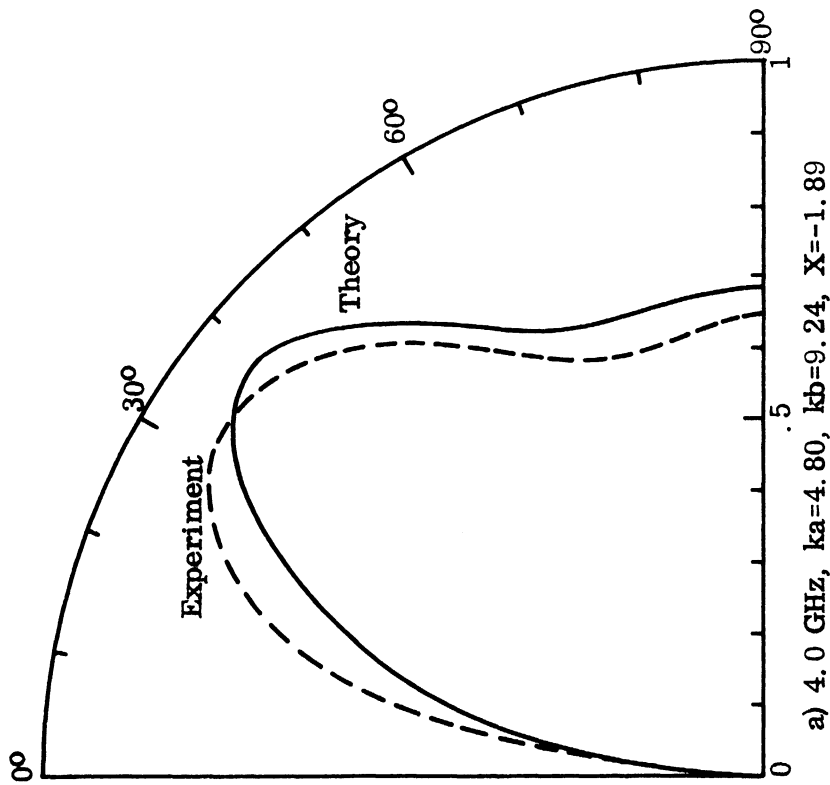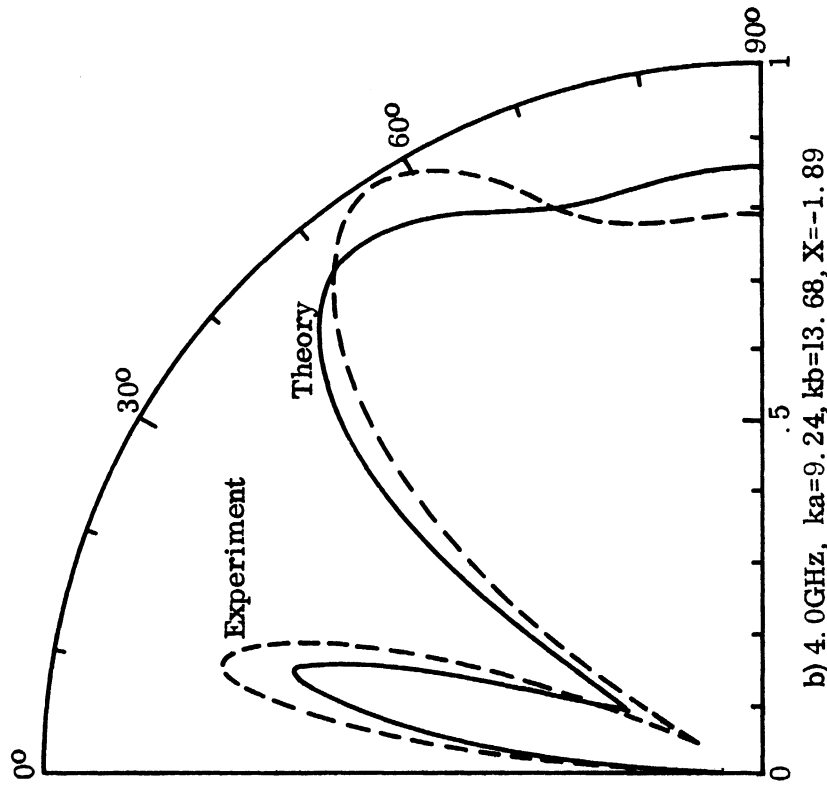
b) 4.0GHz, ka=9.24, kb=13.68, X=-1.89

FIG. 4-7: RADIATION FIELD PATTERNS OF A MONOPOLE OVER AN INFINITE SCREEN WITH ANNULUS OF CAPACITIVE SURFACE REACTANCE.

d) 3.6 GHz, ka=4.32, kb=12.31, X=-3.58.
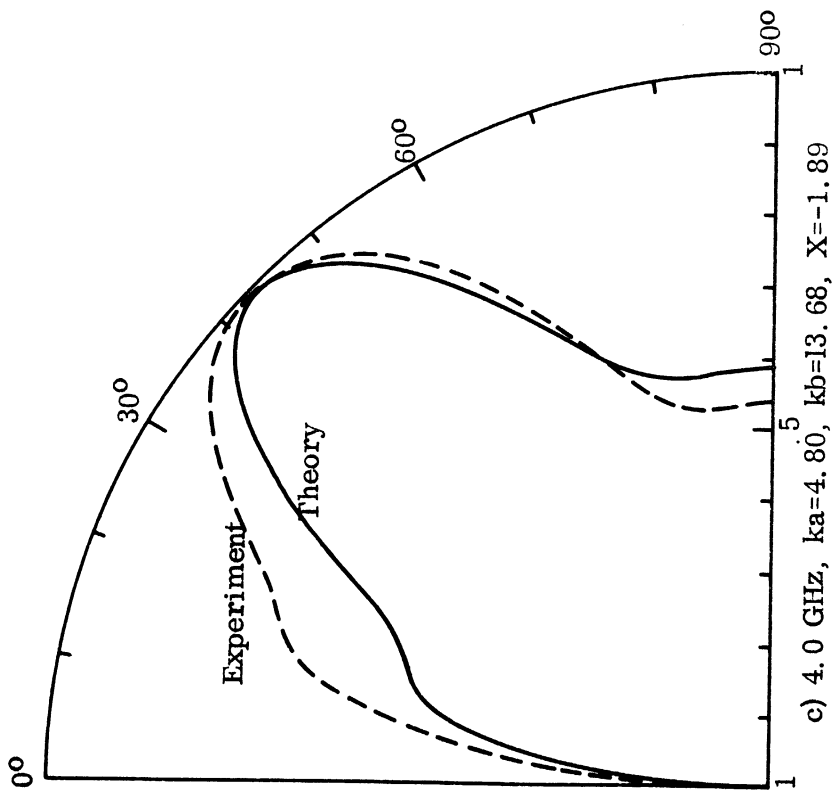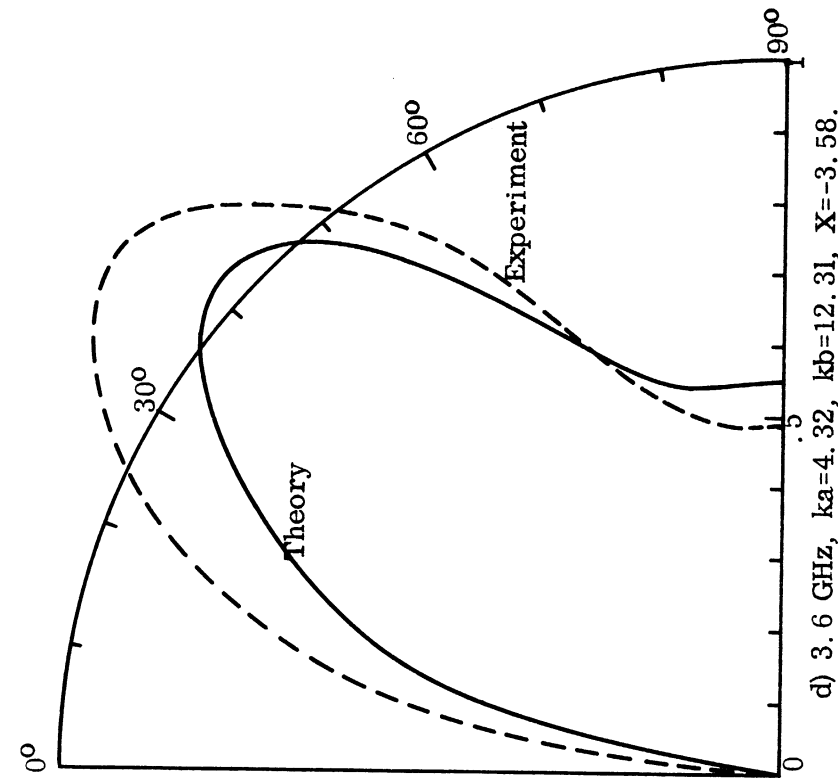
c) 4.0 GHz, ka=4.80, kb=13.68, X=-1.89

FIG. 4-7: Concluded.

The variation with frequency of the basic features of the radiation pattern i. e. position of maximum, half-power beamwidth and level at $\theta=90^\circ$ (along the ground plane) with respect to maximum level are summarized in Fig. 4-8. These data were obtained from several measured radiation patterns of monopole A with corrugations S in the 12' square ground plane. The half-power beamwidth of a quarter wavelength monopole over an infinite, perfectly conducting screen, is 39°.

When the monopole and corrugated dish were tested in a free space environment the level at $\theta=90^\circ$ was 6 dB below the level corresponding to an infinite ground plane as expected. The radiation behind the disk was very small in contrast to the case of a flat disk. The difference is illustrated in Fig. 4-9. In this figure curve A shows the radiation pattern of monopole A over a disk with radius 5.7 cm, equal to the inner radius of the corrugations S; curve B was measured after corrugations S were added.

4. 6 Mutual Coupling

The effect of the reactive loading of the ground plane on the near field coupling of two monopoles was measured using a swept frequency technique. Monopole A was surrounded by corrugations S and monopole B was placed at a distance of 22.8 cm (2.5 λ_0 at 3.3 GHz). The measured coupling with and without the corrugations is shown in Fig. 4-10. Since the power level at the transmitting antenna varies (within narrow limits) as the frequency is swept, a calibration curve representing the - 25 dB level is shown superimposed in Fig. 4-10. The spikes on the calibration curve are due to frequency markers. Since no matching devices were used, the coupling reduction shown in Fig. 4-10 is referenced to the transmission lines connected to the antennas. The reduction of the coupling between the two antennas differs from this figure by the amount of transmission loss or gain due to the different antenna SWR when the corrugations are present. The correction, amounting to no more than 0.5 dB, can be calculated on the basis of the information presented in Section 4.3.
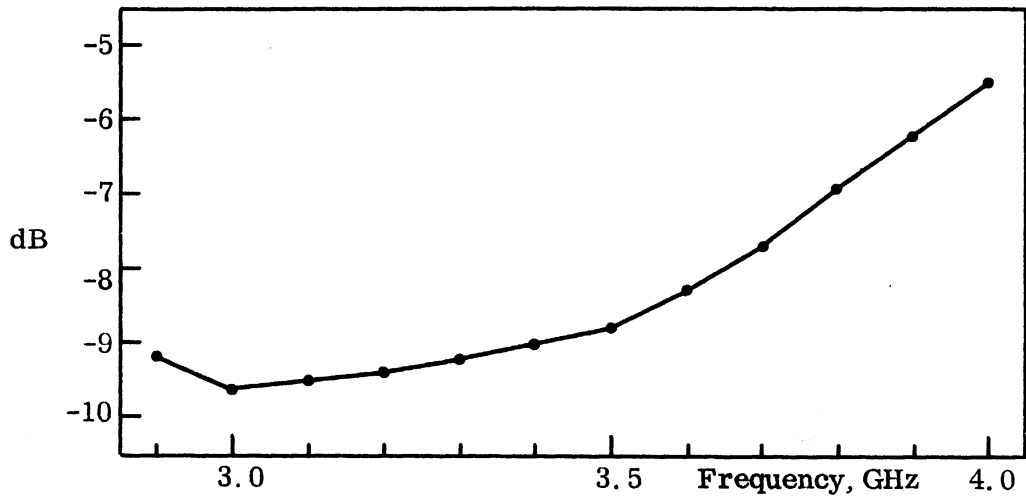
a) Level at 90° with Respect to Maximum.
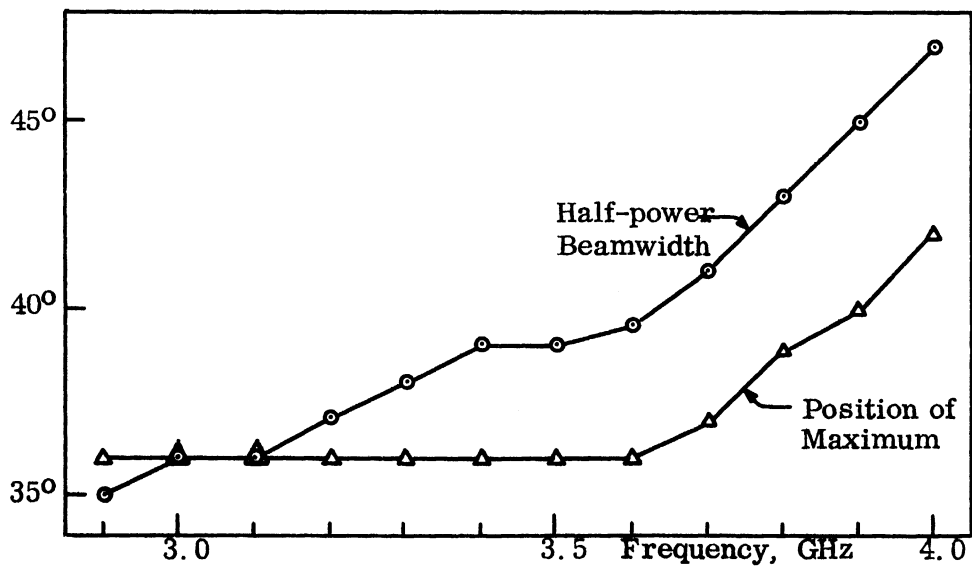
b) Half-power Beamwidth and Position of Maximum.

FIG. 4-8: MEASURED RADIATION PATTERN CHARACTERISTICS OF
MONOPOLE A WITH CORRUGATIONS S .
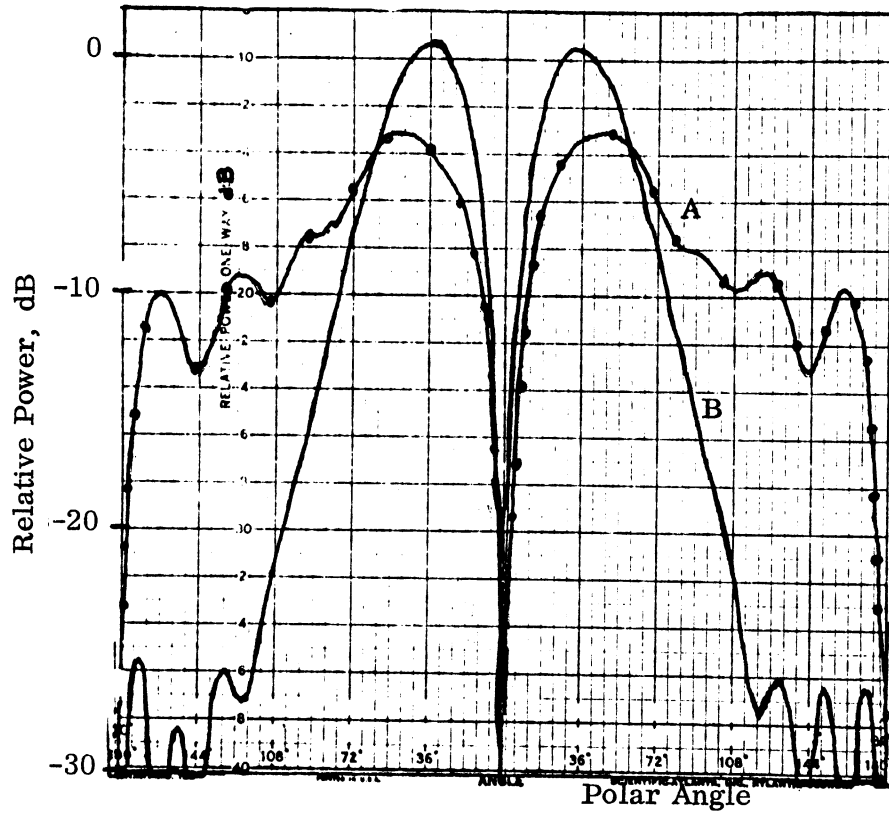
FIG. 4-9: MEASURED RADIATION PATTERNS OF MONOPOLE
A OVER A DISK.

-25 dB Level (Calibration)

Flat Ground Plane

With Corrugations

Coupling (dB)

Frequency (GHz)
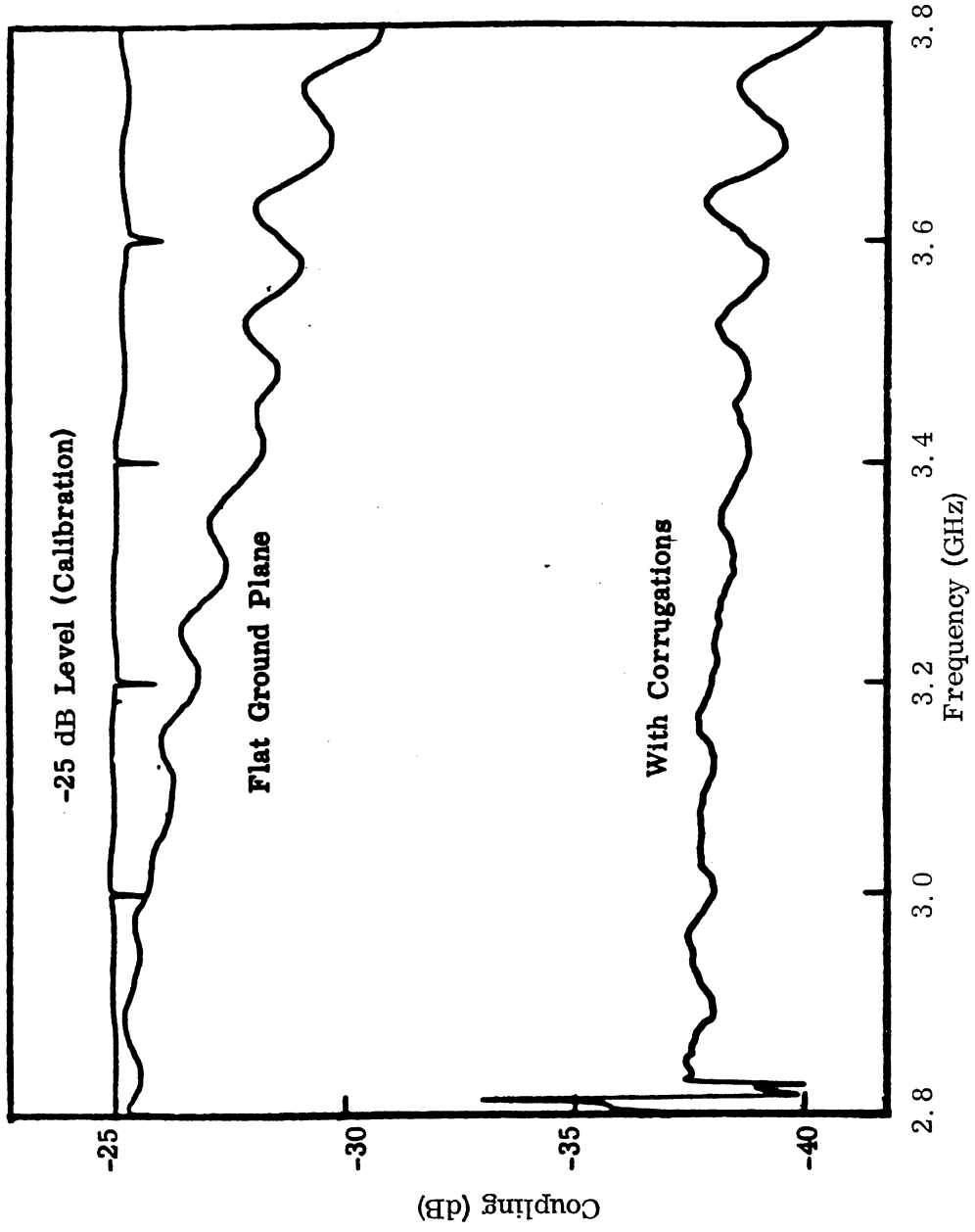
FIG. 4-10: COUPLING OF TWO MONOPOLES SPACED 22.8 CM.

The coupling was also measured for antenna spacings D of 68. 6 cm and 102. 1 cm. The amount of coupling reduction between the two antennas was calculated from these measurements. The results are presented graphically in Fig. 4-11. In the same figure the amount of sidelobe reduction obtained from the radiation patterns is presented for comparison. The coupling reduction is much greater in the near field than in the far field. In the case of a flat ground plane the monopole coupling showed far-field behavior, i. e. it followed Friis formula for monopole spacings greater than 2. 5 λ_o. When the corrugations are present the effective aperture of the antenna increases greatly so that far-field behavior is not observed even at an antenna spacing of 10 λ_o (102. 1 cm).

FIG. 4-11: MEASURED SIDELOBE AND COUPLING REDUCTION.
    A: Sidelobe reduction. Monopole A.
    B: Coupling reduction. Monopoles A and B. D=102.1 cm.
    C: Coupling reduction. Monopoles A and B. D=68.6 cm.
    D: Coupling reduction. Monopoles A and B. D=22.9 cm.
    E: Coupling reduction. Monopoles A and C D=22.9 cm.

V

RADIATION FROM MICROWAVE ANTENNAS WITH REACTIVE LOADING OF THE GROUND PLANE

5.1 Introduction

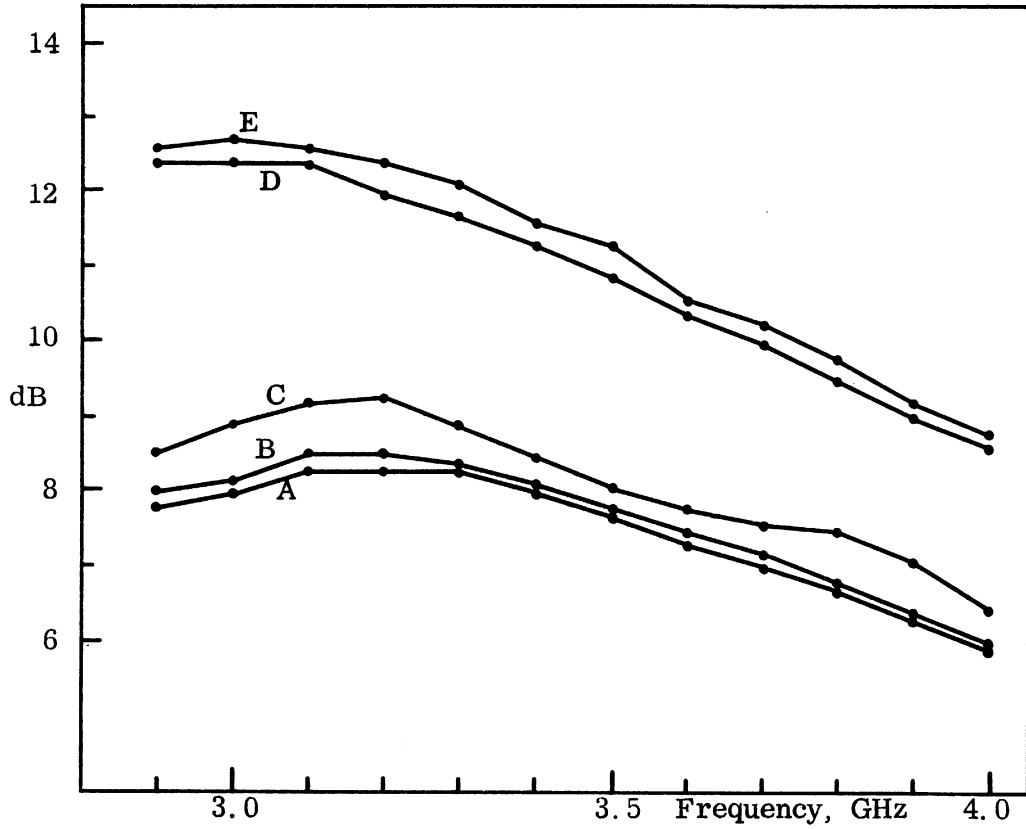This chapter contains the results of an experimental study on the effect of reactive loading of the ground plane on the radiation properties of different types of flush mounted microwave antennas. Some of the most common types of antennas used in aerospace vehicles were studied including the rectangular slot, the thin slot, the sectoral horns, the pyramidal horn and the Archimedean spiral. These antennas exhibit a wide variety of radiation patterns. Their gain along the ground plane varies from maximum (slot, E-plane) to very small (horns) to theoretically zero (spiral). The properties of these antennas that were investigated comprise radiation patterns, input impedance, voltage standing wave ratio and coupling between two similar, adjacent antennas. Both large and small ground planes were used in the measurements of radiation patterns. For all coupling and most impedance measurements the antennas were mounted on the 12 ft. square ground plane, near its center, facing the anechoic chamber. Different areas of the ground plane were modified by means of surface reactive loading, including the case of "isolated loading" as defined in Chapter I. The desired capacitive surface reactance was created by cutting corrugations in the form of circumferential trenches of appropriate dimensions (see Section 4.2.1). Corrugations with parallel and non-parallel walls were considered.

Different sets of corrugated disks were designed, constructed and used at S, X and Ku bands of frequencies. These corrugated disks were so designed that different antennas could be placed at the center of a disk while the disks themselves could be fastened on a larger metal ground plane with the corrugations flush with the surrounding flat surface.

5.2 Broadband Slot with Isolated Reactive Loading

5.2.1. Loading with a Single Trench

The type of antenna examined here is the open ended waveguide. Such slot antennas are often found flush mounted in close proximity. In such cases the

low directivity. that characterizes this type of antenna gives rise to a strong interference which is due to the main lobe of the radiation pattern and not just weak sidelobes.

The capacitive surface impedance on the ground plane was created by means of a single circumferential trench surrounding the aperture of the slot (Fig. 5-1). The small disk shown here could be mounted in the larger ground plane. This antenna was designed for operation at X-band, i. e. 8.2 to 12.4 GHz. As shown, the width of the trench was very small compared to both the depth and the free space wavelength so that higher order modes inside the trench would be quickly attenuated. The trench depth was equal to one quarter of a free space wavelength at 8.0 GHz. Two slot antennas of a transmitter-receiver system were similarly surrounded by trenches and mounted on the large ground plane, at a center-to-center spacing of 11.4 cm, so that their respective E-planes would be aligned. The coupling was measured and compared with that in the case of the two slots in the same geometry but without the trenches. It was observed that with the trenches the coupling was reduced by 9 dB at 8.2 GHz tapering to 4 dB at 10 GHz. In the case where only one of the two slots was surrounded by a trench it was found that the coupling reduction was not dependent upon whether the trench was around the transmitting or receiving antenna. In either case the coupling reduction was equal to half of that observed when both antennas were surrounded by trenches.

In order to examine the behavior of this type of reactive loading at lower frequencies, the trench depths of the transmitter and receiver were modified so that they would be equal to a quarter wavelength at 10.0 GHz and 9.2 GHz respectively. This was realized by the addition of two copper rings which were covered with silver paint. The dimensions of the trenches were then as follows:

depth $= d_t = 0.75$ cm (transmitting slot)

$d_r = 0.82$ cm (receiving slot)
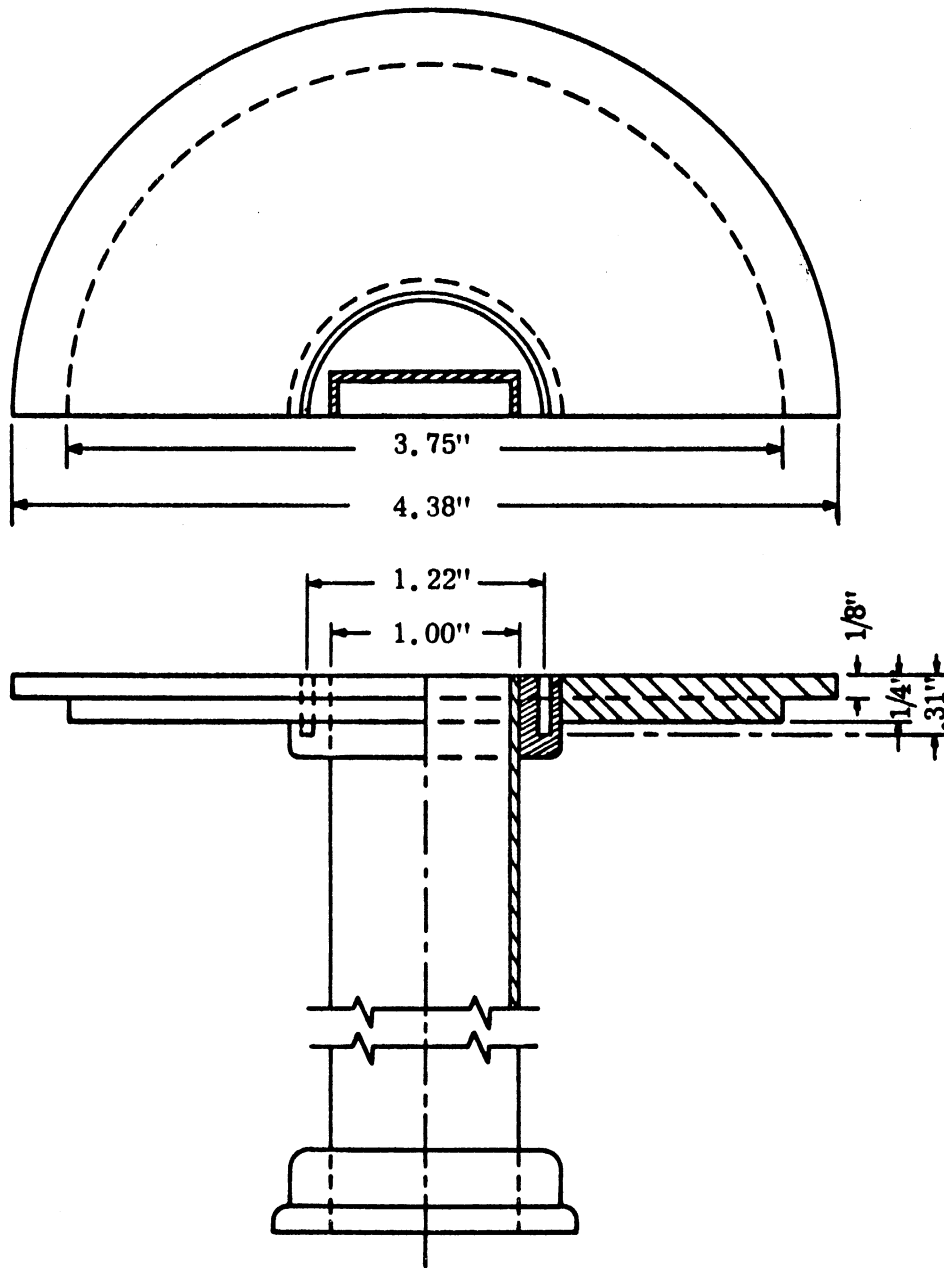
width $= w = 0.16$ cm $(1/16$ in.$)$.

FIG. 5-1: SLOT ANTENNA WITH CIRCUMFERENTIAL
TRENCH.

The E-plane coupling versus frequency for this case is shown in Fig. 5-2. In the same figure the coupling of two slots without a surrounding trench is given as a reference. Also the coupling reduction when only the transmitting slot is surrounded by a trench (depth 0.75 cm) is given. In this case the trench depth is equal to one quarter of the free space wavelength at 10.0 GHz. The coupling reduction then is greatest at 9.4 GHz where the depth is equal to 0.235λ.

Two antenna apertures may occur in any number of different positions with respect to each other. The level of coupling varies greatly depending upon antenna orientation even though the center-to-center distance of the two apertures is constant (Lyon et al, 1966). The coupling variation can be measured by leaving one antenna in a fixed position and rotating the other about its axis. The two most representative geometries are shown in Fig. 5-3. Here the term "E-plane coupling" means that the respective positions of the two antennas are such that the center of the rotating antenna is in the E-plane of the stationary antenna. A similar definition holds for the H-plane coupling.

Patterns of coupling variation with one antenna in a fixed position and the other rotating were measured for the two slots surrounded by trenches and are presented in Fig. 5-4. In the same figure the corresponding coupling variation without the surrounding trenches is shown for comparison. As shown, the amount of coupling reduction in the E-plane coupling is practically constant, i. e. independent of the relative orientation of one slot with respect to the other.

The coupling increase or decrease shown in Fig. 5-2 is due to corresponding changes in the antenna radiation patterns. Such patterns were measured at several frequencies and two representative patterns are shown in Figs. 5-5 and 5-6. The trench with d=0.75 cm was used for these patterns. The two frequencies shown were selected so that one corresponds to $d < \lambda_0/4$ and the other to $d \geq \lambda_0/4$. The corresponding patterns for a slot in a flat ground plane are shown for gain comparison.
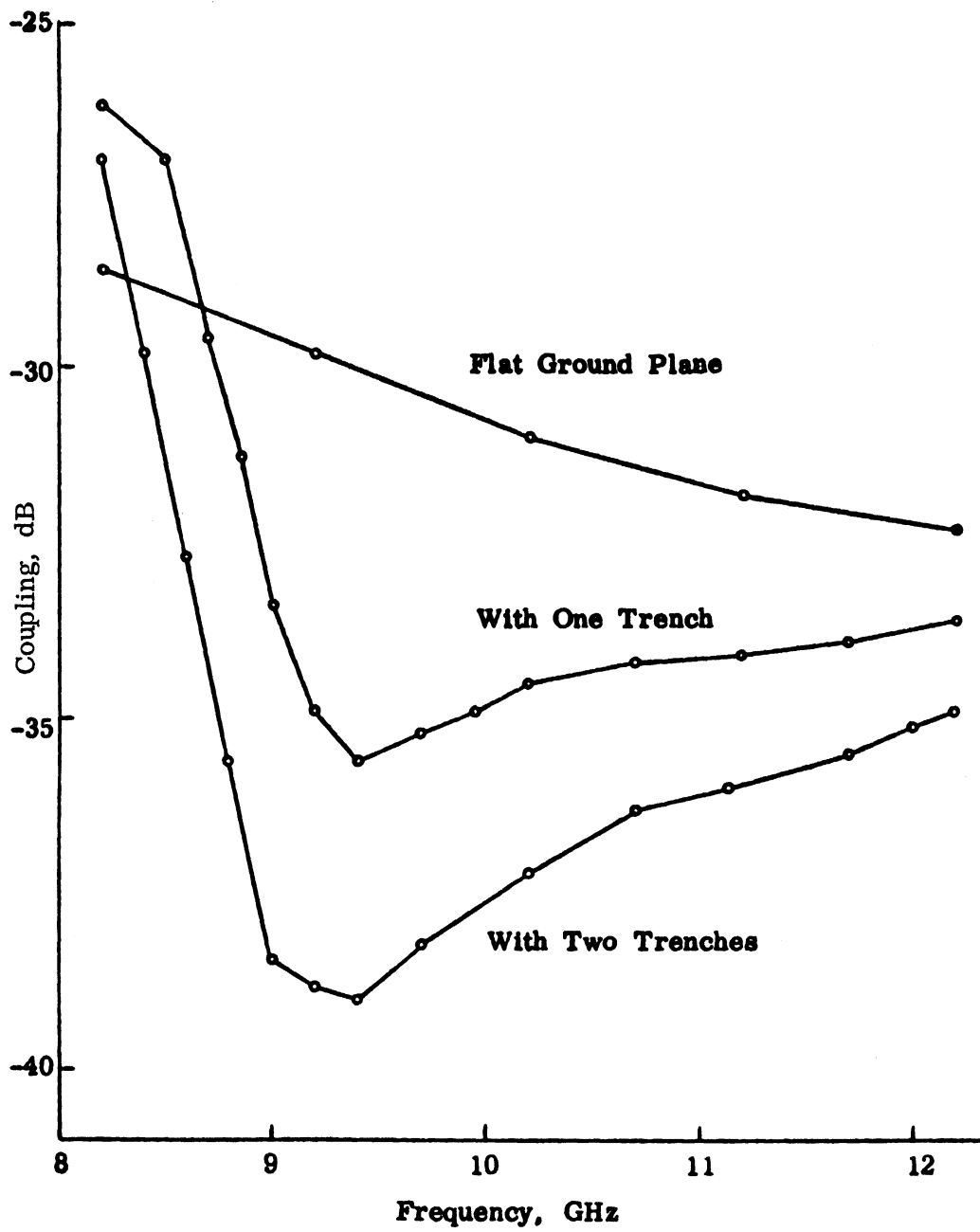
FIG. 5-2: E-PLANE COUPLING OF TWO SLOTS SPACED 11.4 CM.
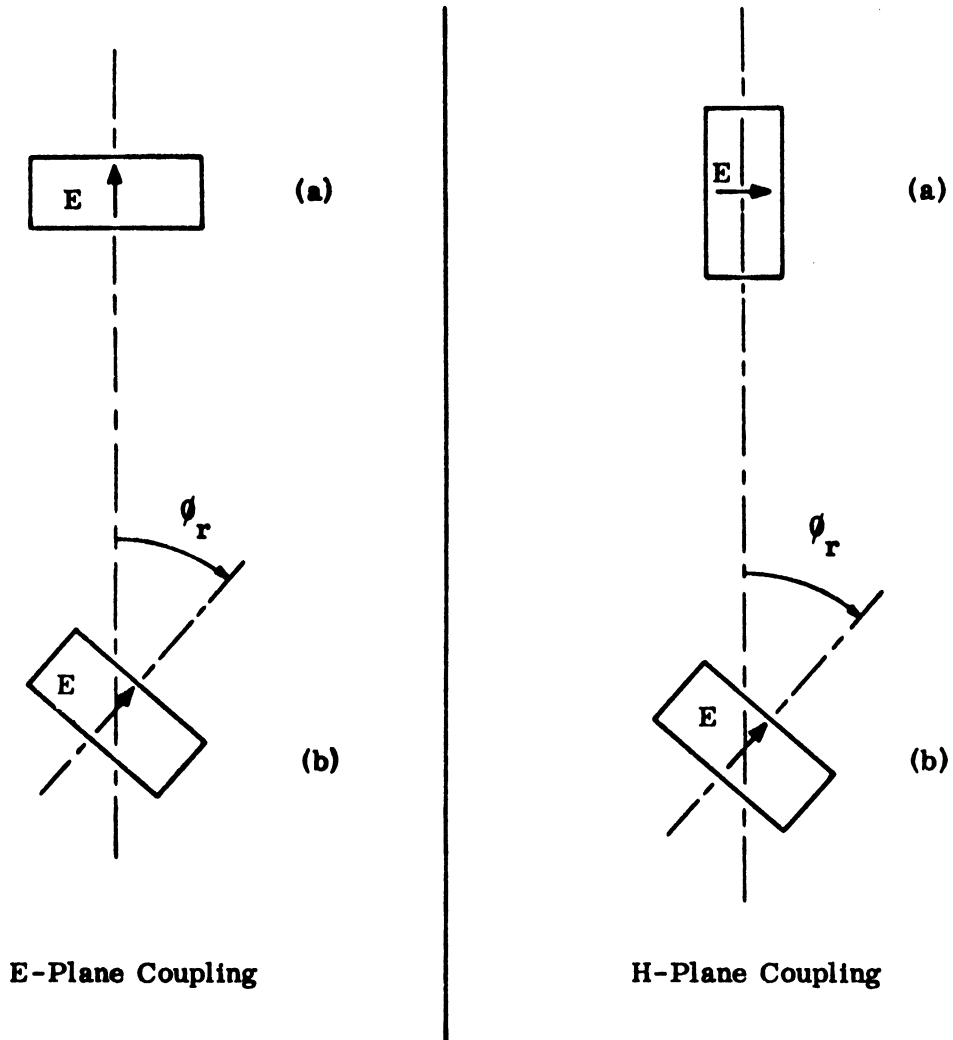
FIG. 5-3: GEOMETRY OF TWO SLOT ANTENNAS SHOWING E- AND H-
PLANE COUPLING. (a) TRANSMITTER-FIXED POSITION
(b) RECEIVER-ROTATABLE.
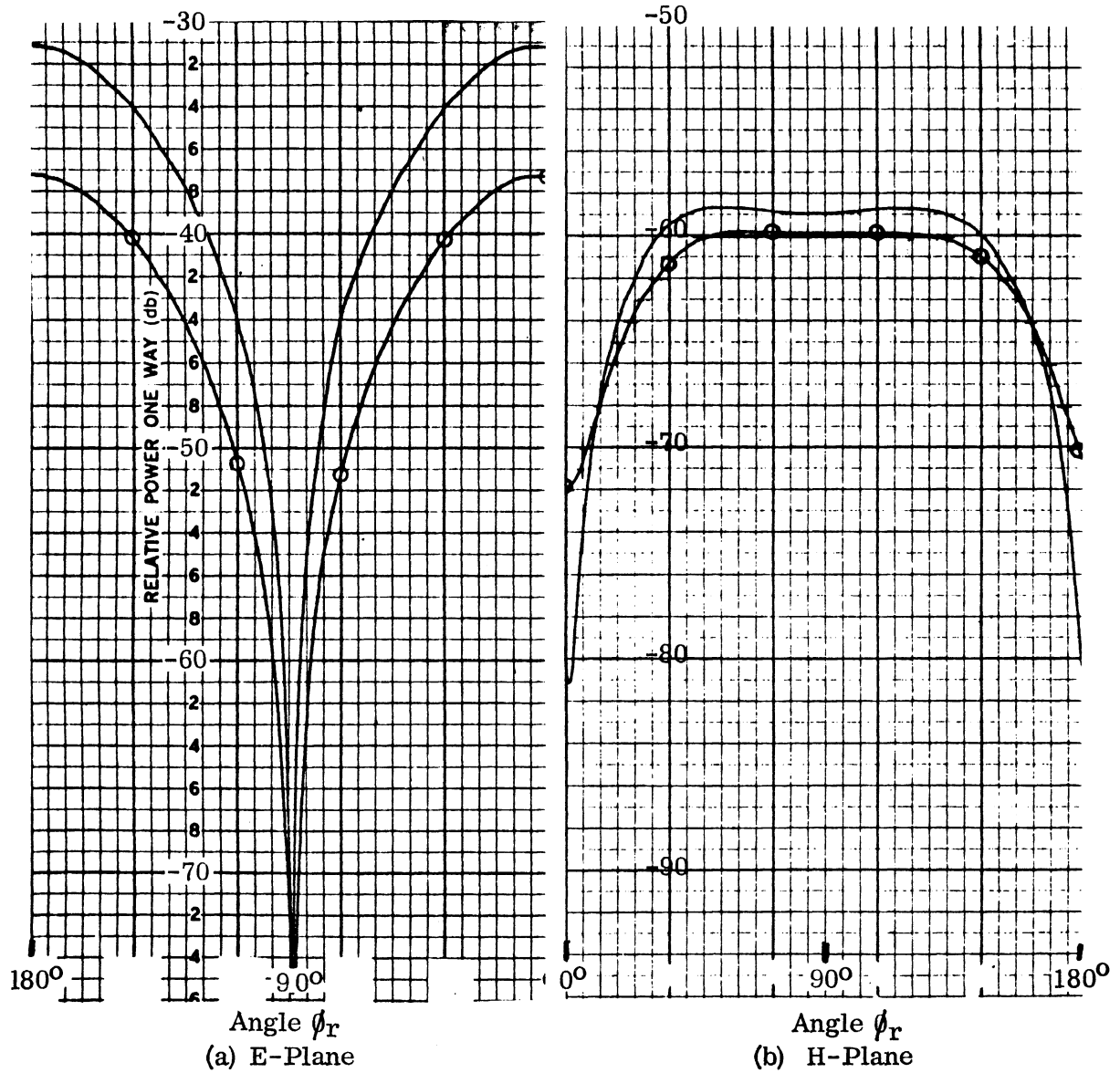
FIG. 5-4: COUPLING PATTERNS FOR TWO SLOTS ON A COMMON GROUND
PLANE SPACED 11.4 CM, 10.030 GHz. (—)Flat Ground Plane,
(—o—) Slots Surrounded by Trenches.
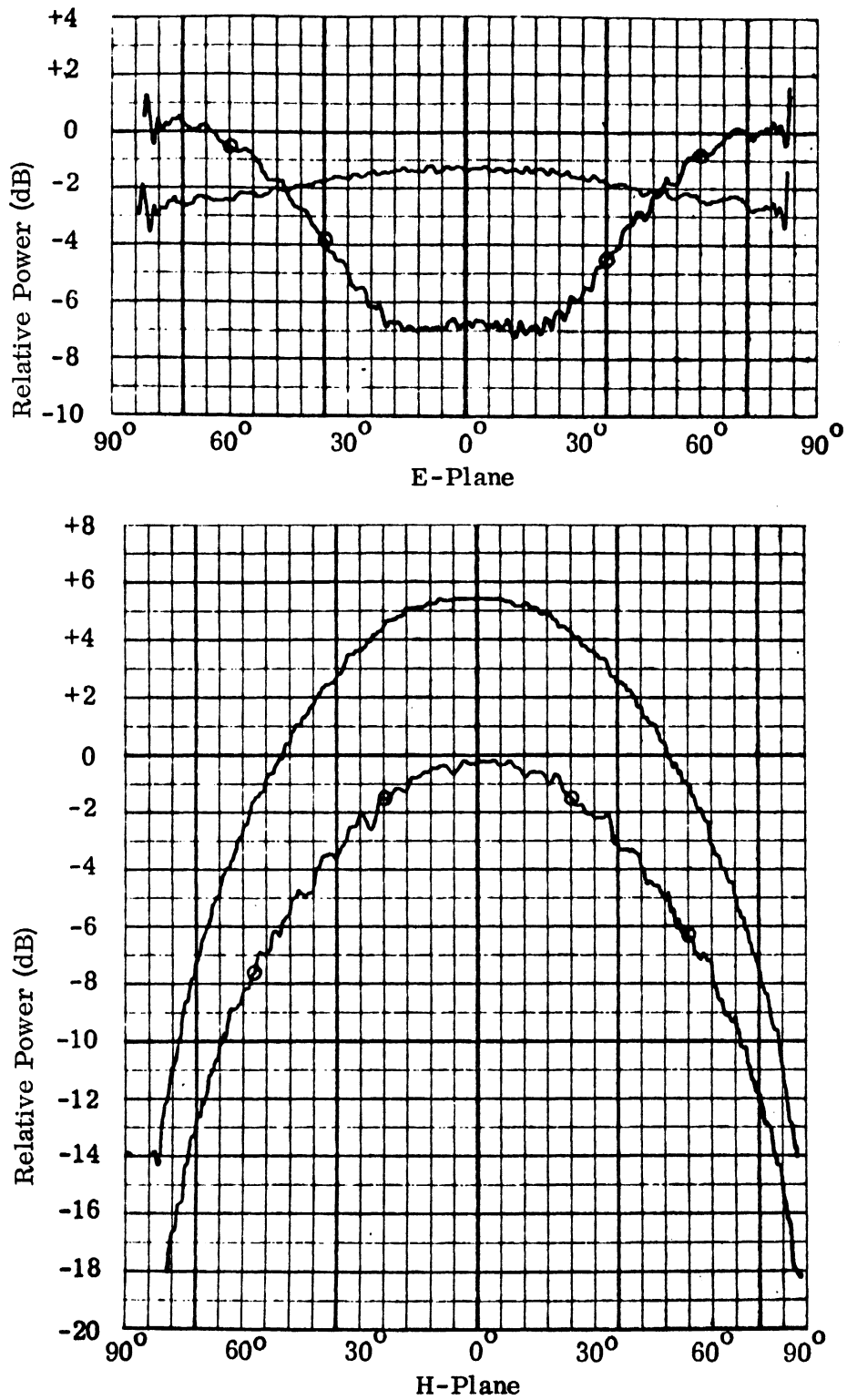
FIG. 5-5: E- AND H-PLANE RADIATION PATTERNS OF PLAIN SLOT (—)
AND SLOT SURROUNDED BY A TRENCH (-⊖-) AT 8.23 GHz.
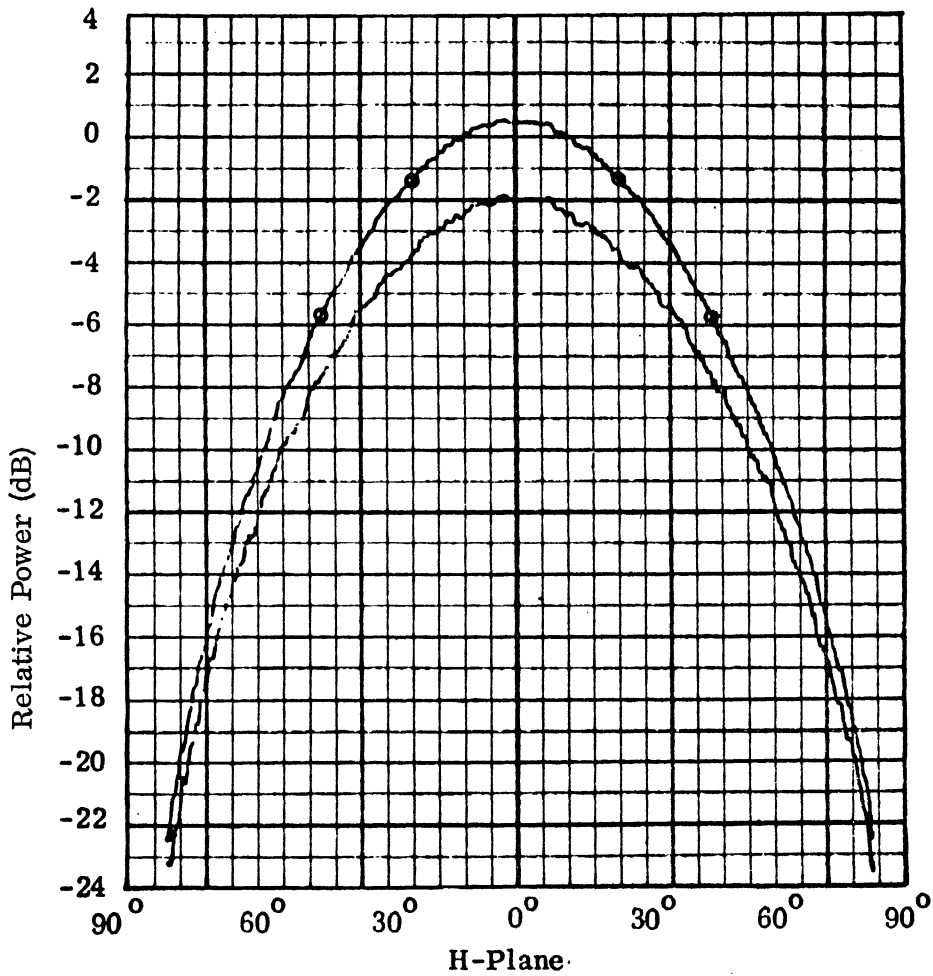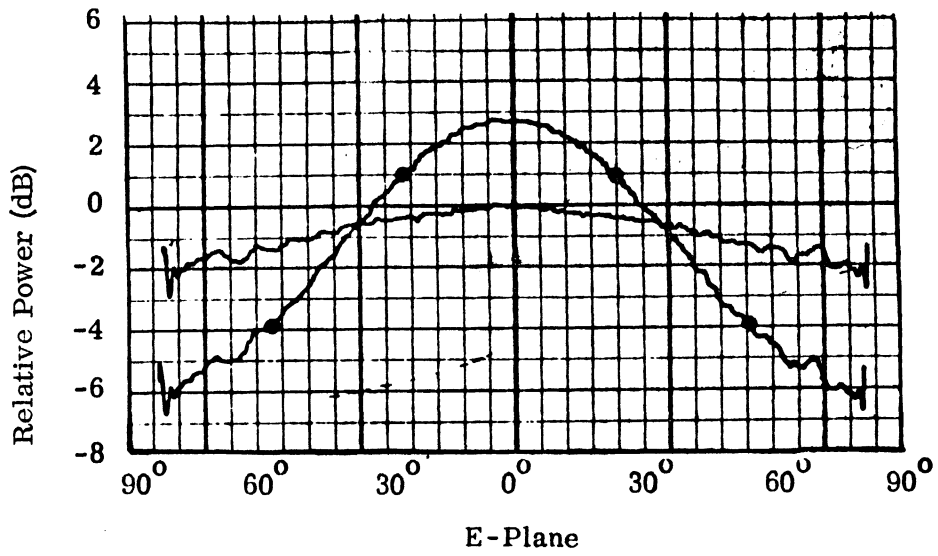
FIG. 5-6: E- AND H-PLANE RADIATION PATTERNS OF PLAIN SLOT (—)
AND SLOT SURROUNDED BY A TRENCH (-⊖-) AT 10.03 GHz.

These radiation patterns were measured with the test antenna mounted at the center of the 12 ft. square ground plane. A small E-sectoral horn with aperture size 2.85 cm by 2.3 cm and gain between 8 and 10 dB across the range of test frequencies was used as a pick-up antenna. This horn was mounted on booms and moved along a circumference at a distance of 1.80 m from the test antenna. The booms were covered with hairflex absorber to reduce reflections. When the two antennas were interchanged the power level of the transmitter and all gain controls were held constant so that the recorded patterns give an accurate picture of the relative gains of the slot with and without the surrounding trench.

As shown, the presence of the circumferential trench changes drastically the radiation pattern of the slot, more so in the E-plane. At 8.23 GHz the trench offers an inductive surface reactance which results in reduced radiation in the broadside direction and increased radiation along the ground plane. The opposite results are obtained at 10.03 GHz where the trench presents a capacitive surface reactance. Thus, the reduction of the main lobe along the ground plane and the associated coupling reduction to any adjacent antenna is accompanied by an increase in antenna gain (2.5 dB) and directivity.

5.2.2 Loading with Four Trenches

In order to obtain greater coupling reduction another antenna was constructed with an X-band waveguide-fed slot surrounded by four circumferential trenches (see Fig. 5-7). The trenches were spaced radially by 0.8 cm, with the one closest to the slot aperture having a radius of 1.9 cm. Each trench had a depth of 0.914 cm, corresponding to $\lambda_0/4$ at 8.2 GHz, and a width of 0.17 cm. This antenna was mounted flush in the 12 ft. square aluminum ground plane.

The radiation patterns of this antenna were measured at several frequencies using the set-up described earlier. Typical radiation patterns measured at 8.23 GHz are shown in Fig. 5-8. At this frequency the radiation along the ground plane is reduced by more than 10 dB in the antenna E-plane while the antenna gain is increased by 3.5 dB. This is reflected in the reduction of E-plane coupling between two slots at a center-to-center spacing of 11.4 cm as shown in Fig. 5-9. The decoupling, however, is gradually reduced at higher frequencies due to the reduced

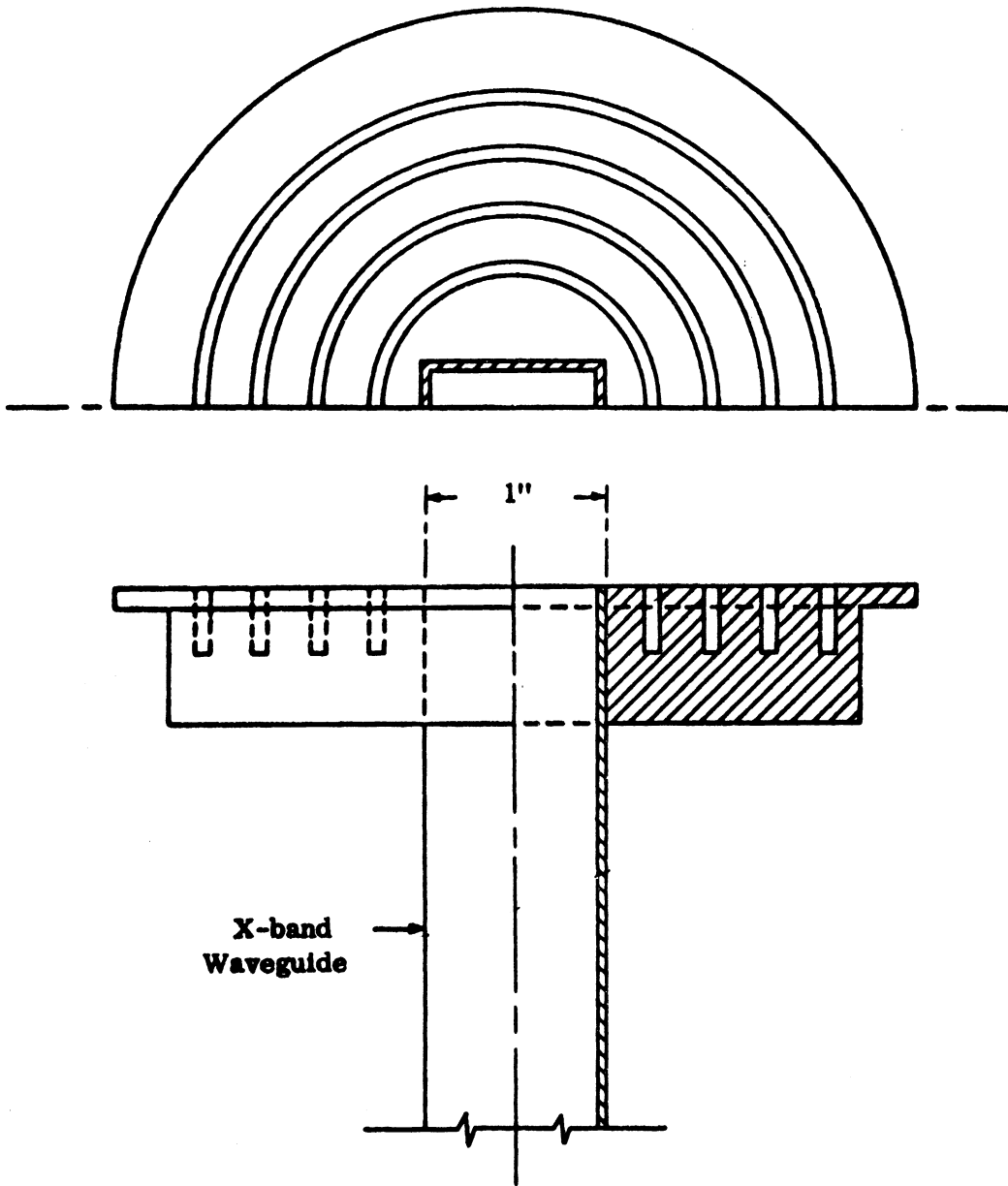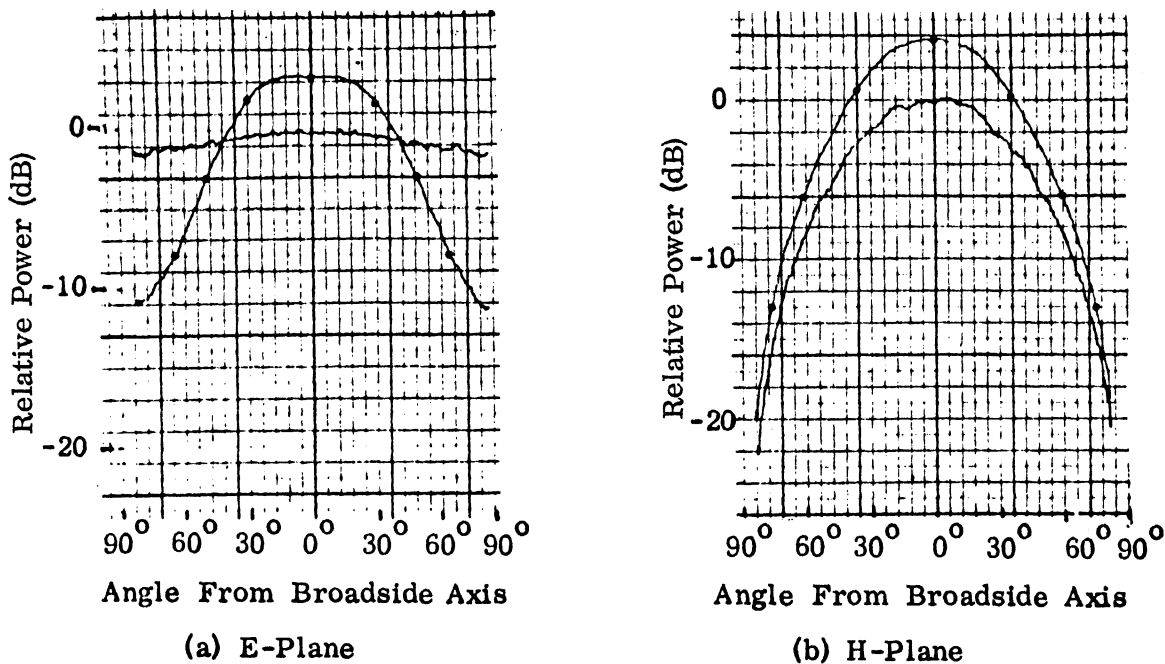FIG. 5-7: SLOT ANTENNA WITH FOUR TRENCHES.

(a) E-Plane

(b) H-Plane

FIG. 5-8: E- AND H-PLANE RADIATION PATTERNS AT 8.23 GHz (—) Flat
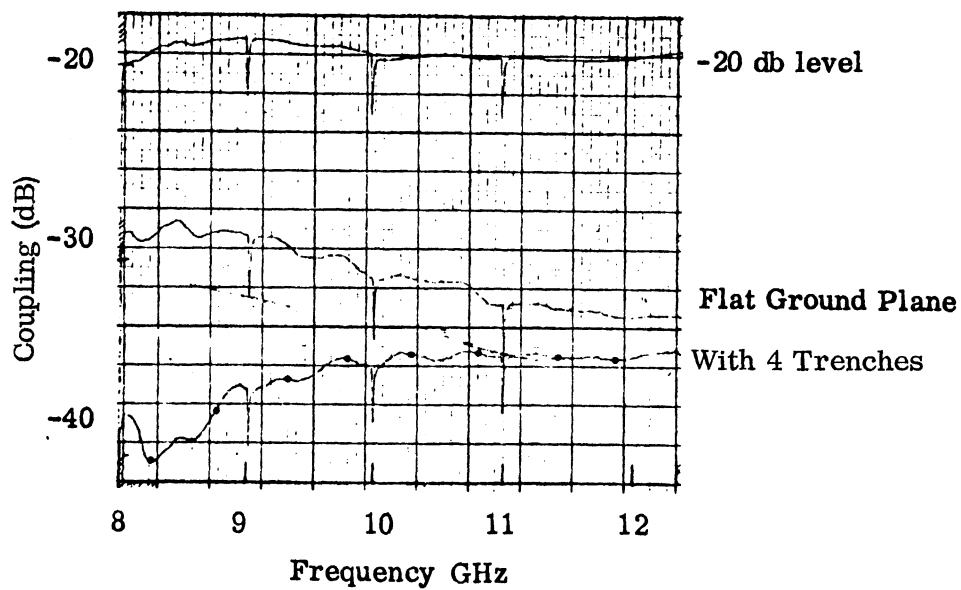Ground Plane, (-o-) With Four Trenches.

FIG. 5-9: E-PLANE COUPLING VS FREQUENCY FOR TWO SLOTS SPACED
11. 43 CM.

surface reactance presented by the trenches. The H-plane coupling was little affected by the presence of the trenches. A modest decoupling of the order of 1 to 2 dB was measured across the same frequency range.

The coupling was measured by using a sweep generator and sweeping the frequency across the entire X-band. The spikes seen along the two coupling curves are due to frequency markers. When using a sweep generator with internal leveling, as was done in this case, the power level at the transmitting antenna varies within certain limits. Therefore, a calibration curve representing the -20 dB level is presented, superimposed in Fig. 5-9. The calibration curve was obtained by mating the waveguide flanges connected to the two antennas, thus creating a direct link between transmitter and receiver, and simultaneously inserting a 20 dB attenuation in the link through a precision attenuator.

The antenna maximum gain was also measured in the frequency range 8 to 12. 4 GHz by sweeping the frequency and was compared to the gain of a similar slot without the reactive loading. It was found that the reactive loading increased the antenna gain throughout this frequency range, with the increase tapering gradually from a maximum of 3. 5 dB at 8. 2 GHz to a minimum of 0. 3 dB at 12. 4 GHz.

5. 3   Broadband Slot with Continuous Reactive Loading
       5. 3. 1 Parallel Wall Corrugations
       The reactive loading of the ground plane around the antenna aperture with one or more isolated circumferential slots gave good results but a relatively modest amount of decoupling. In order to obtain greater coupling reduction, continuous reactive loading was used by modifying the area around the antenna aperture. The modified area was in the shape of an annulus starting very near the antenna and extending out to a radius of one to two free space wavelengths.

Two sets of corrugations with parallel walls and constant depth were constructed with the first stop bands in the S- and X-frequency bands. The dimensions of the trenches of the corrugations designed for S-band have already been given

(see Section 4.2.2). When used with an S-band slot antenna these corrugations extend from an inner radius of 4.76 cm out to a radius of 16.32 cm. So the radial extent of the corrugated area is approximately equal to 1.3 λ_0 at 3.4 GHz. These corrugations are shown in Fig. 5-10 with a broadband, waveguide-fed slot mounted at the center. Subsequently they will be referred to as "corrugations S".

The dimensions of the set of corrugations designed for use at X-band were as follows (all symbols as defined in Section 4.2.1):

$$d = .84 cm, \qquad w = .165 cm, \qquad s = .185 \ cm.$$

The corrugated area, in the form of an annulus, extended from an inner radius of 1.58 cm out to a radius of 4.32 cm for a radial extent of 0.9 λ_0 at 10 GHz. The cut-off frequency for the first pass band is found from Eq. (4.4) to be 8.2 GHz. These corrugations were made by cutting strips of shim stock 0.84 cm wide and soft soldering them to the bottom of a cylindrical cavity cut from a piece of brass (see Fig. 5-11). Subsequently they will be referred to as "corrugations R-1".

5.3.1a. <u>Operation at S-band (2.6 to 4.0 GHz).</u> When "corrugations S" were placed around an S-band slot (aperture dimensions 7.21 cm by 3.40 cm) it was found that the E-plane coupling to an adjacent slot was reduced from a maximum value of -27 dB to -41 dB over almost the entire S-band (see Fig. 5-12). Calibration curves obtained by the procedure described earlier are shown together with the coupling curves. The center-to-center spacing of the two slots was 2.5 λ_0 in the middle of the frequency range considered (3.3 GHz). The experiment also shows that the stop band starts at 2.81 GHz which is 2.1 percent from the calculated value. When the slots are oriented for weak coupling (H-planes colinear) the radiation pattern of each slot exhibits a null in the direction of the other slot and therefore the corrugations cannot be as effective. However, this is not a serious problem since the H-plane coupling level is much lower than the E-plane coupling. In this case the maximum H-plane coupling was reduced from -49 dB to -52 dB when the corrugations were added. In the case of H-plane coupling the stop band starts at 2.73 GHz which is within the limits of measurement error from the calculated value. This agreement with the theoretical result is remarkable
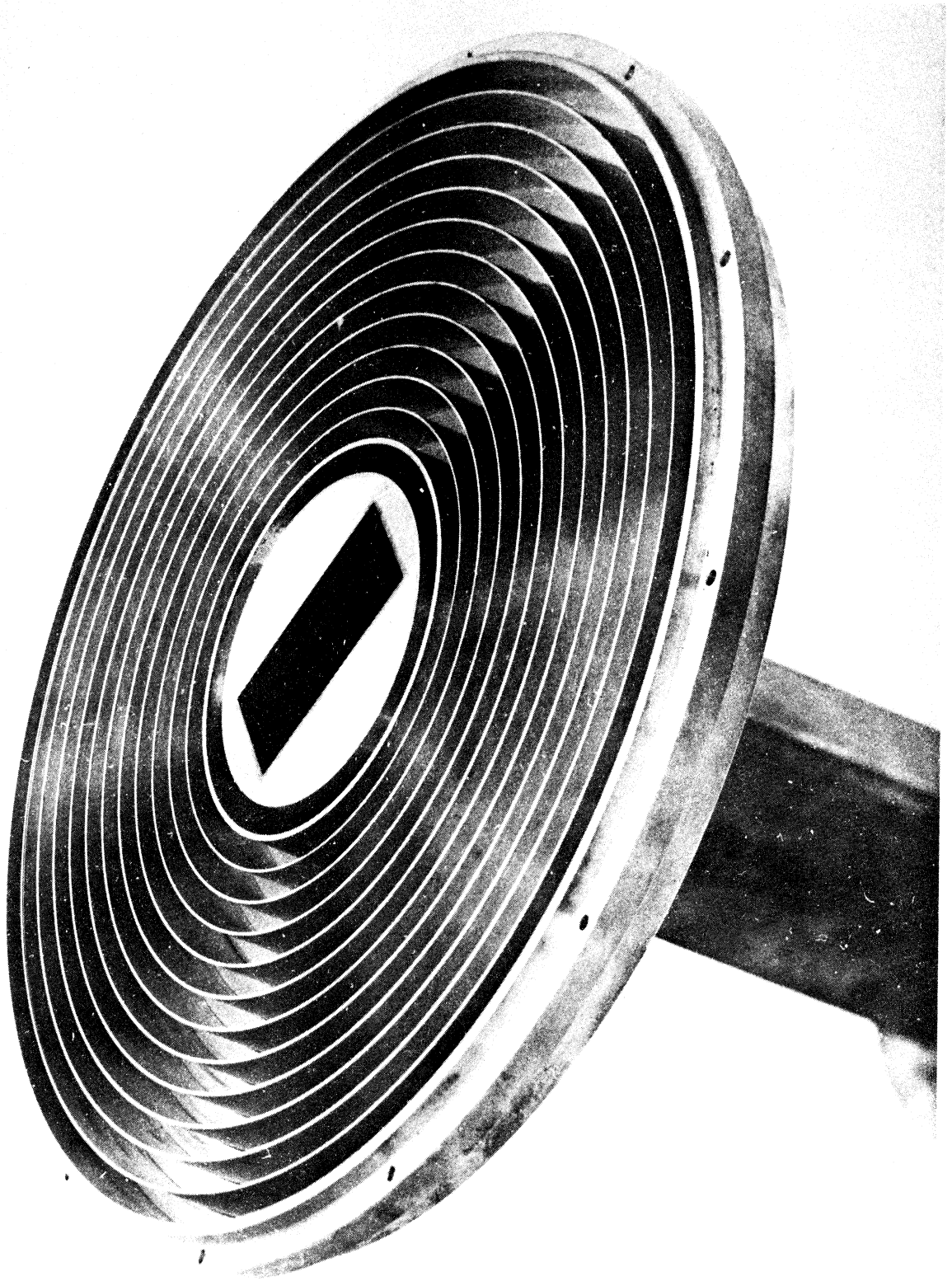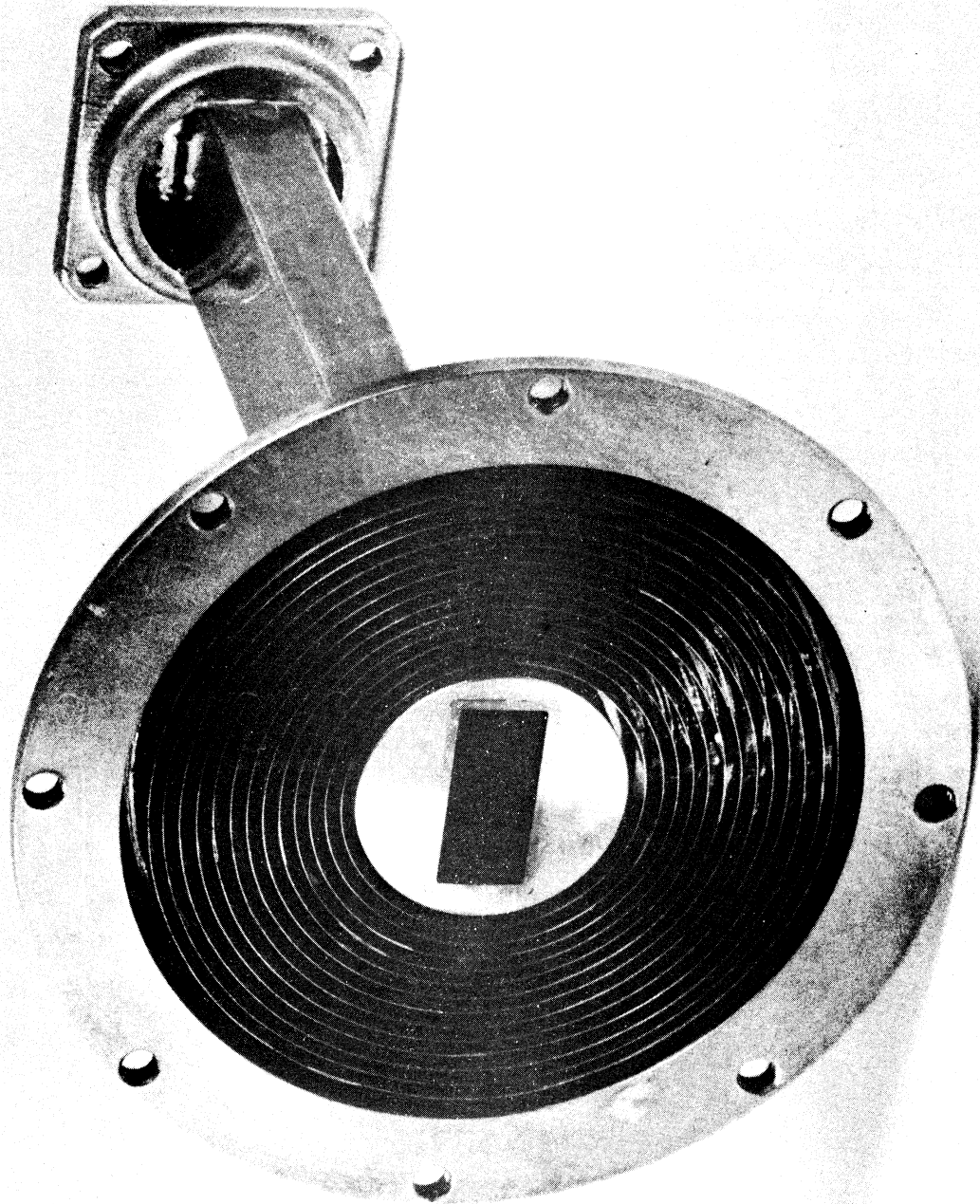
FIG. 5-10: SLOT ANTENNA AND CORRUGATIONS S.

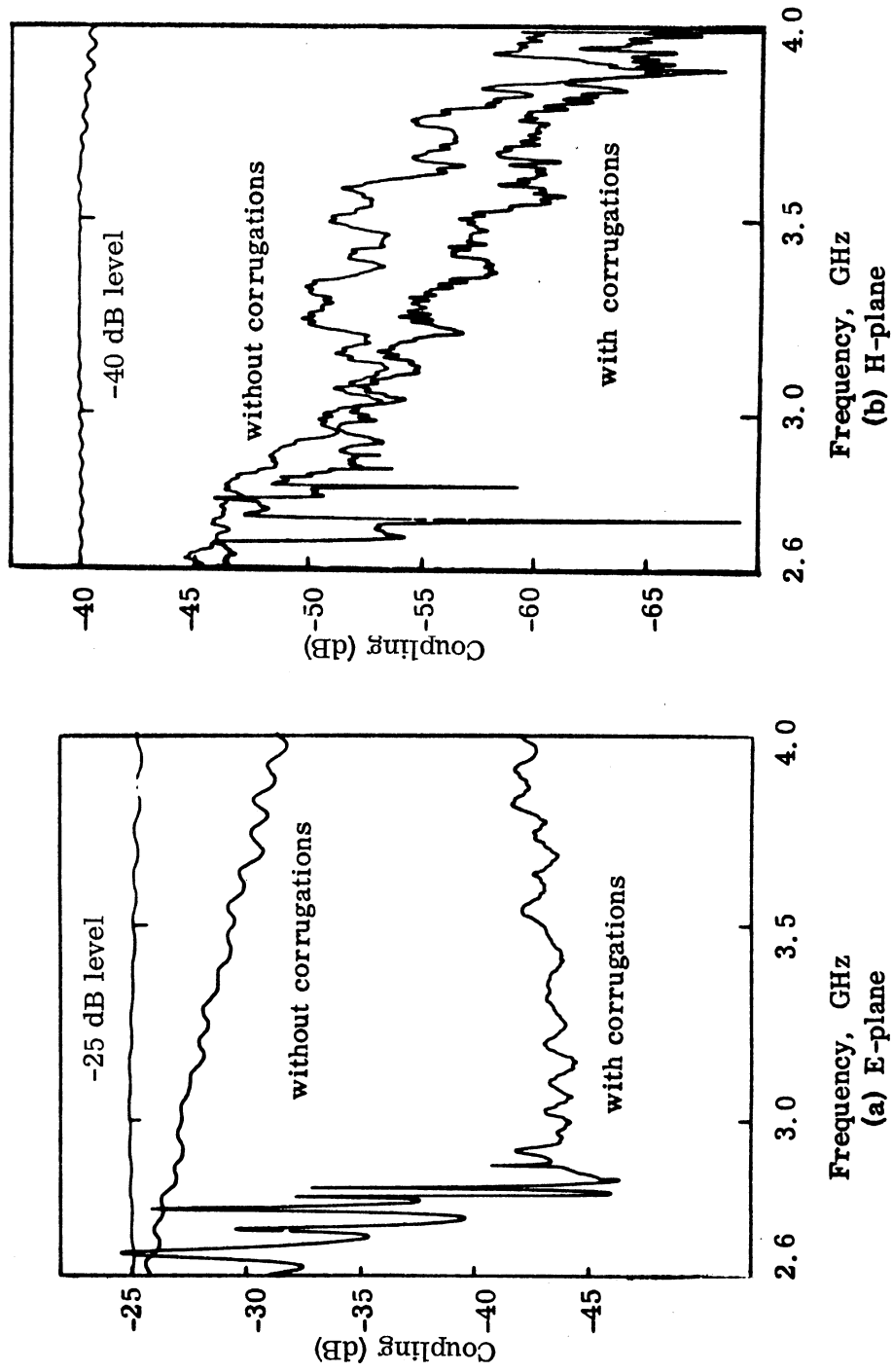FIG. 5-11: SLOT ANTENNA WITH CORRUGATIONS R - 1.

FIG. 5-12: E- AND H-PLANE COUPLING VS FREQUENCY FOR TWO SLOTS SPACED 22.8 CM IN A 12' BY 12' ALUMINUM GROUND PLANE.

since the actual geometry deviates from that assumed to derive Eq. (4. 4) in two respects: a) the structure is not periodic since it extends for only one wavelength rather than continuing to infinity and, b) instead of parallel wall corrugations, one has circumferential corrugations which, strictly speaking, is not a two-dimensional problem.

It has been thought to be of interest to investigate the effect on decoupling of the trenches individually. For this purpose the area of the ground plane surface represented by the corrugations was covered by aluminum foil and the coupling between the two slots measured by sweeping the frequency. The innermost trench was then uncovered and the coupling measured again. The uncovering of subsequent trenches continued until they were all exposed. The results are shown in Fig. 5-13. In this figure the parameter indicates the number of uncovered trenches. The lowest curve in Fig. 5-13 is identical with that of Fig. 5-12. By examining the effect of the individual trenches above the cut-off frequency it is seen that beyond the ninth trench, which is situated at a distance of 1.25 λ_0 (3. 0 GHz) from the center of the slot, the additional decoupling created by more trenches is uniform. Thus, greater coupling reduction can be achieved by extending the corrugated area further. If the corrugations were extended to infinity the radiation along the ground plane would be reduced to zero exactly as in the case of the monopole.

The effect of the corrugations has been qualitatively explained as trapping the power carried by a surface wave along the ground plane and radiating it in the broadside direction. This means that the sidelobe decrease should be accompanied by an antenna gain increase. This was observed experimentally by mounting the slot on a small metal disk (diameter 33.3 cm) and recording the radiation patterns in the two main planes (see Fig. 5-14). A plain and a corrugated disk of the same overall diameter were interchanged and the two radiation patterns were superimposed for comparison. At 3. 0 GHz the corrugations cause an E-plane sidelobe reduction of 12 dB accompanied by a 3 dB gain increase. By orienting the slot for maximum gain and sweeping the frequency (Fig. 5-15) it was demonstrated that the gain increase varies between 1. 5 dB to 5. 0 dB between 2. 6 and 4. 0 GHz.
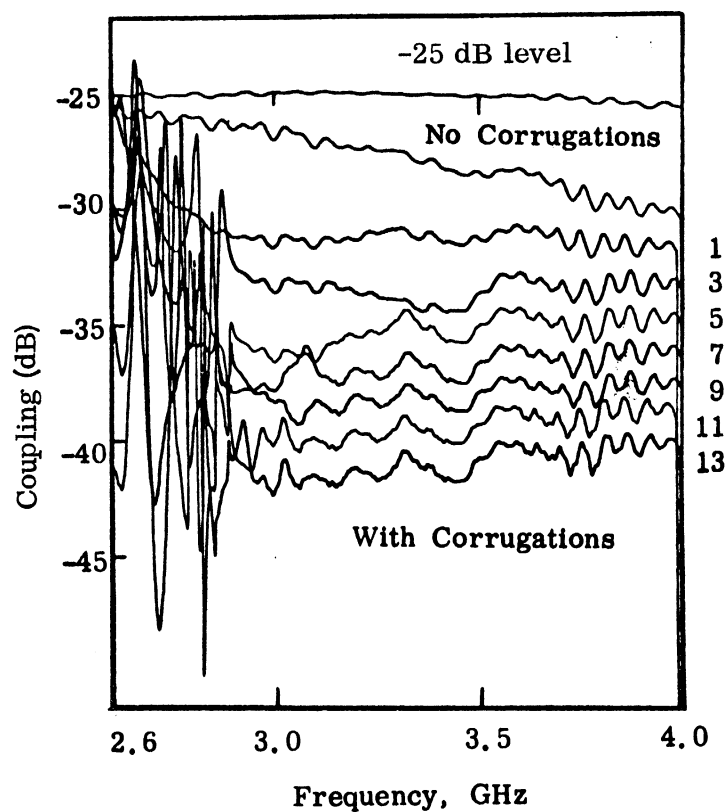
FIG. 5-13: E-PLANE COUPLING VS FREQUENCY FOR TWO
SLOTS SPACED 22.8 CM. Parameter Indicates
the Number of Uncovered Trenches.
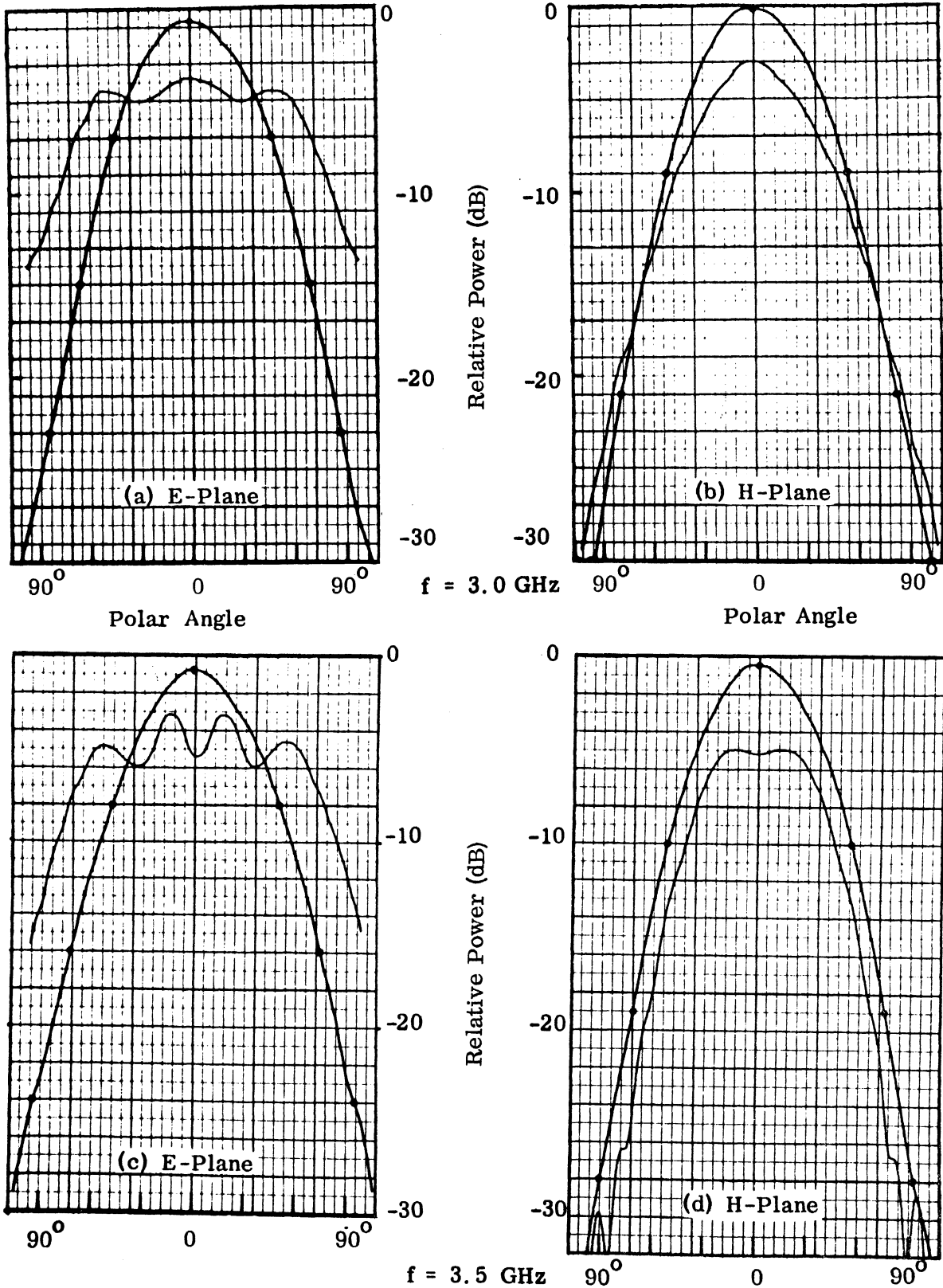
FIG. 5-14: RADIATION PATTERNS FOR S-BAND SLOT IN METAL DISK, 33. 3 CM DIAMETER. (—) Flat Disk, (-●-) Disk with Corrugations.

Relative Power (dB)

0

-10

-20

-30

90°   0   90°   f = 4.0 GHz

Polar angle

FIG. 5-14: (continued)

0

-10

-20

-30

90°   0   90°

Polar angle

With Corrugations

0

Relative Power (dB)

-5

-10

Without Corrugations

2.6   3.0   3.5   4.0

Frequency, GHz

FIG. 5-15: MAXIMUM GAIN VS FREQUENCY FOR S-BAND
SLOT IN METAL DISK, 33.3 CM DIAMETER.

The above radiation patterns were obtained with the test antenna located inside the 50 ft. anechoic chamber at a distance of approximately 30 ft. from the large aluminum ground plane. The latter was covered with hairflex absorber pads except for an opening at a center for a standard gain horn to illuminate the test antenna. The antenna under test was supported by a rotating pedestal and was used as a receiver. The directivity of the standard gain horn used in these measurements varied from 17. 0 to 19. 7 dB in the range of frequencies from 2. 6 to 4. 0 GHz.

When the slot is mounted in the large ground plane (as for the coupling measurements) its radiation pattern is different from that measured in free space. The difference is small near the broadside and larger near the plane of the aperture. At the plane of the aperture the field intensity is doubled when an infinite ground plane is present, i. e. the level of radiated power is higher by 6 dB (Stratton and Chu 1939, Meixner 1956).

When two antennas are in the far field of each other, the mutual coupling can be predicted from their radiation patterns by the Friis transmission formula. In the case of two slots in a large, flat ground plane far field coupling behavior has been observ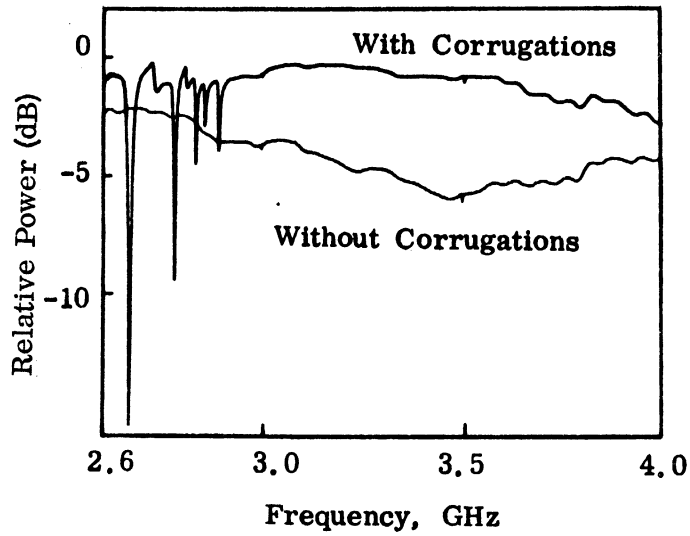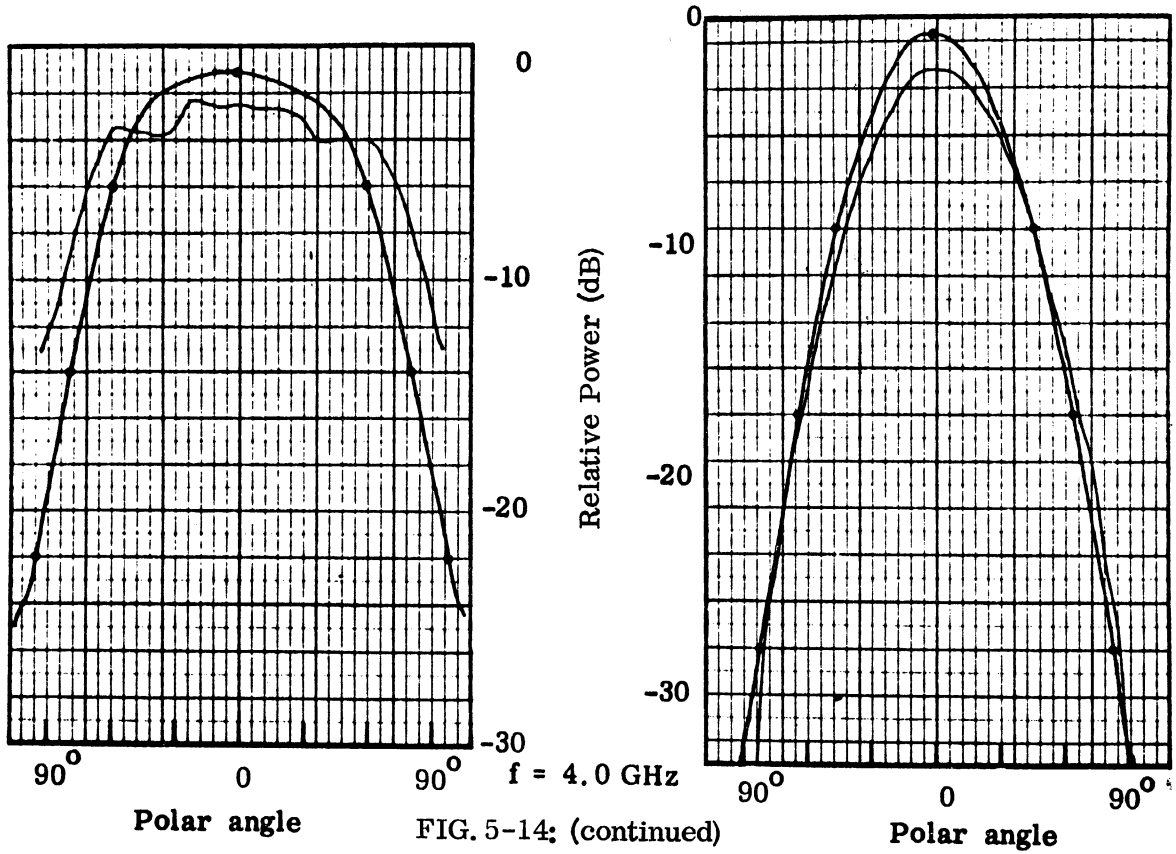ed even at spacings of 2. 5 λ_0 (Lyon et al, 1966). With the addition of the corrugations this is not true any more since the effective antenna aperture is markedly increased and so is the minimum distance for far field behavior. A comparison of the coupling reduction, Δ C, measured in the near field (antenna center-to-center spacing 22. 8 cm) with that which should be expected in the far field is presented in Table V-1. The data for this table were taken from Figs. 5-12 and 5-14. It is interesting to note that the corrugations as used here offer the greater decoupling where it is needed most, i. e. in the near field where the coupling is the strongest and the interference problem more acute.

TABLE V-1: COUPLING REDUCTION WITH CORRUGATIONS S.

Frequency , GHz	3. 0	3. 5	4. 0
ΔC, Near Field, dB	16. 0	13. 5	10. 5
Δ C, Far Field, dB	12. 5	10. 0	7. 0

The slot standing wave ratio and input impedance were measured with the antenna mounted in the 12 ft. square aluminum ground plane. Two sets of readings were taken, one with a flat ground plane and one with the corrugations surrounding the slot. In the experimental set-up the waveguide feeding the slot was connected to a waveguide slotted section having a residual standing wave ratio less than 1.01. A broadband crystal detector was used with the slotted section. Between the slotted section and the waveguide to coaxial adapter, where the source output was fed, a waveguide attenuator was inserted to minimize any reflections from the adapter. This attenuator, having an SWR less than 1.15, was set between 10 and 20 dB. A flat plate was placed at the waveguide aperture to create a short characterized by an SWR greater than 20 dB.

The variation of the slot SWR with and without the corrugations is shown in Fig. 5-16. The presence of the corrugations does not increase the maximum SWR of the slot in the frequency range of operation. The resistance and reactance of the slot in the two cases are shown in Fig. 5-17. These values are normalized with
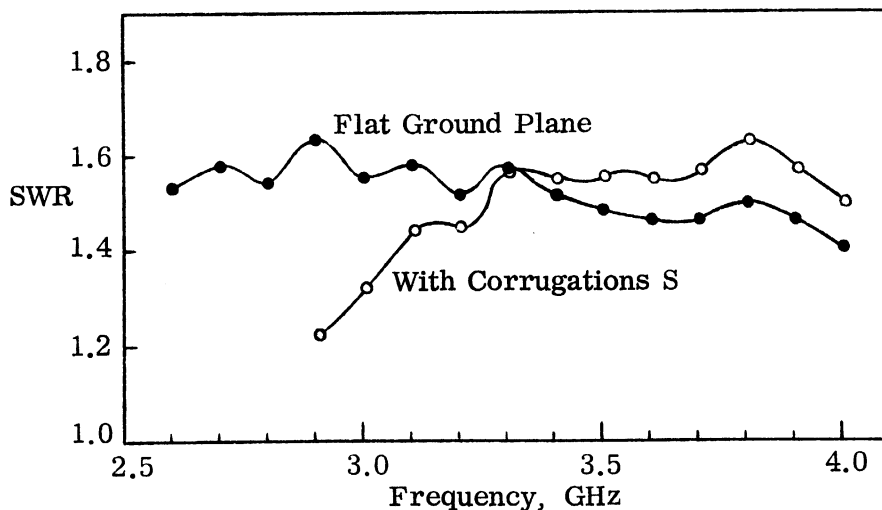

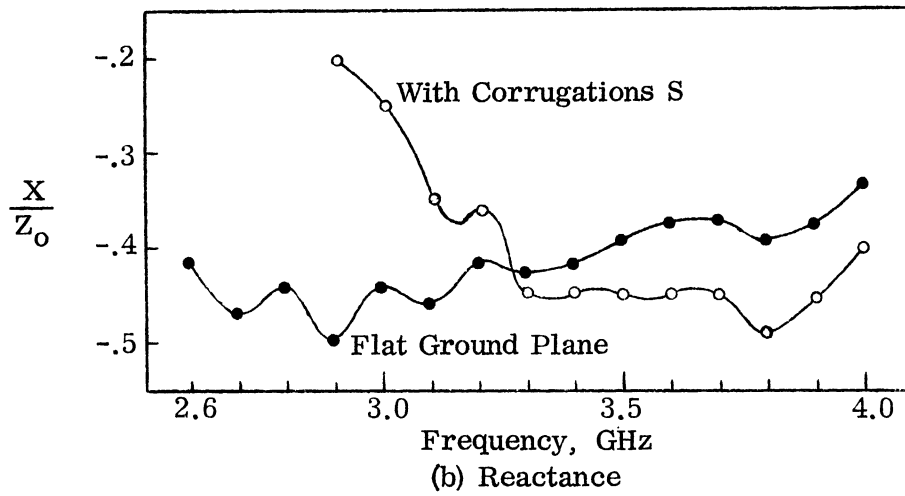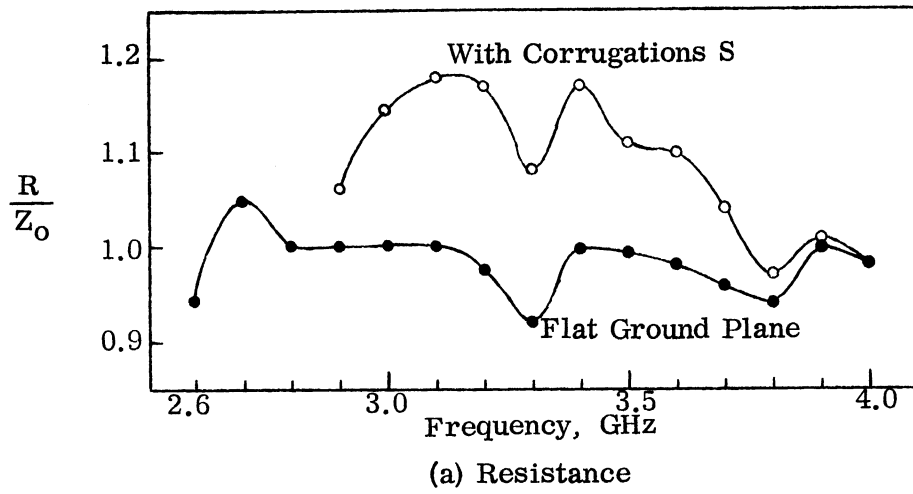FIG. 5-16: STANDING WAVE RATIO OF SLOT ANTENNA.

(a) Resistance

(b) Reactance

FIG. 5-17: APERTURE IMPEDANCE OF WAVEGUIDE
TERMINATED IN INFINITE GROUND PLANE.

respect to the waveguide characteristic impedance Z_0. When the waveguide operates in TE_{10} mode Z_0 is given by

$$Z_0 = \frac{\pi}{2} \, 377 \cdot \frac{b}{a} \cdot \frac{\lambda_g}{\lambda_0} \quad \text{(ohms)} ,$$

where a and b are the width and height of the waveguide, respectively, λ_0 is the free space wavelength, and λ_g is the wavelength in the rectangular waveguide. This value of characteristic impedance is obtained by taking the ratio of the voltage between the top and bottom surfaces of the guide to the current flowing in the walls of the guide. The results for the case of flat ground plane are in general agreement with previously published data (Radio Research Laboratory, 1947).

The slot impedance was also measured when the waveguide was terminated in a disk flange of 33.3 cm diameter instead of the 12 ft. square ground plane. Two cases were considered, flat disk and disk with corrugations. In either case the measured values were very close to the values obtained in the respective cases employing the large ground plane, therefore, those results are omitted .

5.3.1b. **Operation at X-band (8.2 to 12.4 GHz) and Ku Band (12.4 to 18.0 GHz).** The scaling of the dimensions of an antenna so that it can operate at different frequencies generally does not present any new problems and once a model has been studied the results apply equally well to all antennas created by scaling the first model. Therefore the building and testing of a second model would not seem to provide much new information. The above notwithstanding, the corrugations designed for operation at X-band frequencies were tested and the more important results are presented below mainly for two reasons. First, the coupling has been measured over a frequency range of 2 : 1, a measurement which was not performed with corrugations S due to non-availability of the necessary equipment. Since in some applications it is of interest to obtain increased isolation between two systems operating over frequency ranges of 2 : 1 this additional information is important. Secondly, due to the smaller wavelength at X-band it has been possible to measure radiation patterns when the antenna was mounted on the large (for practical purposes, infinite) ground plane and compare them with the radiation patterns of the same antenna in free space. The antenna used for these measurements was a rectangular

slot of dimensions 2.3 cm by 1.0 cm fed by a waveguide.

When corrugations R-1 were placed around the slot antenna, the E-plane coupling to an adjacent identical slot, spaced 11.4 cm, was reduced by 10 dB over a 30 percent bandwidth, as shown in Fig. 5-18(a). The measurements were extended to the next higher waveguide band by using the same slots fed by the X-band waveguide with tapered transitions to the Ku-band waveguide. Figure 5-18(b) shows the measured coupling in this case. It should be recalled that in reading the coupling from Fig. 5-18 at any frequency, the distance along the ordinate from the calibration curve should be measured and then read using the scale of ordinates to the left. Note also that the scales of ordinates in Figs. 5-18(a) and (b) are not the same. The maximum coupling reduction was observed at 8.2 GHz as predicted by Eq. (4.4). Corrugations R-1 were not exactly symmetrical and this was reflected in the coupling measurements. Different orientations of the corrugations with respect to the two slots resulted in slightly different coupling curves.

The effect of the corrugations on the radiation pattern of the slot in a large ground plane is shown in Fig. 5-19. In this case the slot and corrugated disk were mounted flush in the 12 ft. square ground plane. A swept-frequency measurement of the maximum gain (broadside to the ground plane) shows that the reactive loading of the ground plane increases the gain of the slot over the entire X-band (see Fig. 5-20). The gain figures serve only to indicate the relative gains of the slot in the two cases and not the absolute gain. The gain shown depends upon the changing frequency and the gain versus frequency characteristic of the pick-up antenna.

Since a slot antenna may be used on vehicles of considerably smaller dimensions and since the size of the ground plane does affect the pattern significantly, the radiation patterns of the slot surrounded by corrugations were also measured in a free space environment. For this test the antenna was used exactly as shown in Fig. 5-11 except that the mounting screw holes were covered with aluminum foil. For a control case the slot was used with a flat disk flange of the same overall diameter as the disk with the corrugations (11.1)cm. The radiation patterns were measured with a standard gain horn and are shown in Fig. 5-21.
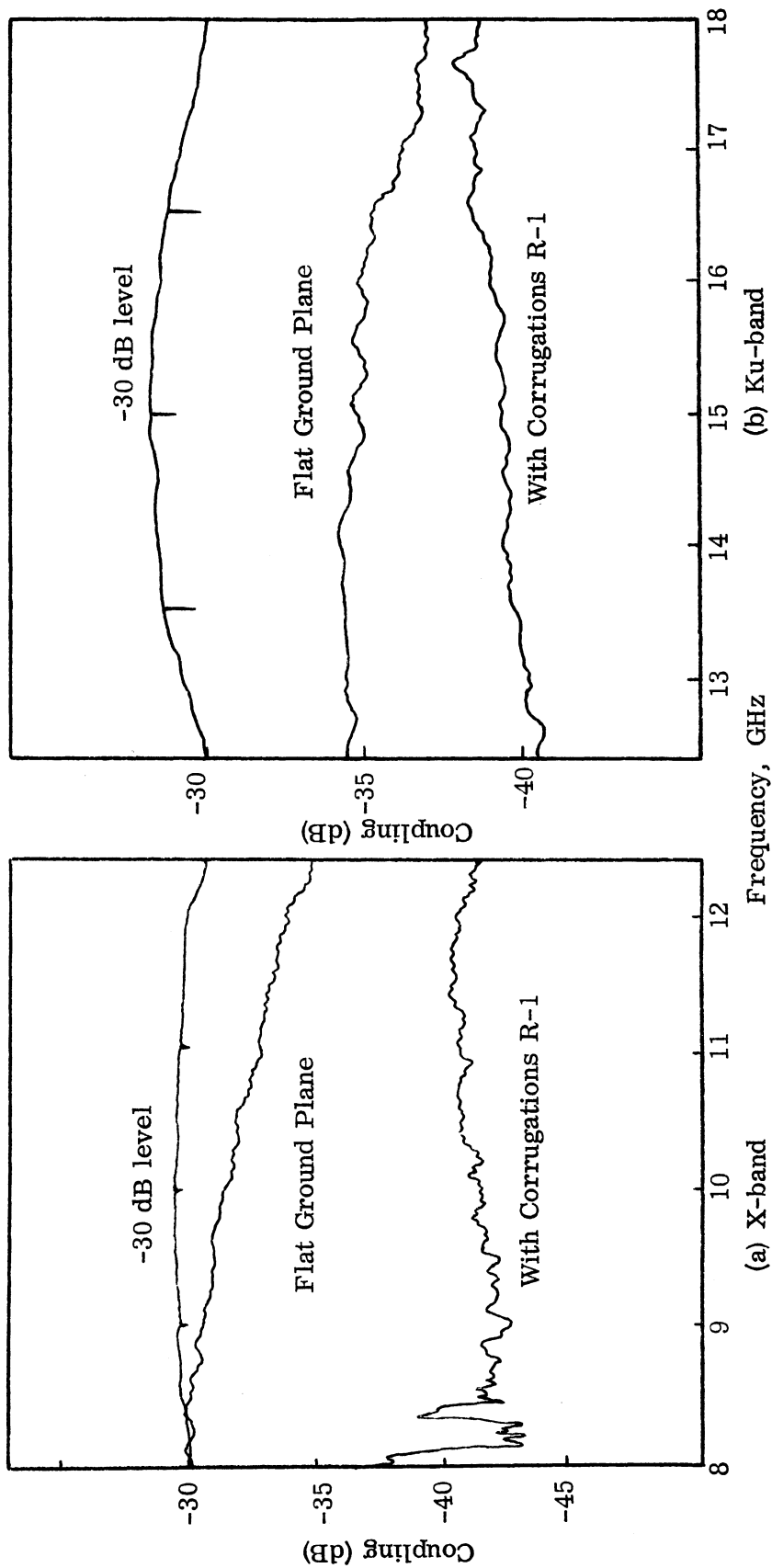
FIG. 5-18: E-PLANE COUPLING OF TWO SLOTS SPACED 11. 4 CM.

111
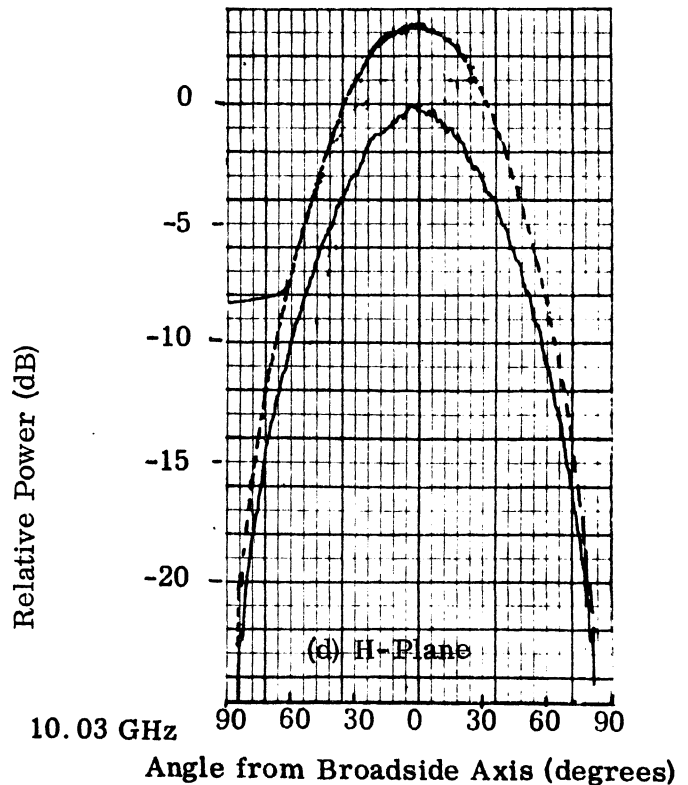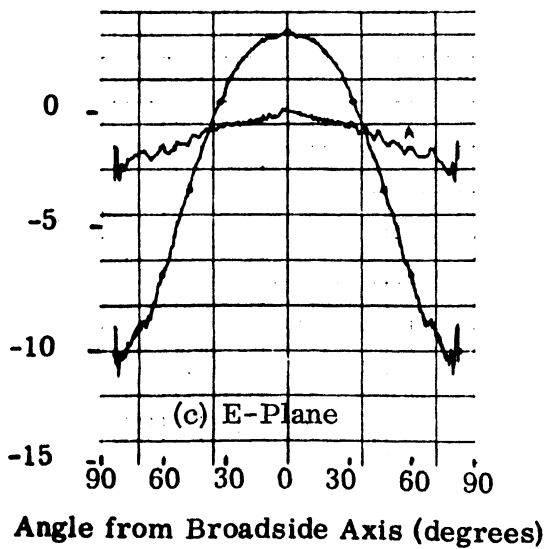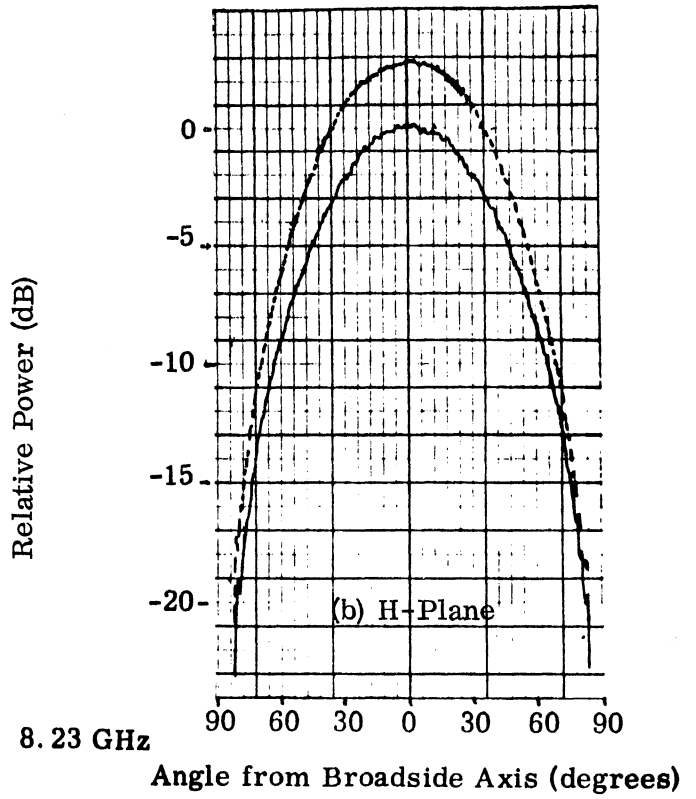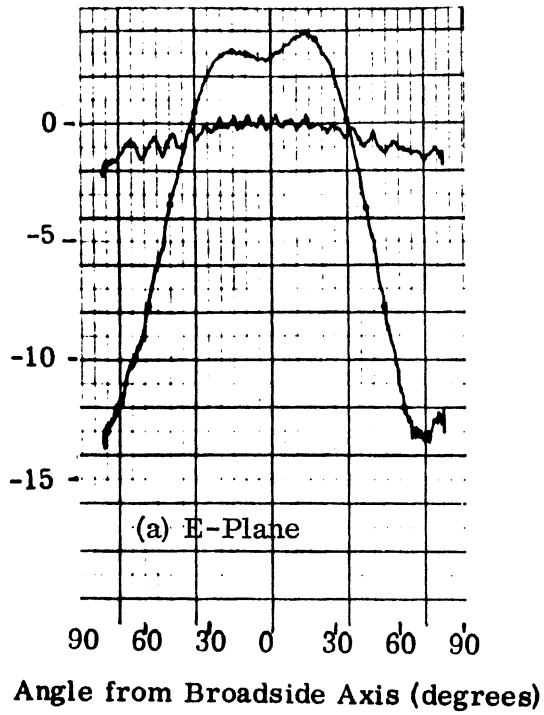
FIG. 5-19: E- AND H-PLANE RADIATION PATTERNS (—)Plain Slot; (-•-) or (---)
Slot with Corrugations R-1.

(e) E-Plane

(f) H-Plane

12.03 GHz

Angle from Broadside Axis (degrees)

Angle from Broadside Axis (degrees)

FIG. 5-19 (continued)

Slot with corrugations

Plain slot

FIG. 5-20: MAXIMUM GAIN VERSUS FREQUENCY.
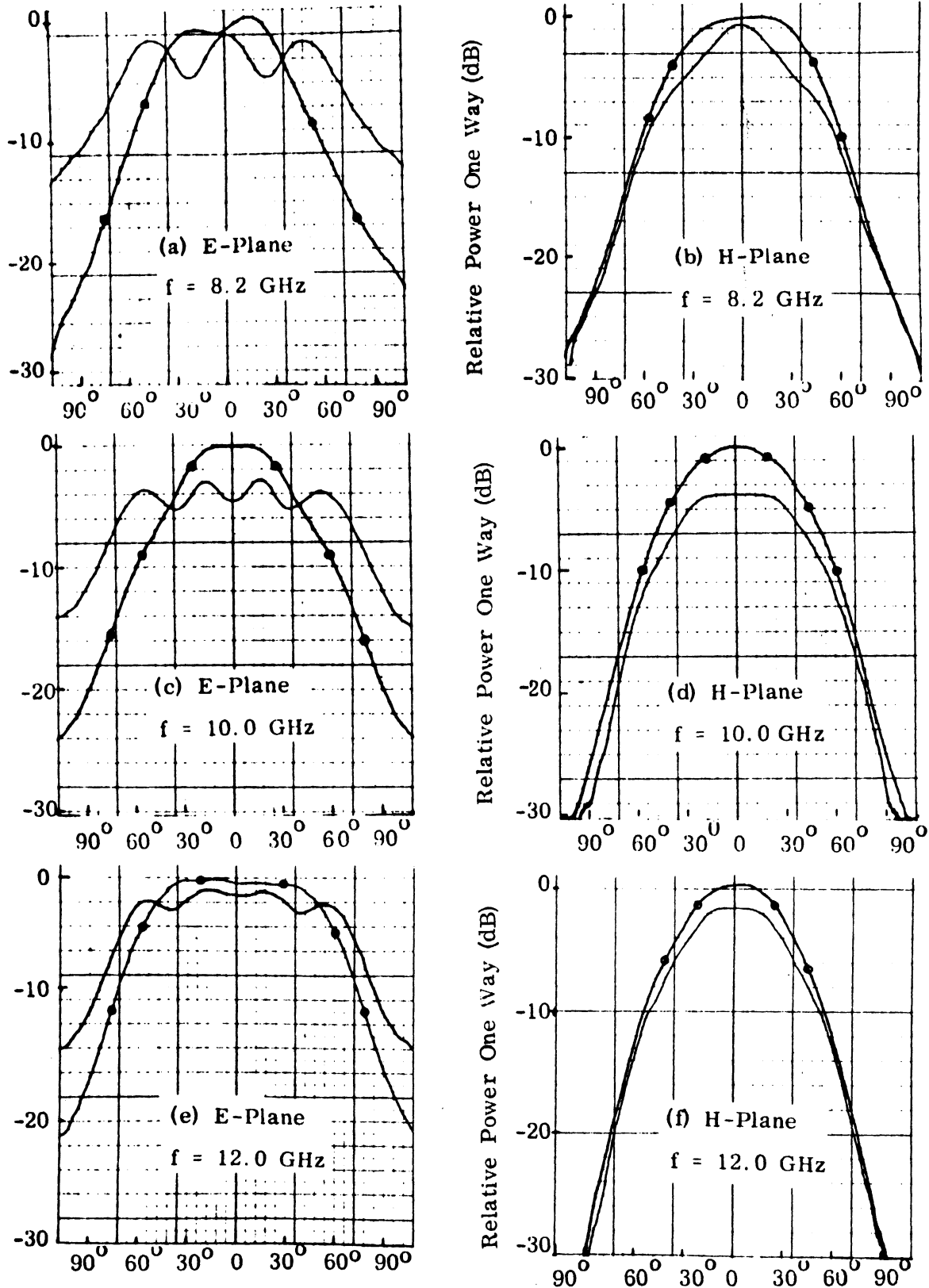
FIG. 5-21: RADIATION PATTERNS FOR SLOT IN METAL DISK, 11. 1 CM
DIAMETER (—) Plain Disk, (—•—)Disk with Corrugations R-1.

Two curves are presented superimposed in each case representing the radiation pattern of a plain slot and of the slot surrounded by corrugations. In each case the transmitter and receiver gains were left constant so that these figures also provide information about the effect of the corrugations on the antenna gain. The undulations present in the patterns of the plain slot are well known and have been explained by assuming additional radiation sources at the edges of the sheet. It is interesting to note that the corrugations virtually eliminate these undulations by preventing the propagation of a surface wave and thus reducing the diffraction from the ground plane edges.

The coupling measurements reported thus far have demonstrated the effectiveness of the corrugations creating a capacitive surface reactance in reducing coupling over a continuous frequency range exceeding a 2:1 bandwidth. However, this is not the ultimate frequency limit. A corrugated structure has an infinite number of stop bands interlaced with pass bands. Regarding the corrugations designed for S-band the second stop band occurs at nearly the third harmonic frequencies of the first stop band which in this case would be X-band.

An X-band slot surrounded by a small flat disk was placed at the center of the S-band corrugations. Then the coupling to a second slot on the same ground plane was measured when the corrugations S were covered by aluminum foil and when they were uncovered. The results are shown in 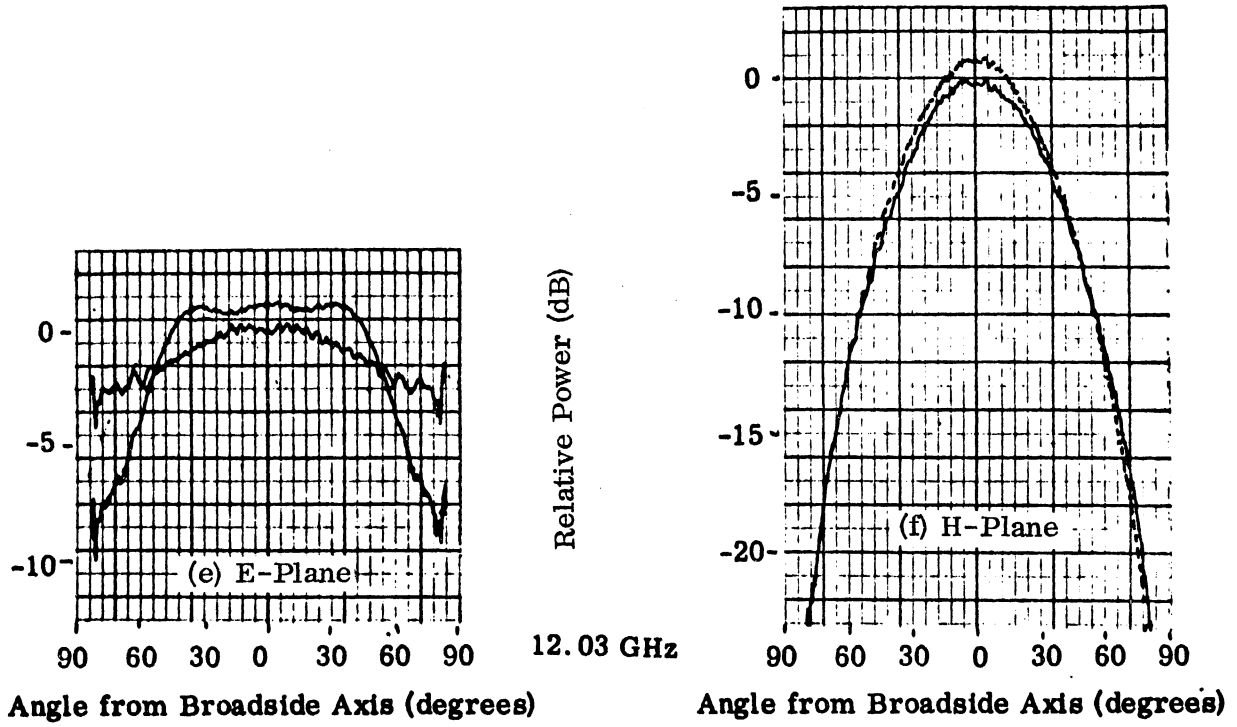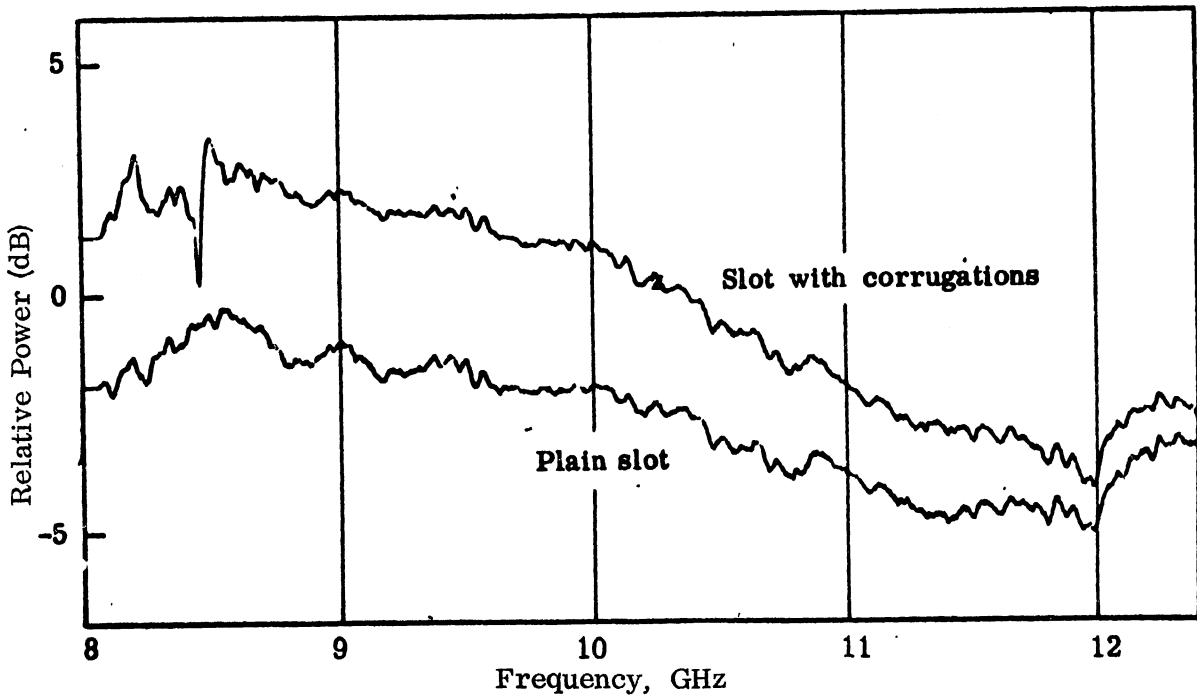Fig. 5-22 (second and fourth curves from the top, respectively). It is seen that the stop band starts at 8.34 GHz which is again within measurement error from the theoretically computed value of 8.31 GHz. Then the disk between the slot and corrugations S was replaced by corrugations R-1. Again two measurements were made with the corrugations S covered and uncovered. The results are shown in Fig. 5-22 (third and fifth curves from the top, respectively). The maximum E-plane coupling over almost all of the X-band has been reduced from -35.5 dB to -50.5 dB.
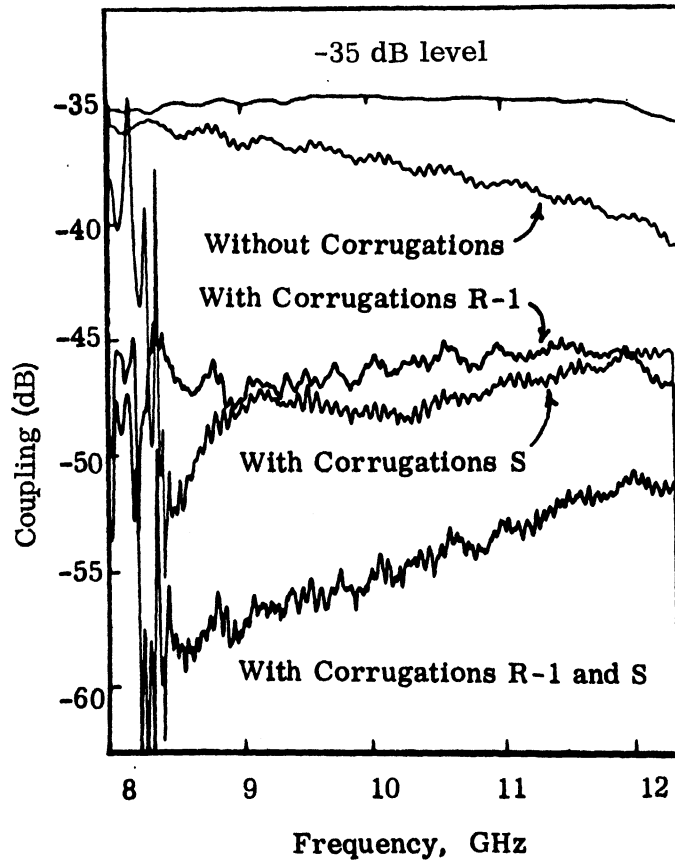
FIG. 5-22: E-PLANE COUPLING VERSUS FREQUENCY
FOR TWO X-BAND SLOTS SPACED 22.8 CM.

In conclusion it is seen that the corrugations are inherently effective also in reducing coupling at the third harmonic frequencies of the original design frequency range. This is an important feature because of the third harmonic content in the output of microwave oscillators in particular and in the radiation of various antennas in general. Due to this phenomenon several interference problems have been reported between antennas operating at different frequencies .

The inherent frequency dependence of the surface reactance created by a corrugated structure could be avoided by filling the trenches with materials exhibiting a desired variation of their characteristics with frequency. It is easy to calculate the desired dependence of the permittivity and permeability of a material upon frequency, so that corrugations would have a constant depth in terms of wavelengths. Consider for example, a piece of rectangular waveguide, of width a, terminated by a short. If the waveguide is filled with a material of relative permittivity ϵ_r and permeability μ_r, the wavelength inside the guide will be given by

$$\lambda_g = \frac{c}{\sqrt{f^2 \mu_r \epsilon_r - (c/2a)^2}} \tag{5.2}$$

where c is the speed of light. In order to have a constant λ_g as the frequency, f, is varied, it is necessary and sufficient that

$$f^2 \mu_r \epsilon_r = \text{constant} . \tag{5.3}$$

Materials with such properties can be manufactured but they are inherently lossy. A lossy material is not desirable because the attenuation of the waves inside the corrugations greatly reduces their action.

5.3.2 Tapered Wall Corrugations

It has been thought to be of interest to investigate the properties of a different type of currugated surface, with tapered width trenches. One motive in this investigation is that circular trenches of this profile can be easily machined in contrast to the parallel wall trenches.

A derivation of the surface impedance created by the corrugations with tapered trenches is presented in Appendix B. The results of this analysis show that the tapering of the trench walls restricts somewhat the frequency range over which the corrugations offer a capacitive surface impedance. Even then, the tapered wall corrugations are effective in reducing coupling over at least one waveguide band of frequencies. What is gained in exchange for the smaller bandwidth is an easily milled profile which also allows the wall width at the top of the trenches to become practically zero which, as mentioned earlier (Ch. IV), increases the amount of coupling reduction.

Three sets of circumferential corrugations with different cut-off frequencies and profiles were manufactured and tested. Each set had six trenches; their dimensions are given below in Table V-2 (all symbols as defined in Section 4.2.1 and Appendix B). The reactance annulus created by these structures extended radially from 1.49 cm to 4.49 cm. Each of these sets was machined from a solid piece of brass.

TABLE V-2: DIMENSIONS OF TAPERED CORRUGATIONS (cm).
Tolerance of r_L, $r_i = \pm 0.03$ cm.

Set	r_L	r_i	s	t
R4	0.25	0.97	0.50	≤ 0.01
R5	0.05	0.98	0.50	≤ 0.01
R6	0.36	1.36	0.50	≤ 0.01

For the coupling measurements these sets of corrugations were placed exactly as the previously described corrugations R-1. The E-plane coupling with and without corrugations around one slot is shown in Figs. 5-23 and 5-24 for two of the above described sets. The reductions in E-plane coupling obtained over a 1.5:1 frequency range with each of the sets R-4, R-5 and R-6 are 11 dB, 12 dB and 11 dB respectively. These figures are nearly the same with the coupling reduction obtained with the parallel wall corrugations R-1. Only corrugations R-6 were measured over a 2:1 bandwidth and there the maximum coupling was reduced by 8 dB which is approximately 2 dB less than the respective figure obtained with corrugations R-1.
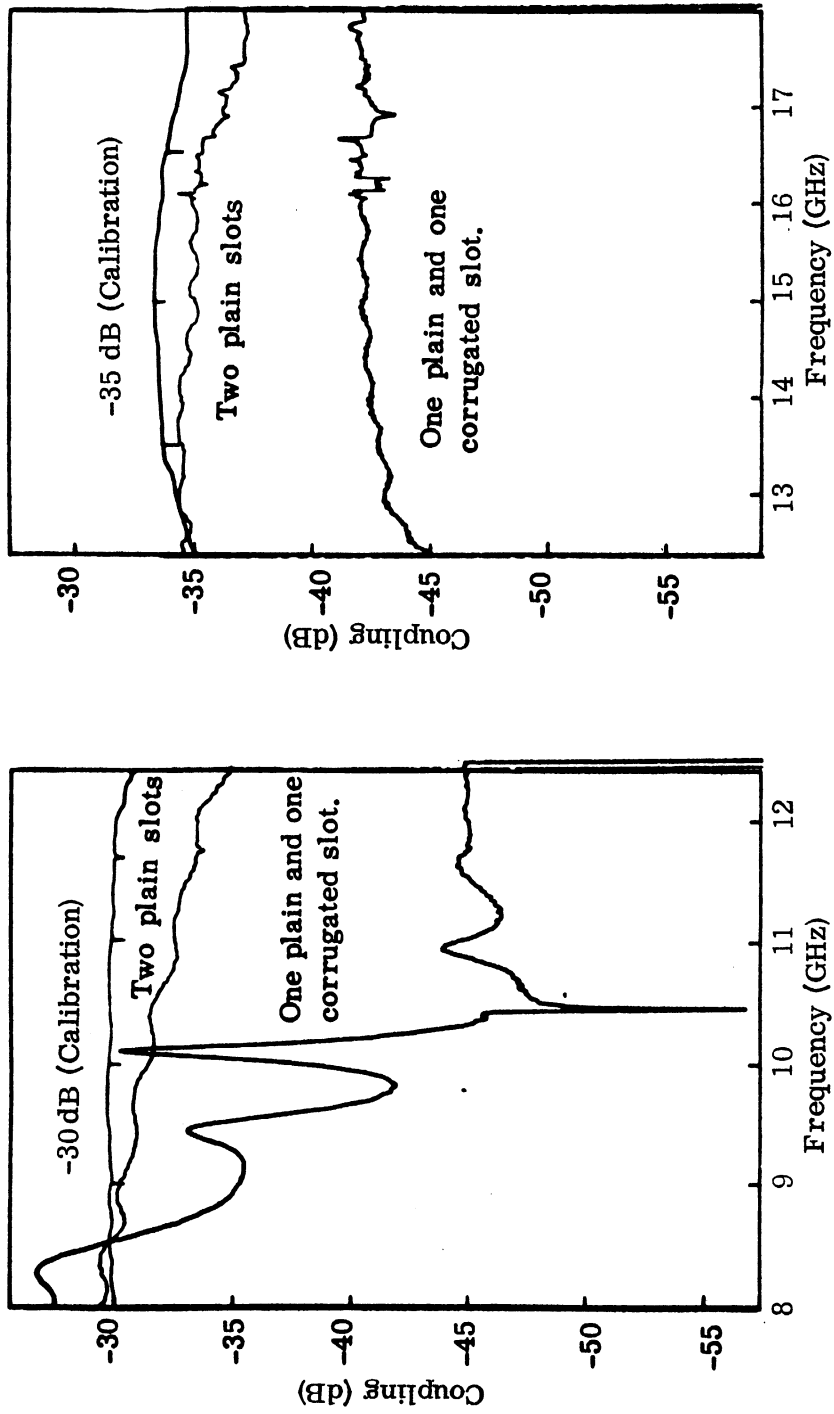
118

FIG. 5-23: E-PLANE COUPLING VS FREQUENCY FOR TWO SLOTS SPACED 11.4 CM (Corrugations R-5).
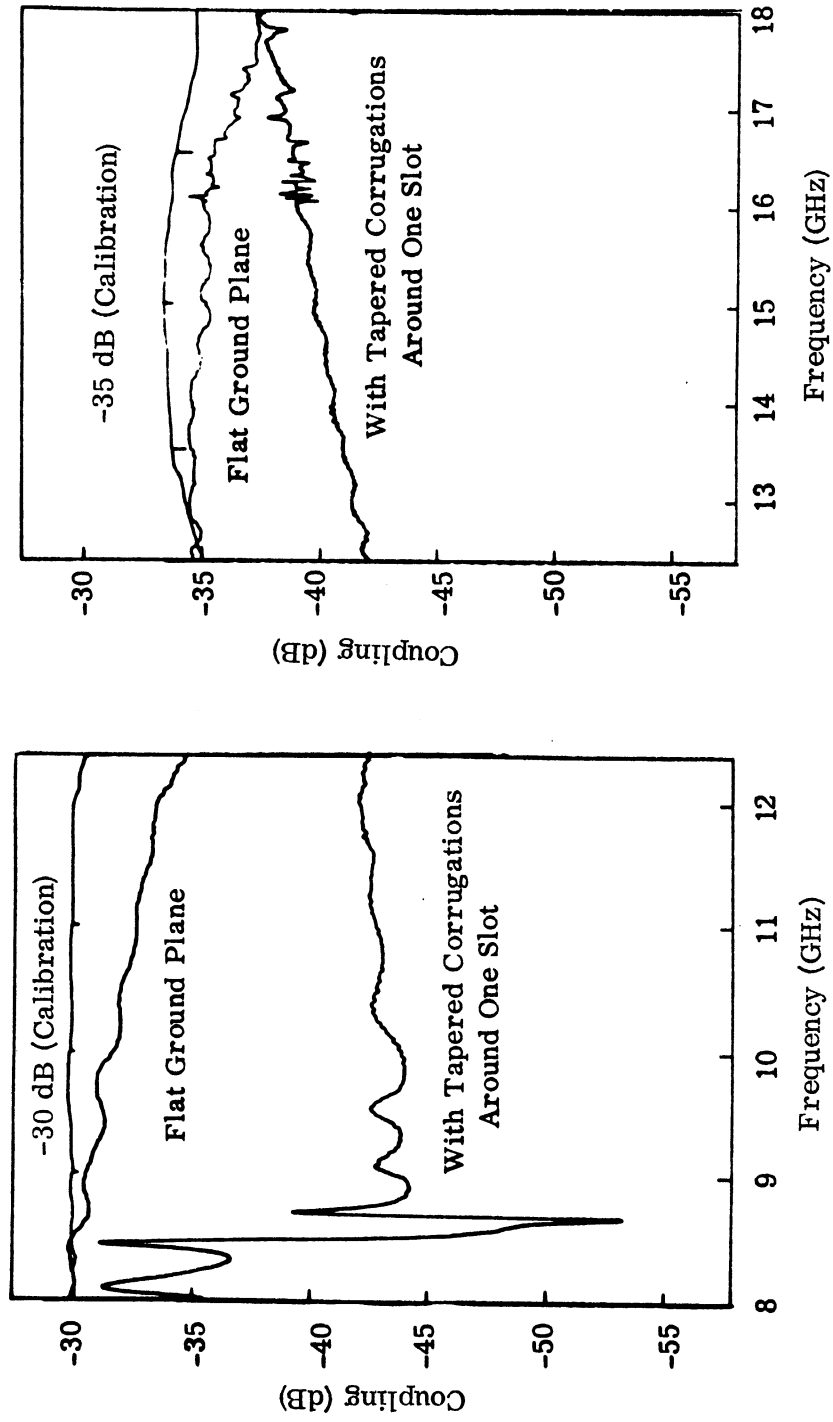
FIG. 5-24: E-PLANE COUPLING VS FREQUENCY FOR TWO SLOTS SPACED 11. 4 CM (Corrugations R-6).

Typical radiation patterns for a slot surrounded by tapered-trench corrugations in a 60 cm by 90 cm (2'x3') rectangular ground plane are shown in Fig. 5-25. This figure shows that the sidelobe decrease is accompanied by a considerable increase in antenna gain. This was examined in more detail, in a swept frequency measurement of maximum gain. The reactive loading increases the antenna gain by as much as 5 dB at some frequencies.

A comparison of the frequencies where the top band starts in each of the three models, between the experimental data and the theoretical derivation of Appendix B, shows that the theoretically predicted values are always too high by 3 to 5 percent. The agreement is very good considering that the analysis was based on a two-dimensional model with infinitely thin walls at the top. The good agreement is due to the fact that all three experimental models had very thin walls at the top. In the case where the trenches are separated by thick walls the more accurate analysis using space harmonics should be used.

The coupling reduction data presented so far were obtained by applying a given modification to one antenna only of a receiver-transmitter pair. It has been stated that twice as much coupling reduction (in dB) would be obtained if both antennas were similarly modified. A justification of this statement is provided by the following experiment. Two slot antennas at a center-to-center spacing of 22.8 cm (7.6λ at 10 GHz) were each surrounded by corrugations. The corrugated disks R-1 and R-6 were used. The coupling reduction obtained when each set of corrugations was used alone and when they were used simultaneously is shown in Fig. 5-26. From this figure it can be verified that the total coupling reduction is equal to the sum of the coupling reductions obtained by each method individually (when all quantities are expressed in dB). See also Fig. 5-22.

5.4 Thin Slot

Thin slots are used in many applications, operating over a narrow band of frequencies. The thin slot is the complimentary antenna of the half-wave dipole. Therefore, it is a low directivity antenna. A slot cut in a large metal sheet and fed by a waveguide or backed by a cavity so that all the radiation is confined to one
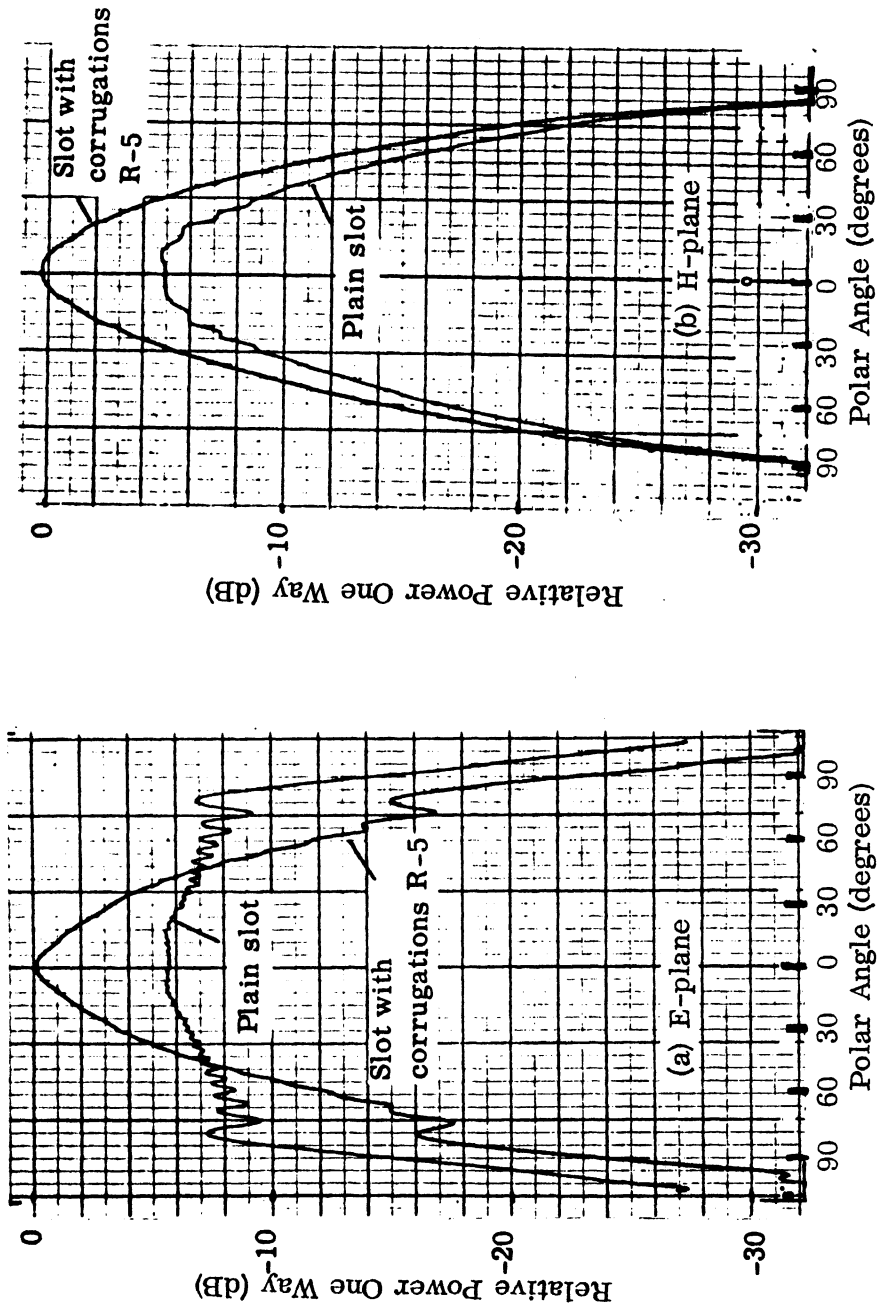
FIG. 5-25: E- AND H-PLANE RADIATION PATTERNS FOR SLOT IN 2'x3' METAL PLANE AT 12 GHz.
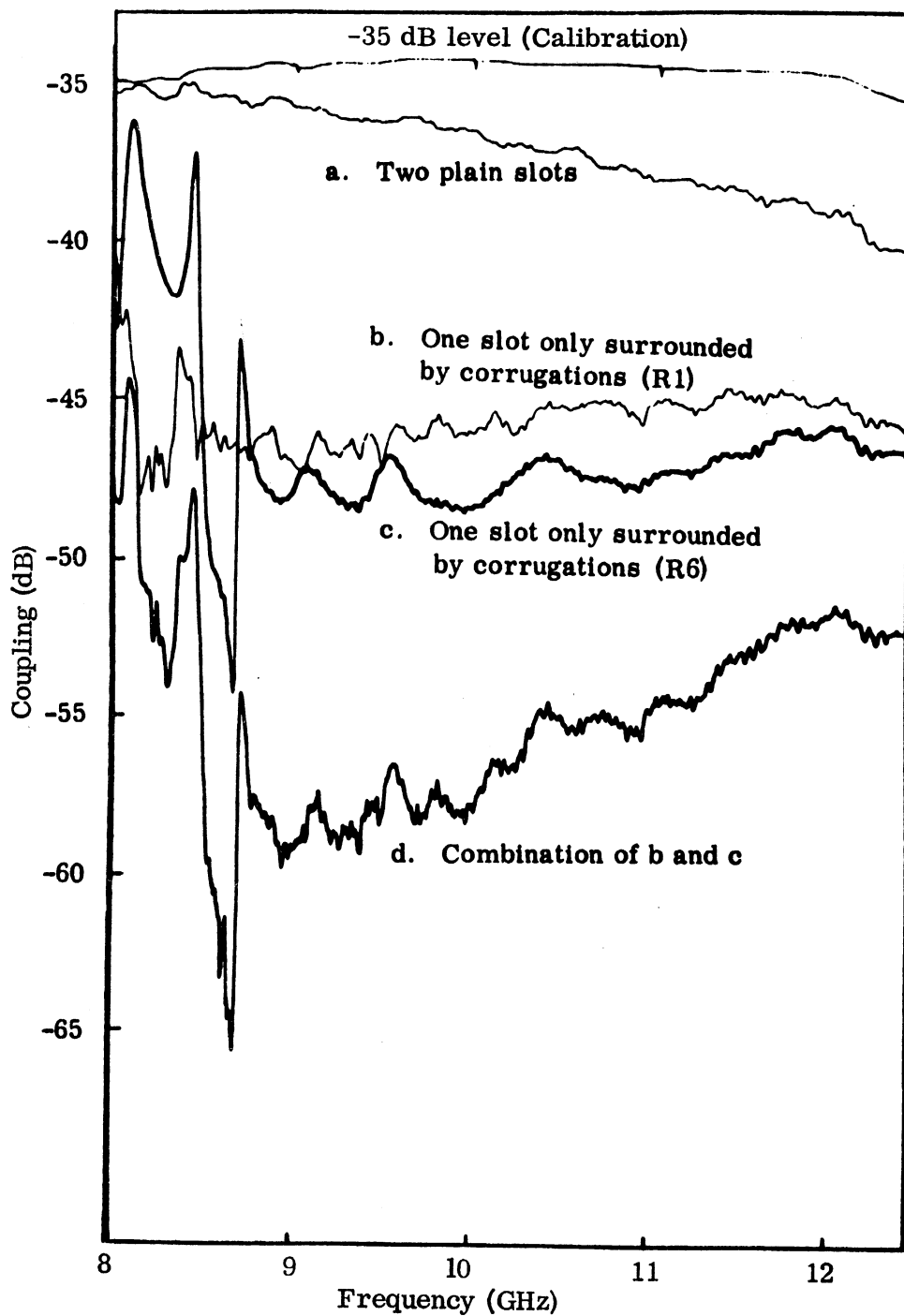
FIG. 5-26: REDUCTION OF E-PLANE COUPLING OF TWO SLOTS SPACED
22.8 CM BY MEANS OF CORRUGATIONS.

side of the sheet, has a directivity of approximately 2 dB above a semi-isotropic radiator (5 dB above isotropic). The use of capacitive reactive loading in the ground plane increases the maximum gain of this antenna by more than 3 dB while at the same time decreases the gain along the ground plane by 10 dB. Thus a slot with ground plane loading can produce a radiation pattern similar to that of a small horn. This may be useful in aerospace applications where it is required that the antenna have a minimum penetration below the surface and therefore the use of a horn is unacceptable.

For the radiation patterns shown in Fig. 5-27, a thin slot of dimensions 2.29 cm by 0.15 cm was mounted in a 12 ft. square ground plane. The slot was fed by an X-band waveguide with tapered walls in the E-plane. Corrugations R-1 were used to create the capacitive surface impedance. The radiation patterns were taken with a probe describing a circumference of radius 1.75 m. A leveled sweep generator was used as a source for all patterns. Because of the high standing wave ratio in the feeding waveguide created by the tapered walls, a tuner was used at every frequency and before the recording of each curve the SWR in the transmission line was reduced to less than 1.2. A very minor tuning was necessary when changing from the flat ground plane to the corrugations, in order to achieve maximum radiated power.

The reduction of the (absolute) gain of the slot at higher frequencies was expected since the slot operated further away from the resonance. The decrease in the amount of sidelobe reduction is due to the fact that the corrugations also operate further away from the design cut-off frequency (cf. with Fig. 5-18). It is interesting to note the split beam appearing at 12 GHz. When the same corrugations were used with a broadband slot no such beam splitting was observed (see Fig. 5-19). The reason for the difference is that when the thin slot was used the distance between the edge of the slot and the beginning of the corrugations, measured along the E-plane, was greater than $\lambda_0 / 2$ at 12 GHz. To be exact, this distance (1.5cm) is equal to $0.55 \lambda_0$ at 11.0 GHz (where no pattern splitting occurs) and to $0.60 \lambda_0$ at 12 GHz (split beam). This then, provides an experimental estimate of how close
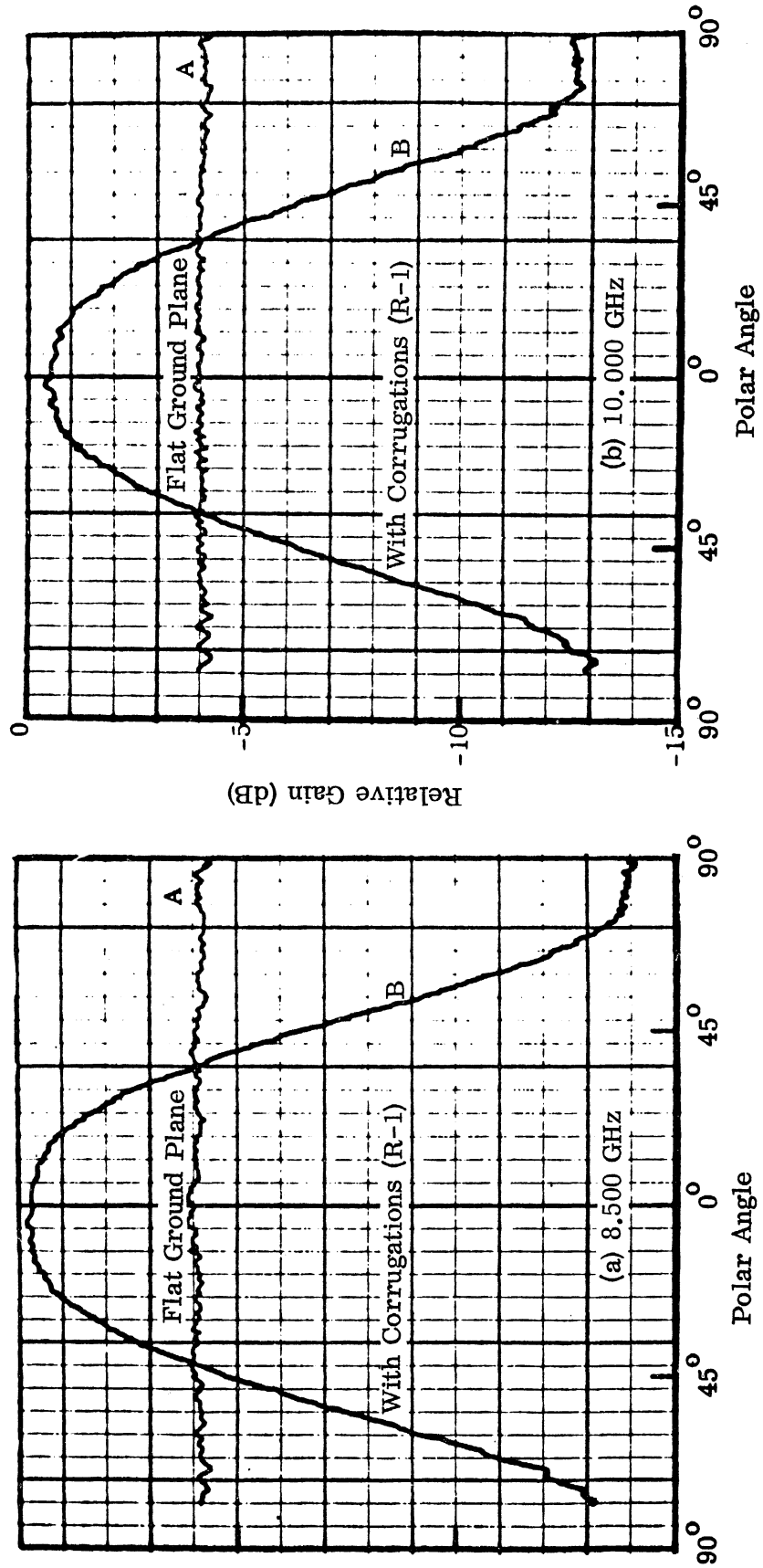
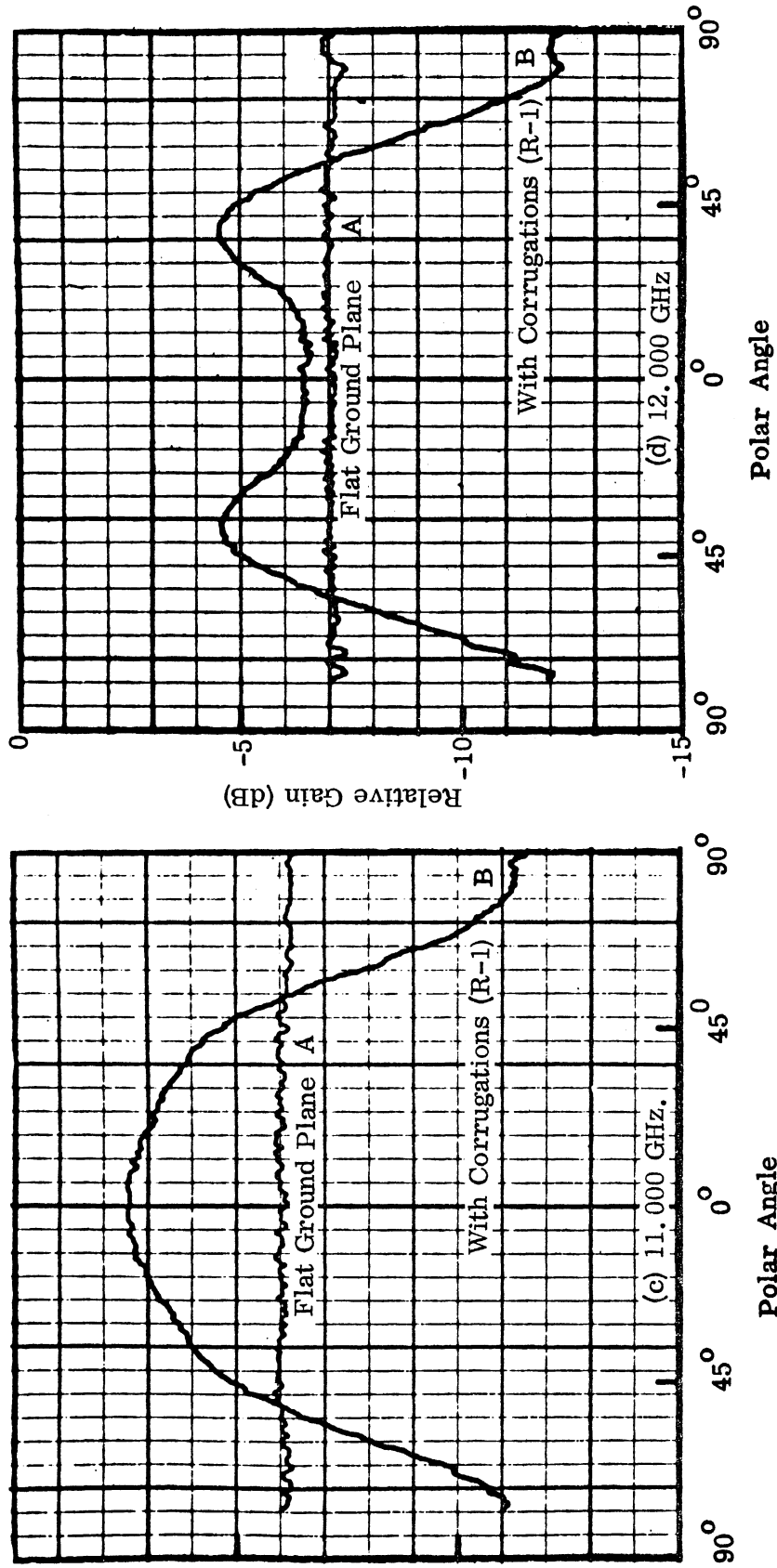FIG. 5-27: E-PLANE PATTERNS OF THIN SLOT (continued on next page).

FIG. 5-27: E-PLANE PATTERNS OF THIN SLOT (continued from previous page).

to the aperture the loading should be in order to avoid splitting of the beam. The more general conclusion is that the reactive loading of the ground plane cannot be considered per se as a method of coupling reduction in a system of two or more antennas, but rather it should be considered in conjunction with an antenna as a means of modification of the properties thereof. Naturally, in order to have maximum effect it is desirable that the loading be adjacent to the antenna aperture.

5. 5 E-Sectoral Horn

The radiation pattern of the E-plane sectoral horn has nulls in the H-plane, as does that of the slot, and very low sidelobes in the E-plane. Therefore the coupling level between two such horns even when aligned with their E-planes collinear is much smaller than the coupling of two slots. Three additional parameters are necessary in order to determine the coupling of two horns; the dimensions of the aperture and the flare angle. The two identical E-sectoral horns that were used for the measurements described below had aperture dimensions 3. 9 cm by 2. 3 cm and a flare angle of 20°. They were fed from the X-band waveguide. The reactive loading was accomplished by placing the corrugated disk S around the horn aperture. These corrugations were designed for use at S-band, however, as it has already been stated, they are also effective at X-band. Due to the smaller wavelength, at X-band the corrugated surface has about 3 trenches per wavelength. The corrugated disk was mounted flush with the surrounding flat area of the ground plane.

The decoupling accomplished with reactive loading around one antenna aperture only is shown in Fig. 5-28. The maximum coupling, over the X-band, was reduced by 9 dB. In this case the antenna center-to-center spacing was on the average 7. 5 wavelengths (22. 8 cm). Radiation patterns were recorded with the transmitting antenna in the same configuration except that the receiving horn aperture was covered, to form a smooth flat surface around the area with the corrugations. The maximum sidelobe reduction of the order of 20 dB, was observed at 8. 64 GHz. The E-plane radiation pattern for this frequency is shown in Fig. 5-29. E-plane radiation patterns are also presented for two more frequencies (Figure 5-30a and b). The corresponding H-plane patterns are not shown because they did not show any appreciable change. A special fixture allowing the pick-up antenna to come as close
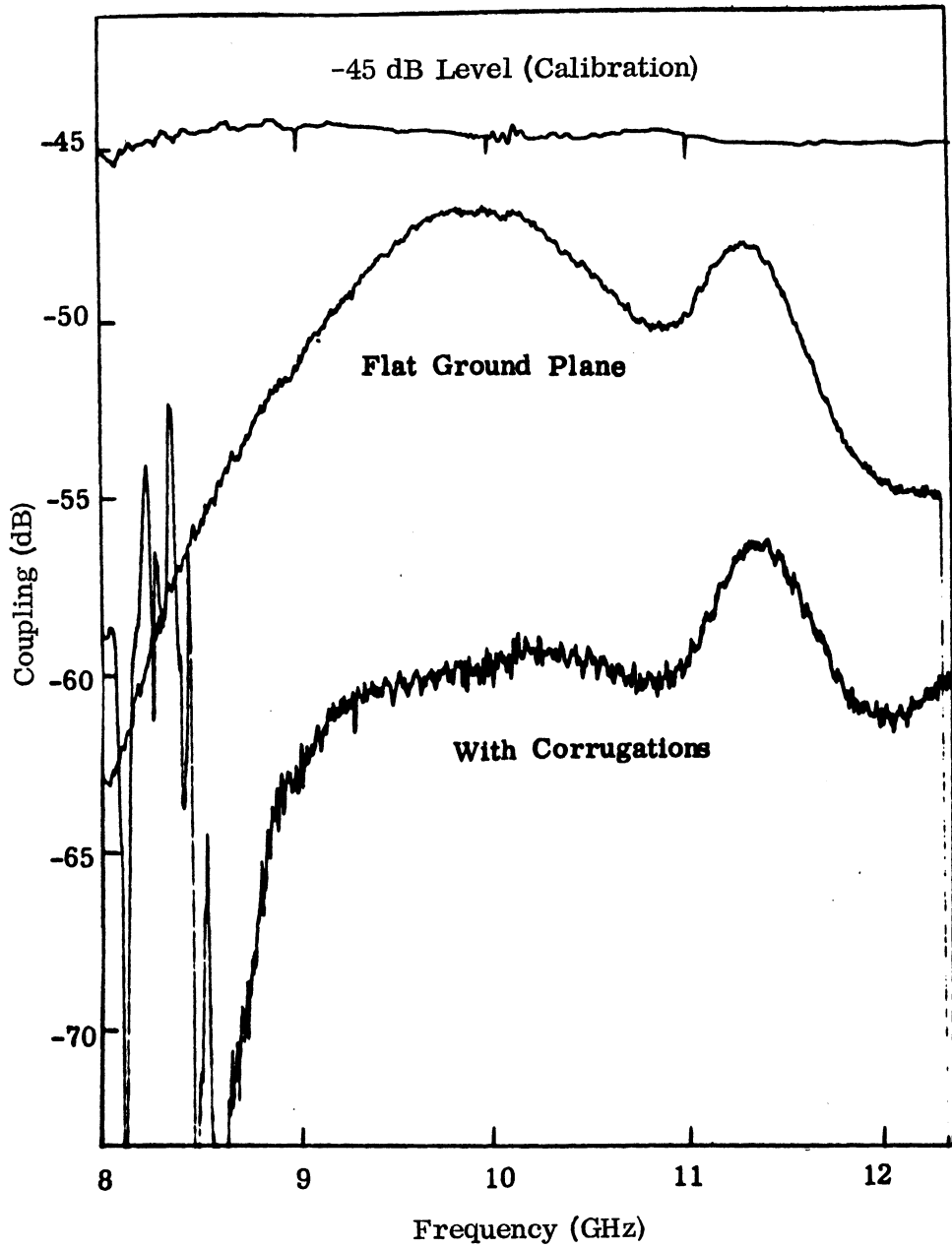
FIG. 5-28: E-PLANE COUPLING OF TWO E-SECTORAL HORNS SPACED 22.8 CM.
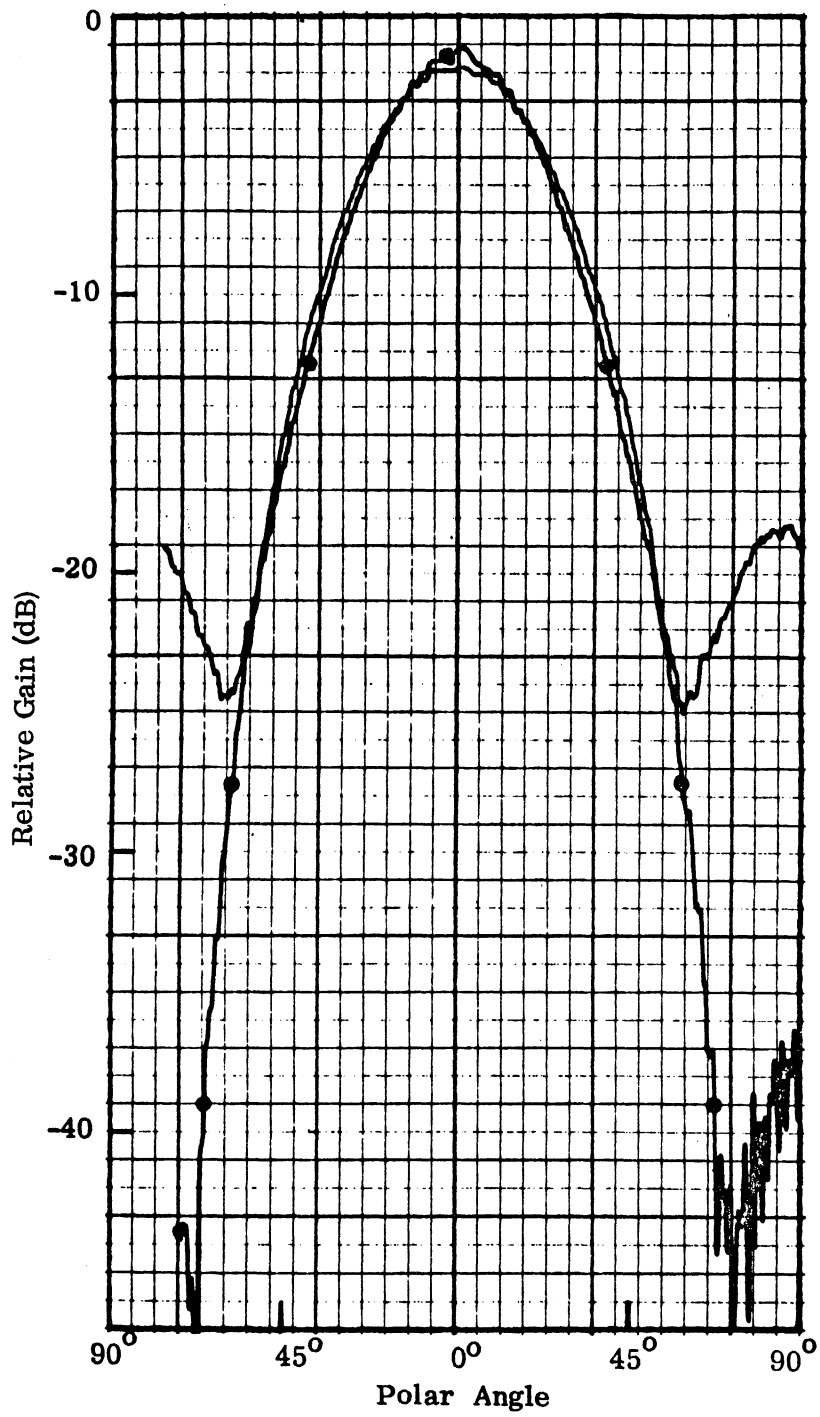
FIG. 5-29: E-PLANE RADIATION PATTERN OF E-SECTORAL
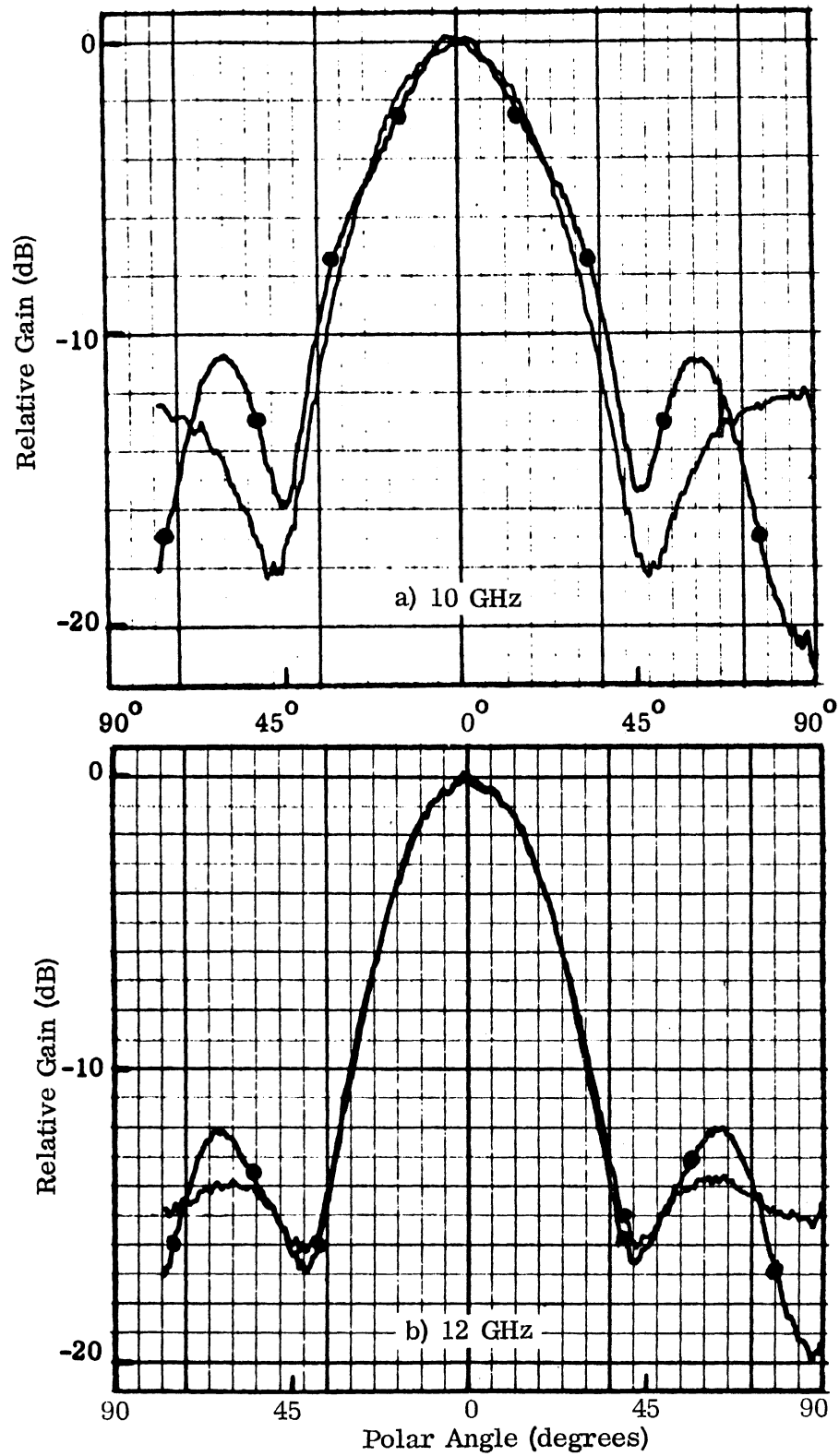HORN AT 8. 64 GHz (—)Flat Ground Plane,
(—•—) With Corrugations.

FIG. 5-30: E-PLANE RADIATION PATTERN OF E-SECTORAL HORN.
(—) Flat Ground Plane (-●-) With Corrugations.

as 0.5° from the ground plane was used for these radiation patterns. Because of this fixture the pick-up antenna travel in the other direction near the ground plane was limited to about 75° and so the patterns may appear as being asymmetrical. Actually only a redundant portion of the patterns has been omitted.

The sidelobe reduction was accompanied by a very small (less than or equal to 0.6 dB) broadside gain increase in contrast to the substantial gain increase which was observed when low directivity antennas were used (cf. with Sect. 5. 3). This is partly due to the fact that in an antenna with medium to high gain in the broadside direction, only a small amount of energy is radiated along the ground plane. By redirecting this energy towards the broadside a small term is added to a large term and therefore only a small change results. Another reason, applicable to the particular case examined here, is that for the experiments of this section, components that were readily available were used. Although the combination gave good results, it did not represent an optimum overall design, the main deficiency being that the distance between the E-plane horn aperture edge and the corrugated area was 3. 8 cm, i. e. more than one wavelength. It has been seen (Fig. 5-13) that the closer the loading to the antenna aperture, the more effective it is and that for a distance between aperture and loading area greater than $\lambda_0/2$, splitting of the beam occurs. Such a beam splitting action appears in the sidelobe shape of the E-plane radiation patterns at 10 and 12 GHz. Higher broadside gain, lower sidelobes and greater coupling reduction than that demonstrated in this section, can be obtained by reactively loading the area in the immediate vicinity of the horn aperture.

Measurements of the standing wave ratio of the sectoral horn with and without the circumferential corrugations showed a very small change.

5. 6 Pyramidal Horn

The pyramidal horn is another example of a flush mounted antenna characterized by medium to high directivity and low sidelobes. Depending upon the aperture dimensions and flare angles, the variation of coupling with frequency may take different forms. The two identical horns used for the coupling measurements had a flare angle of 21° in both the E- and H-plane and aperture dimensions

6. 0 cm (H-plane) by 4. 8 cm. Their gain at 9 GHz was 12 dB. The two horns were flush mounted in the 12 ft. square ground plane at a center-to-center spacing of 22. 8 cm, i. e. in the near field of each other. The set of corrugations S was used around the aperture of one of the two horns. The distance from the edge of the horn aperture to the beginning of the corrugated area measured in the E-plane was 3. 33 cm.

The swept frequency coupling measurement (Fig. 5-31) shows that the maximum coupling over the X-band is reduced from -41 dB to -54 dB. The system coupling reduction of 13 dB would be twice as much if similar loading was employed around both apertures. The maximum gain is slightly higher at some frequencies, with the surface loading (see Fig. 5-32). The sidelobe levels of the horn with and without the surface loading are shown in the same figure. The sidelobe levels were recorded at an angle of 89. 5° from the broadside direction with an 8 dB gain E-sectoral horn used as a pick-up antenna. With the reactive loading of the ground plane the sidelobe level shows a null at 8. 32 GHz as predicted by Eq. (4. 4). (It should be noted that in Fig. 5-32 the curves showing maximum gain have been printed 5 dB lower with respect to the curves showing the sidelobe level for figure compactness. This is reflected in the scale of the axis of ordinates.) The reduction in the sidelobe level represents the reduction in antenna coupling that should be expected if the two antennas were in the far field of each other. A comparison of the near field coupling reduction with that expected in the far field shows that greater reduction is achieved in the near field exactly as in the case of monopoles where the phenomenon was studied in more detail.

Radiation patterns for the E-plane at 9 and 10 GHz are shown in Fig. 5-33a and 5-33b . The reactive loading did not affect the H-plane patterns by more than 0. 5 dB at the most and therefore their presentation is not justified. The comments that were made for the radiation patterns of the E-sectoral horn apply here as well .
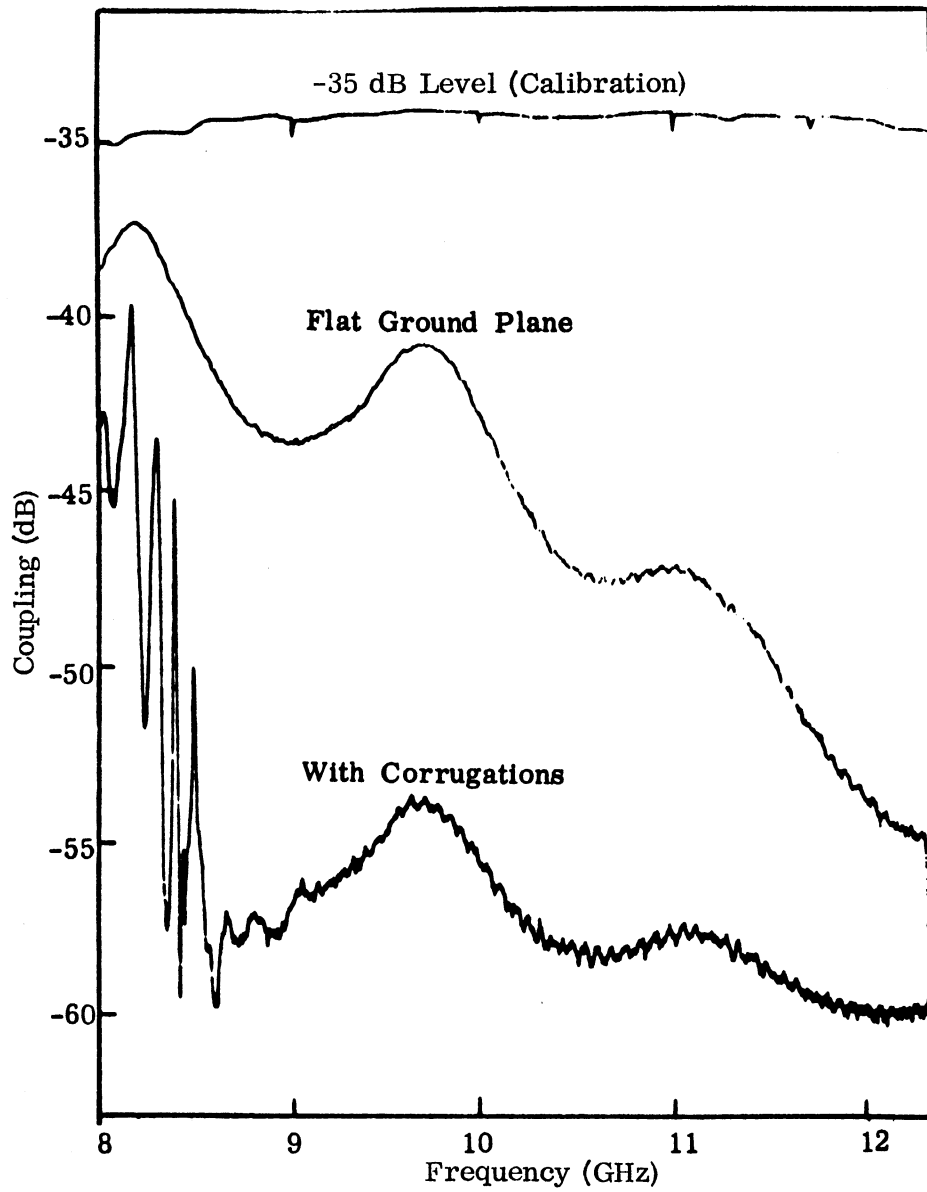
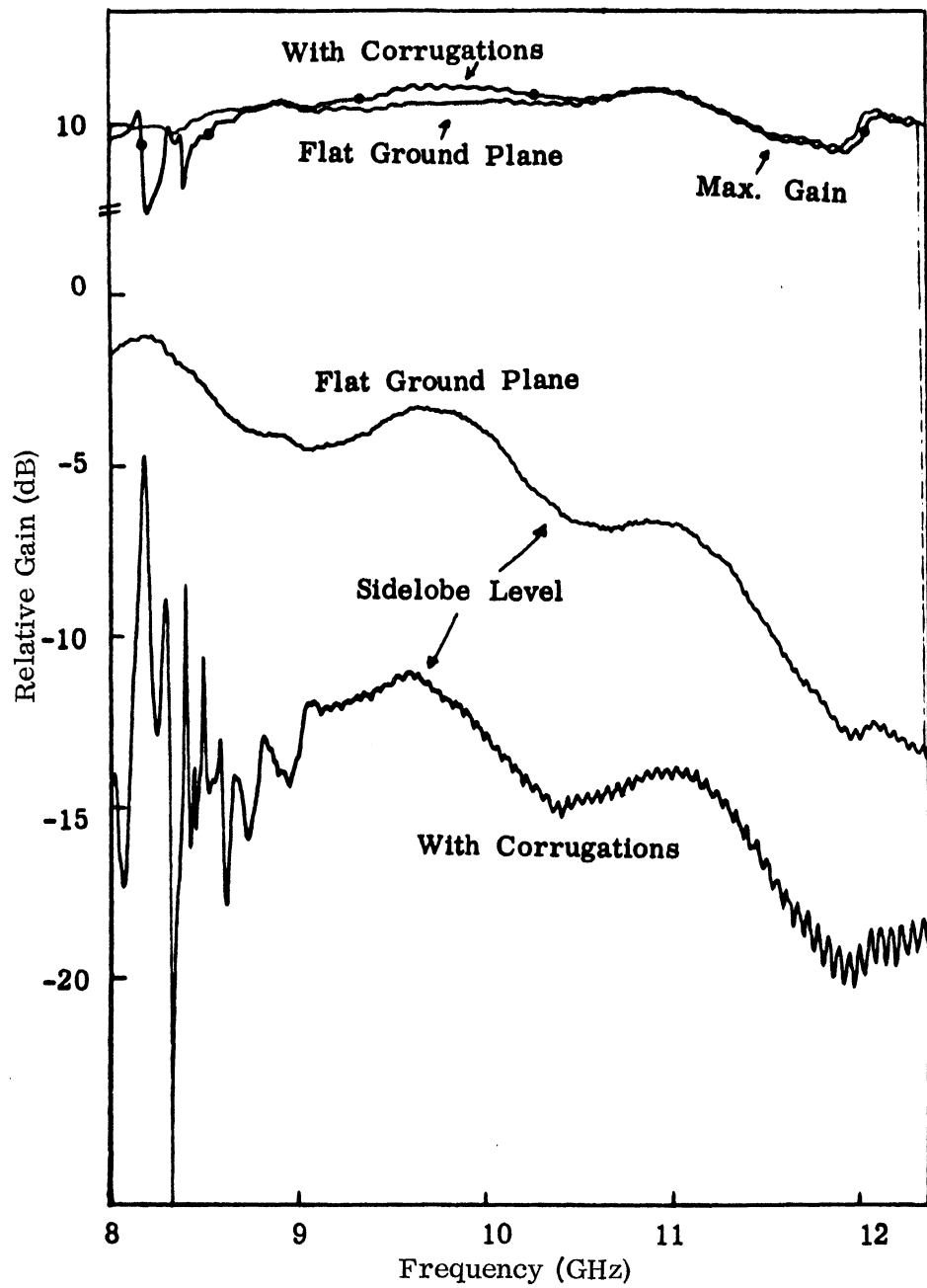FIG. 5-31: E-PLANE COUPLING OF TWO PYRAMIDAL HORNS
SPACED 22.8 CM.

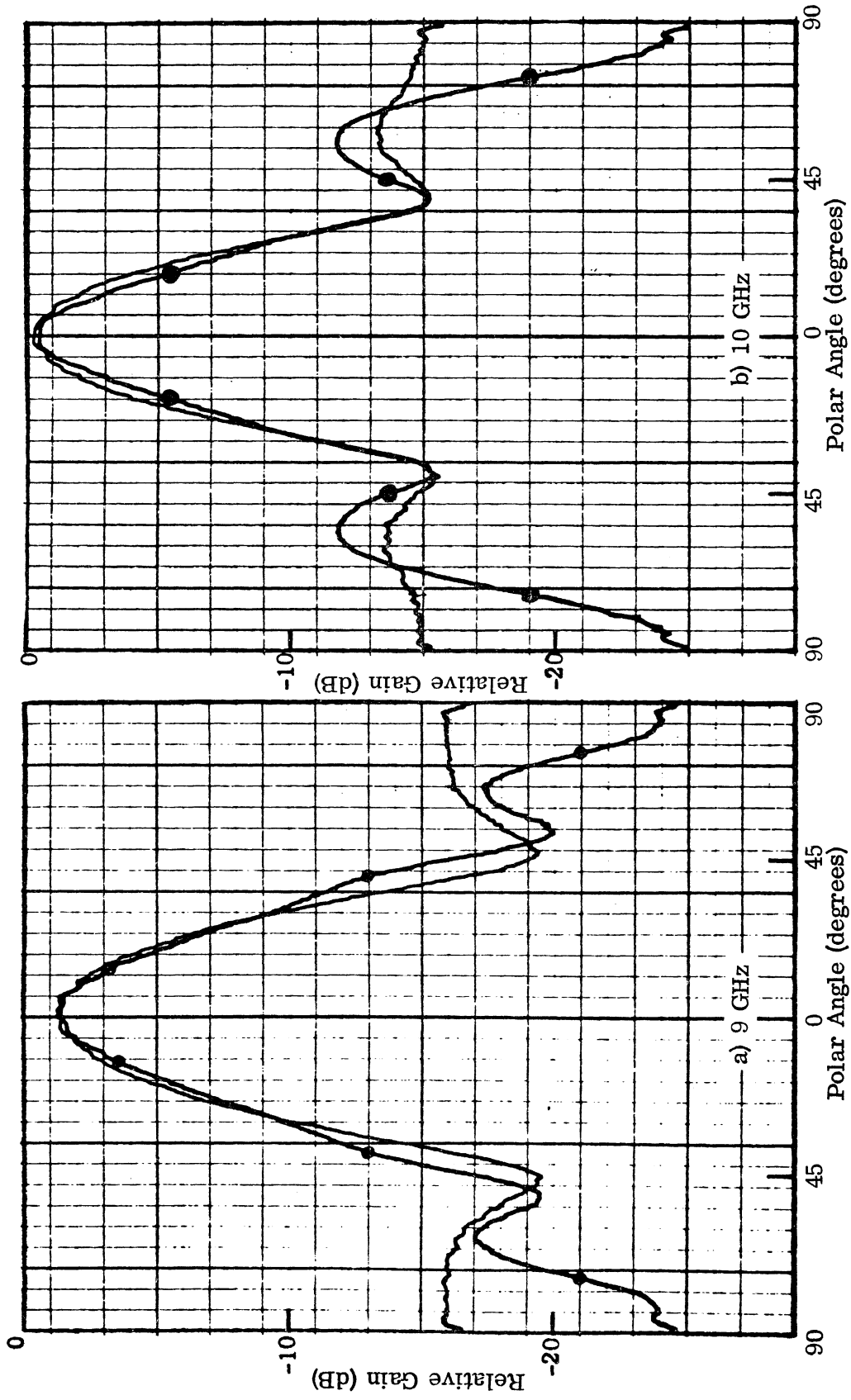FIG. 5-32: MAXIMUM GAIN AND SIDELOBE LEVEL OF PYRAMIDAL HORN.

FIG. 5-33: E-PLANE RADIATION PATTERNS OF PYRAMIDAL HORN (—) Flat Ground Plane,
(—•—) With Corrugations.

5. 7 Archimedean Spiral

The Archimedean spiral provides a practical way of producing circularly polarized radiation over a wide band of frequencies and so it differs from the antennas examined thus far which produce linearly polarized radiation. It is usually mounted flush in a conducting ground plane and backed by a cavity. It may be wound either clockwise or counterclockwise depending on the sense of circular polarization desired. Spiral antennas are usually fed out of phase in order to achieve maximum radiation in the axial direction (axial mode). A balun is used to provide a balanced feed.

When a spiral operates in a pure axial (or first order) mode there is a null along the ground plane and the coupling to another spiral in the same ground plane should be zero. In actual operation, however, reflections from the ends of the spiral elements may occur giving rise to a standing wave along the spiral arms. Also small in-phase currents at the feed excite additional modes, of order zero, two, etc. The zero order mode in particular will cause a considerable amount of radiation along the ground plane. These feed and termination defects are considered to be primarily responsible for the coupling between two spirals. Therefore, this is a case of weak coupling comparable to the H-plane coupling of slots.

Two similar Archimedean spirals made by Aero Geo Astro Corporation (Model AGA-100-3-2) for the frequency range 2 to 4 GHz were used for the measurement of coupling. Each spiral had 13 turns with conductor width 0. 15 cm, spacing of adjacent turns 0. 15 cm, a strip-line Roberts type balun and was backed by a cavity of 10 cm diameter. The two spirals were mounted in a large(12'x12') ground plane at a center-to-center spacing of 22. 8 cm (2. 5λ at 3.3 GHz). The coupling measurements were made by a swept frequency technique. Due to this no matching devices were used between the transmission line and the antennas. A spot check, however, indicated that the use of matching devices results in no more than 1 dB difference in the coupling level. However the defects of the feeds to the spiral are emphasized in swept frequency methods.

For the coupling measurements the two spirals were positioned in three different ways as shown in Fig. 5-34. In this figure the positions of the spirals are determined from the relative orientation of the feed terminals. One of the spiral antennas was surrounded by circumferential corrugations S and then the coupling was measured with the corrugations covered and then uncovered. Similar coupling curves were obtained for the three different combinations of orientations of the feed terminals. The coupling corresponding to two different positions is shown in Fig. 5-35. For any given frequency the coupling depends upon the relative orientation of the two spirals. However, the swept frequency coupling patterns taken for different orientations exhibit the same general characteristics except that the peaks and troughs occur at different frequencies. The corrugations accomplished a moderate coupling reduction of 6 dB in the frequency range 2.8 to 4.0 GHz.

The effects of the corrugations on the spiral radiation pattern at different frequencies are shown in Fig. 5-36. These patterns were obtained by illuminating the spiral with a linearly polarized standard gain horn. The polarization was chosen so that the E-field vector would be perpendicular to the ground plane at $\theta=90^\circ$. The patterns are shown for two different orientations of the spiral; one where the (imaginary) line determined by the two feed points is parallel to the E-field and another where it is perpendicular. A sidelobe decrease of the order of 6 to 11 dB is observed, accompanied by a gain increase. The gain increase due to the corrugations varies from 1 dB at the low end of the frequency range to 0 dB at the high end.

The change in antenna SWR when the ground plane is reactively loaded is summarized in Table V-3.

TABLE V-3: SPIRAL STANDING WAVE RATIO

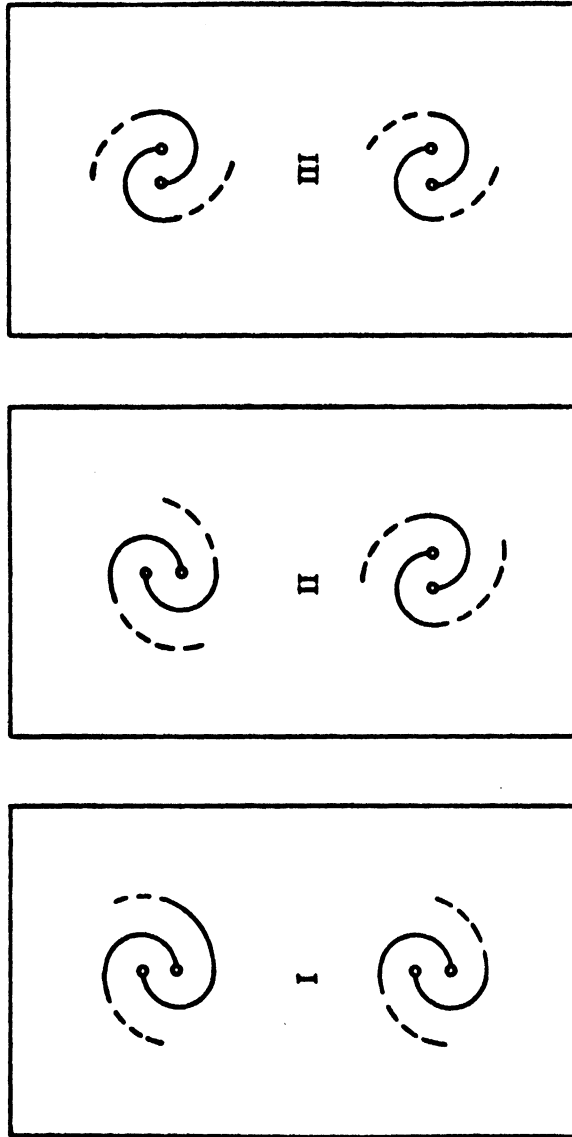| Frequency (GHz)	2.75	3.00	3.25	3.50	3.75	4.00
Flat Ground Plane	1.45	1.33	1.26	1.90	1.79	1.75
With Corrugations	1.60	1.42	1.47	1.31	1.40	1.37

137

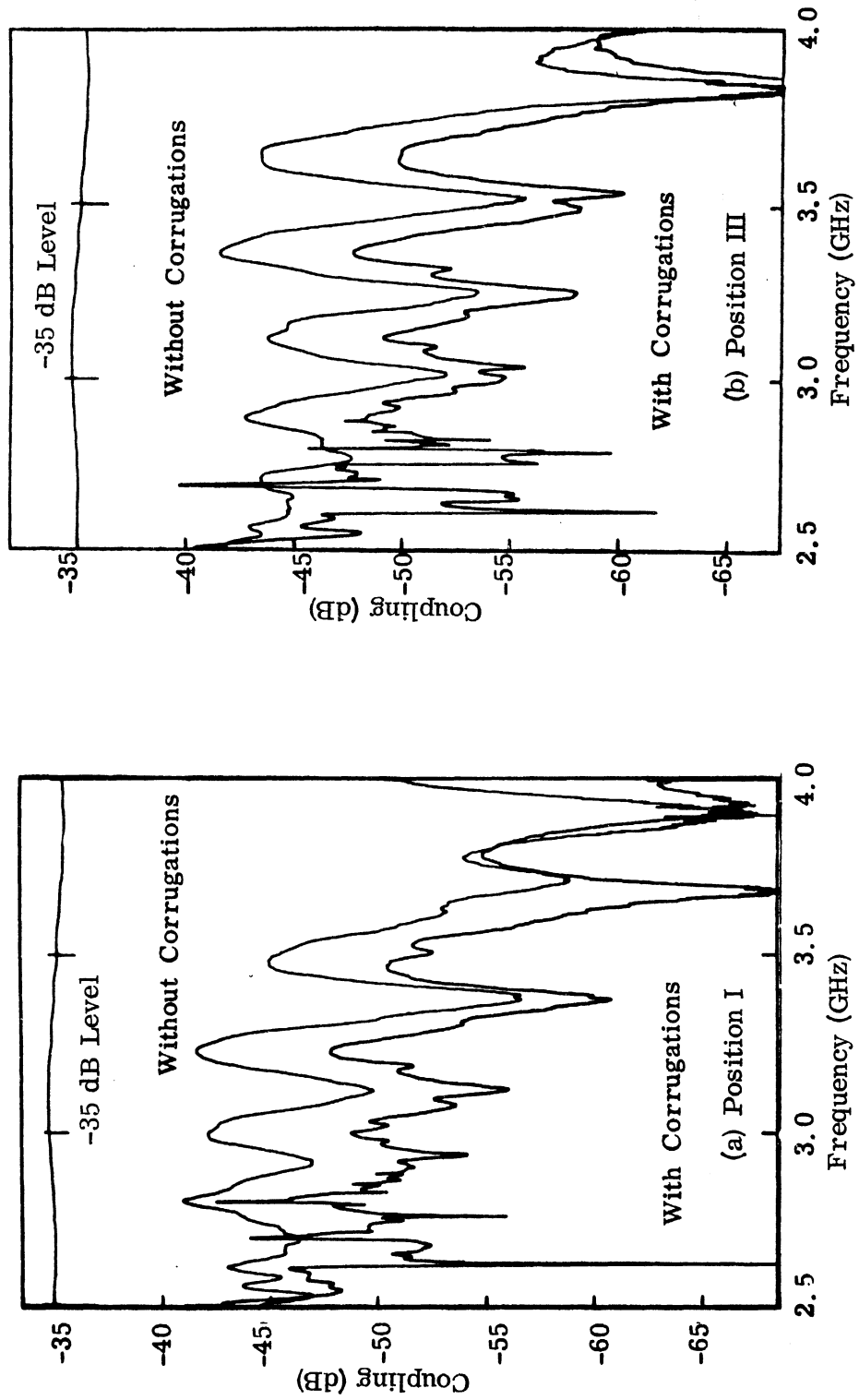FIG. 5-34: RELATIVE POSITIONS OF CIRCULAR SPIRALS (FEEDS).

FIG. 5-35: COUPLING VS FREQUENCY FOR TWO ARCHIMEDEAN SPIRALS SPACED 22.8 CM.
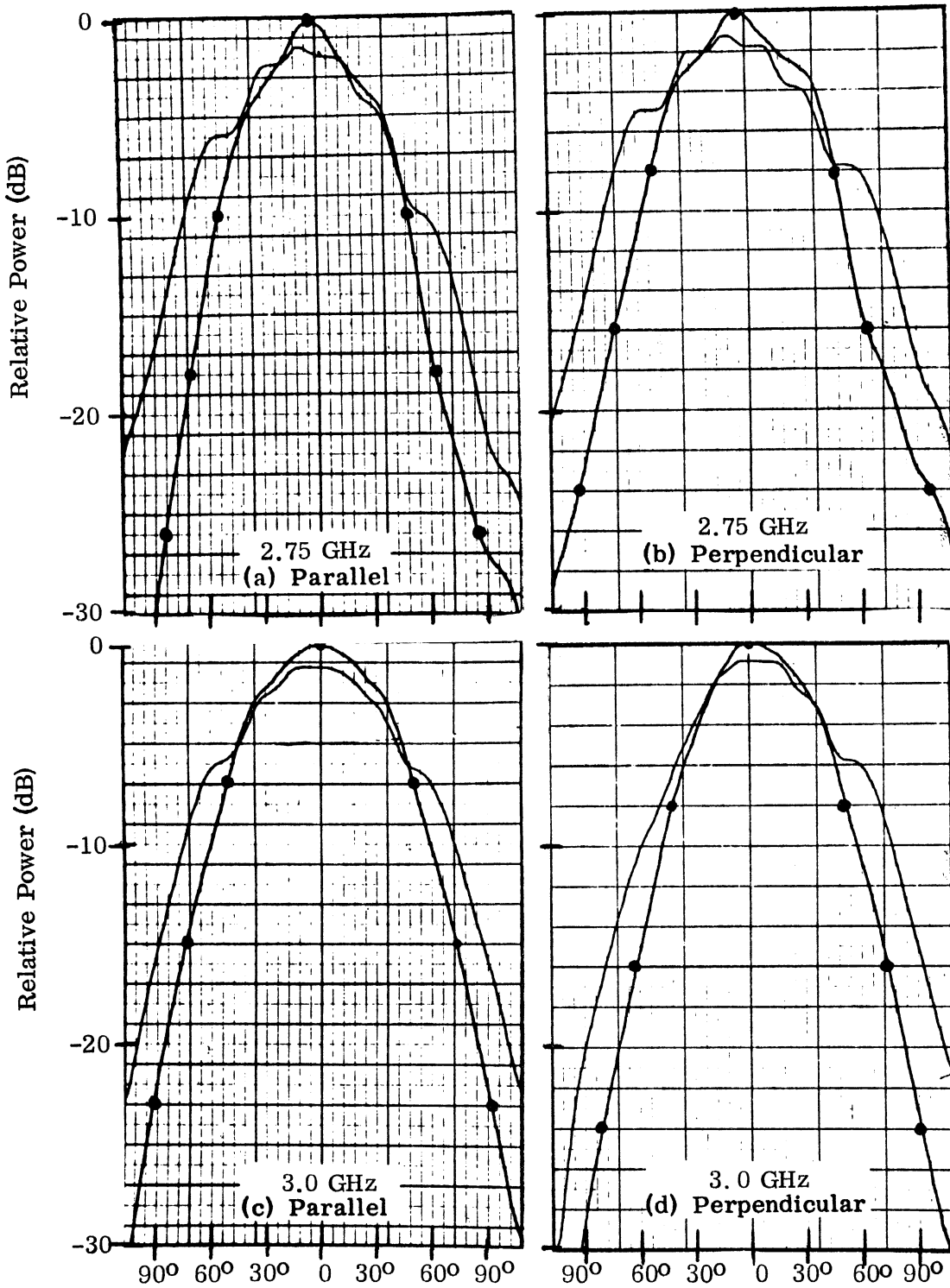
FIG. 5-36: RADIATION PATTERNS OF ARCHIMEDEAN SPIRAL IN 2'x3'
METAL GROUND PLANE FOR TWO NORMAL LINEAR
POLARIZATIONS (—)Flat Plane (-●-) With Corrugations.

VI

CONCLUSIONS

Although a great deal of work has been done regarding the propagation of surface waves above corrugated surfaces and their radiation, very little was known about the performance of finite extent corrugated surfaces below the surface wave cut-off frequency. The present study without being exhaustive on the subject has resulted in several original contributions.

1. The use of capacitive surface reactance loading of the ground plane has been proved successful as a method of reducing the mutual coupling and the antenna sidelobes in a frequency range extending over at least one waveguide band of frequencies.

2. Expressions were derived for the radiation resistance and directivity of a short monopole as well as a quarter-wavelength monopole antenna over an infinite screen with a capacitive surface reactance. The variation of the direction of maximum radiation was studied as a function of the surface reactance.

3. The radiation pattern of a short monopole over an infinite screen with an annulus of capacitive surface impedance was obtained theoretically. This result was then used to study the optimum position of the annulus for maximum coupling reduction and maximum antenna gain. The monopole input impedance, near field coupling and radiation pattern were obtained experimentally. The comparison between the experimental and theoretical radiation patterns has shown a reasonably good agreement, the relative difference being less than 10 percent for $30^{\circ} \leqq \theta \leqq 90^{\circ}$ and X= -1.89. With the use of annular loading (ka$\neq$ 0) the significant reduction in antenna radiation resistance, which occurs when ka=0, is avoided. The radiation resistance must be considerably larger than the ohmic losses in order to have reasonable antenna efficiency and good matching with the characteristic impedance of conventional transmission lines.

4. The effect of capacitive surface loading on the radiation pattern, impedance (or SWR) and near field coupling of various types of slot, horn and spiral antennas was studied experimentally. It was generally found that the sidelobe reduction is accompanied by an increase in antenna gain which was more pronounced in the case of low-gain antennas.

5. Corrugations with a trapezoidal profile were used. Their surface impedance was theoretically derived assuming that only the dominant TEM mode propagates inside the trenches.

The position of the loaded area with respect to the antenna was found to be a very important factor indicating that in any case of ground plane loading the problem of the antenna with the appropriate boundary condition must be solved. A model based solely on the attenuation of a wave as it passes over a finite zone of capacitive reactance may lead to gross inaccuracies as to the predicted coupling reduction. Indiscriminate positioning of loading could also create significant degradation in the antenna radiation pattern. This has been demonstrated in the present study and elsewhere (Lyon, et al, 1968).

The control over the direction of the monopole maximum gain obtained by surface loading may be useful in certain applications. For example, the command antenna of the Nimbus Meteorological Satellite is a monopole with the requirement of maximum gain at $\theta=58^{\circ}$(Post, 1967). On the basis of the increased directivity of a slot with capacitive loading, the loading may also be considered as a size reduction method since instead of using e.g. a horn to obtain a certain directivity, one may use a thin slot with surface loading. Thus there is a trade-off between volume and surface.

When the capacitive surface reactance is created by means of corrugations, the frequency dependence of the reactance imposes a restriction on the bandwidth over which the method is effective. Maximum coupling reduction is obtained at the surface wave cut-off frequency. The amount of this reduction gradually decreases as the frequency is increased until it becomes nearly zero at the frequency where the depth of the corrugations is equal to $\lambda_0/2$. However, this disadvantage is off set to some extent by the fact that the coupling is also frequency dependent. When the antennas are oriented so that their E-planes coincide, the coupling is reduced at a rate of 6 dB per octave of frequency while when the H-planes coincide the reduction is 12 dB per octave - provided that the distance between the two antennas is greater than two wavelengths. Besides, the interlacing of stop bands with pass bands which is inherent in the corrugations extends their usefulness to other frequency ranges roughly corresponding to the odd-harmonics of the first stop band. An upper limit is imposed since the number

of corrugations per wavelength should be at least three.

The extension of the theory to ground planes terminating at the outer radius of the corrugations is straightforward. Instead of using image theory, as was done in Chapter III, one would have to add the contribution of the surface currents in region 1 (which is of a simple form) to that of the surface currents in region 2 - which has already been obtained.

For future work it is suggested that an exact solution be obtained for the problem posed in Chapter III. An approximate analysis based on the modified geometrical theory of diffraction (Keller, 1957, 1962) may also be used. The corresponding canonical problem for this formulation is that of a plane wave propagating along a plane which at first is perfectly conducting and at some point changes into a capacitive surface impedance. A more accurate solution based on the actual configuration of the physical model, rather than the impedance boundary condition, would be desirable.

Approximate analyses of the radiation properties of aperture antennas with reactive loading seem to be easier to carry out. Such studies could be based on a distribution of short electric monopoles or a magnetic line source on the E-plane edge of the antenna aperture to represent the wave diffracted by the edge. One would then proceed with an assumed current distribution based on the corresponding canonical problem - as was done for the monopole.

A study of the loading with variable impedance may also be of interest.

BIBLIOGRAPHY

Allen, J. (1965), "Mutual Coupling — Why Worry About It?," IEEE International Ant. and Prop. Symp. Digest, pp. 133-137.

Andersen, J. B. (1967), "An Analysis of Surface Wave Antennas," Electromagnetic Wave Theory (Proceedings of URSI-Delft Symposium, September 1965), Pergamon Press, pp. 729-738.

Barlow, H. M. and A. L. Cullen (1953), "Surface Waves," Proc. IEE (London), Pt. III, 100, pp. 329-341.

Borgiotti, G. (1963), "Fourier Transform Method in Aperture Antenna Problems," Alta Frequenza, 32, pp. 808-816.

Bouwkamp, C. J. (1950), "On Sommerfeld's Surface Wave," Phys. Rev., 80, p. 294.

Carl, J. R. and S. A. Guccione (1966), "Gemini Rendezvous Radar Error," Microwave J., 9, pp. 75-78.

Cullen, A. L. (1954), "The Excitation of Plane Surface Waves," Proc. IEE (London), Pt. IV, 101, pp. 225-234.

Cutler, C. C. (1944), "Electromagnetic Waves Guided by Corrugated Conducting Surfaces," Bell Telephone Laboratory Report MM-44-160-218 (October).

Edelberg, S. and A. A. Oliner (1960), "Mutual Coupling Effects in Large Antenna Arrays-II: Compensation Effects,". IRE Trans. Ant. Prop., AP-8, pp. 360-367.

Ehrlich, M. J. and L. L. Newkirk (1953), "Corrugated Surface Antennas," IRE Nat'l Conv. Record, Part 2, pp. 18-33.

Elliott, R. S (1954), "On the Theory of Corrugated Plane Surfaces," IRE Trans. Ant. Prop., AP-2, pp. 71-81.

Epstein, P. S. (1947), "Radio Wave Propagation and Electromagnetic Surface Waves," Proc. Nat. Acad. Sci., 33, pp. 195-199.

Erdélyi, A. (1956), Asymptotic Expansions, Dover Publications, New York.

Fernando, W. M. G. and H E. M. Barlow (1956), "An Investigation of the Properties of Radial Cylindrical Surface Waves Launched over Flat Reactive Surfaces," Proc. IEE (London), 103, pp. 307-318.

Furutsu, K. (1959), "On the Electromagnetic Radiation from a Vertical Dipole Over the Surface of Arbitrary Surface Impedance," J. Rad. Res. Labs. (Tokyo), 6, pp. 269-291.

Furutsu, K. (1959), "On the Excitation of the Waves of Proper Solutions," IRE Trans. Ant. Prop., Special Issue, AP-7, pp. S 209-S 218 .

Jones, E. M. T. (1952), "An Annular Corrugated-Surface Antenna," Proc. IRE, 40, pp. 721-725.

Hurd, R. A. (1954), "The Propagation of an Electromagnetic Wave Along an Infinite Corrugated Surface," Can. J. Phys., 32, pp. 727-734.

Kane, J. (1963), "The Mathematical Theory of a Class of Surface Wave Antennas," Quart. of Appl. Math., 21, pp. 199-214.

Kay, A. F. (1959), "Scattering of a Surface Wave by a Discontinuity in Reactance," IRE Trans. Ant. Prop., AP-7, pp. 22-31.

Kay, A. F. (1964), "The Scalar Feed," TRG Inc., Sci. Report No. 5, AFCRL-64-347. (March).----

Keller, J. B. and F. C. Karal, Jr. (1960), "Surface Wave Excitation and Propagation," J. Appl. Phys., 31, pp. 1039-1046.

Keller, J. B. (1957), "Diffraction by an Aperture," J. Appl. Phys., 28, pp. 426-444.

Keller, J. B. (1962), "Geometrical Theory of Diffraction," J. Opt. Soc. Amer., 52, pp. 116-130.

Khan, P. J., W. R. DeHart, R. M. Kalafus, A. I. Simanyi, R. B. Harris, W. S. Heath, and D. M. Oliver (1964), "Derivation of Aerospace Antenna Coupling Factor Interference Prediction Techniques," The University of Michigan Cooley Electronics Laboratory Report 4957-8-F.

Knott, E. F. (1965), "Design and Operation of a Surface Field Measurement Facility," The University of Michigan Radiation Laboratory Report 7030-7-T, AD-482481 (December).

Kottler, F. (1923), "Elektromagnetische Theorie der Beugung an schwartzen Schirmen," Ann. der Physik, 71, pp. 457-508.

LaGrone, A. H. and G. F. Roberts (1966), "Minor Lobe Suppression in a Rectangular Horn Antenna Through the Utilization of a High Impedance Choke Flange," IEEE Trans. Ant. Prop., AP-14, pp. 102-104.

Lawrie, R., L. Peters, Jr. and C. Davis (1965), "Antenna Lobe Suppression-Vol. I: Modification of Horn Antennas for Low Sidelobe Levels," The Ohio State University Report RADC-TR-65-186 (October).

Lawrie, R. E. and L. Peters, Jr. (1966), "The Control of the Echo Area of Ogives by Cut-off Corrugated Surfaces," IEEE Trans. Ant. Prop., AP-14, pp. 798-799.

Lechtreck, L. W. (1968), "Effects of Coupling Accumulation in Antenna Arrays," IEEE Trans. Ant. Prop., AP-16, pp. 31-37

Levine, H. and J. Schwinger (1950), "On the Theory of Electromagnetic Wave Diffraction by an Aperture in an Infinite Plane Conducting Screen," Comm. Pure and Appl. Math., III, pp. 355-391.

Lyon, J. A. M., C. J. Digenis, W. W. Parker and M. A. H. Ibrahim (1968), "Electromagnetic Coupling Reduction Techniques, " The University of Michigan Radiation Laboratory Report 7692-1-F, AFAL-TR-68-132, AD 834 900 (June).

Lyon, J. A. M., R. M. Kalafus, Y-K Kwon, C. J. Digenis, M. A. H. Ibrahim and C-C Chen (1966), "Derivation of Aerospace Antenna Coupling Factor Interference Prediction Techniques, " The University of Michigan Radiation Laboratory Report 6633-1-F, AFAL-TR-66-57, AD 483051 (April).

Magnus, W., F. Oberhettinger and R. P. Soni, (1966), Formulas and Theorems for the Special Functions of Mathematical Physics, Springer-Verlag, New York, 3rd Ed.

Meixner, J. (1956), "The Radiation Pattern and Induced Current in a Circular Antenna with an Annular Slit, " IRE Trans. Ant. Prop., AP-4, pp. 408-411.

Post, C. C. (1967), "A Description of the Antenna Systems for the Nimbus-B Meteorological Satellite, " Proceedings of the 17th Annual Symposium of USAF Antenna Research and Development, Monticello, Illinois.

Radio Research Laboratory Staff (1947), Very High Frequency Techniques, Harvard University Press.

Rhodes, D. R. (1964), "On a Fundamental Principle in the Theory of Planar Antennas, " Proc. IEEE, 52, pp. 1013-1021.

Rotman, W. (1951), "A Study of Single-Surface Corrugated Guides, " Proc. IRE, 39, pp. 952-959.

Saunders, W. K. (1956), "Control of Surface Currents by the Use of Channels, " IRE Trans. Ant. Prop., AP-4, pp. 85-87.

Schelkunoff, S. A. (1939), "On Diffraction and Radiation of Electromagnetic Waves, " Phys. Rev., 56, pp. 308-316.

Schelkunoff, S. A. and H. T. Friis (1952), Antennas: Theory and Practice, J. Wiley and Sons, New York, p. 214.

Sommerfeld, A. (1909), " Über die Ausbreitung der Wellen in der Drahtlosen Telegraphie, " Ann. Physik., 28, p. 665.

Sommerfeld, A. (1949), Partial Differential Equations in Physics , Academic Press, New York, p. 246.

Stratton, J. A. and L. J. Chu (1939), "Diffraction Theory of Electromagnetic Waves, " Phys. Rev., 56, pp. 99-107.

Tai, C-T (1967), "The Induced MMF Method, " IEEE Trans. Ant. Prop., AP-15, pp. 527-530.

Toraldo di Francia, G. (1953), Electromagnetic Waves, Interscience, New York p. 218.

Tseng, D. T. (1967), "Guiding and Scattering of Electromagnetic Fields by Corrugated Structures," Polytechnic Institute of Brooklyn Sci. Rep. PIB MRI-1371-67 (July).

Wait, J. R. (1957), "Excitation of Surface Waves on Conducting, Stratified, Dielectric-Clad and Corrugated Structures," J. Res. NBS, 59, pp. 365-377.

Watkins, D. A. (1958), Topics in Electromagnetic Theory, J. Wiley and Sons, New York. p. 18.

Whiteside, II. (1962), "Electromagnetic Field Probes," Harvard Cruft Laboratory Report 377 (October).

Zucker, F. J. (1961), "Surface and Leaky Wave Antennas," Antenna Engineering Handbook (Ed. Jasik), Ch. 16., McGraw-Hill Book Company, New York.

APPENDIX A

NUMERICAL COMPUTATIONS

The numerical computations for the radiation patterns presented in Chs. III and IV were performed on an IBM 360/67 Computer. For an overall check of the expressions derived in Ch. III and the computer program, the integrand of I (Eq. 3. 42) was computed and plotted versus x and then I was obtained by a graphical integration. Thus, using different limits for the integral both functions $\Phi(x)$ and $\psi(x)$ were checked.

The useful domain of $\Phi(x)$ and $\psi(x)$ depends on X as well as x and θ. Thus a new function $\Omega(x)$ was introduced in the main computer program defined by

$$\Omega(x) = \begin{cases} \Phi(x) \text{ if } x \leqq x_{max} \text{ or } x \sin\theta \leqq 5 \\ \\ \psi(x) + j \sin\theta (1 - \dfrac{\cos\theta}{\cos^2\theta + X^2}) \text{ , otherwise} \end{cases} \qquad (A.1)$$

and the functions $\Phi(x)$ and $\psi(x)$ were programmed as subroutines. The domain of $\Phi(x)$ has an upper bound $x = x_1$ established by the limit in the round-off error in the infinite series. The domain of $\psi(x)$ has two low bounds $x\sin\theta = 5$ and $x = x_2$ which serve to guarantee the accuracy of the asymptotic expansions for $J_1(x\sin\theta)$ and $G(x)$ respectively. Thus x_{max} is the minimum of x_1 and x_2. Whenever either function could be used $\psi(x)$ was preferred because it required fewer computations. Evidently when $x_1 < x_2$ or $x \sin\theta < 5$ and $x > x_1$ neither function can be used. However, in the wide variety of parameter values that were used the first condition never occurred while the second occurred only for $\theta < 20^o$ and $x > 15$ (for $X = -1$) or $x > 8.5$ (for $X = -2.5$). Actually for a given X, x_{max} was determined directly by comparing the two expressions for $\Omega(x)$ at $\theta = 90^o$. The relative differences thus obtained were $\Delta = .002$ for $X = -1$ and $x = 12$ and $\Delta = .00004$ for $X = -2.5$ and $x = 5$. For $-1 < X < 0$ only $\Phi(x)$ was used.

147

In the subroutine for Φ (x) the terms of the finite series (eq. 3. 56) were multiplied by m! and the terms of the infinite series were divided by m! in order to avoid the presence of very small and very large numbers in the intermediate computations. The computation of terms of the inner and outer infinite series stopped when the ratio of the latest term to the partial sum was absolutely less than 10^{-8} and 10^{-5} respectively. In the subroutine for Ψ (x) the number n_0 (eq. 3. 64) was determined on the basis of the convergence of G(x) (eq. 3. 18). Thus n_0 was chosen as the minimum of the index of the first term that was absolutely less than 10^{-3} times the corresponding partial sum and the index of the absolutely smallest term.

In several tests comparing the two expressions for Ω (x) it was noticed that whenever n_0 was determined by the smallest term, the error in Ψ (x) could be significantly reduced (by a factor of 10) if Ψ (x) was determined as the average of the four partial sums closest to the partial sum through the smallest term of the asymptotic series. This was based on the observation that a line joining the points in a complex plane representing the partial sums formed a loop whose "center" was very close to the point representing Ψ (x) exactly. It was not found necessary to use the averaging described above although it might be useful in other cases. No theorem is known to the author stating that an asymptotic series always behaves in this fashion.

APPENDIX B

SURFACE IMPEDANCE OF TAPERED WALL CORRUGATIONS

Consider a single tapered trench as in Fig. B-1(b) which extends to infinity in the z and r directions. This can be viewed as a non-uniform transmission line in the r direction. The impedance of this line can be determined as follows. Let $\bar{E} = E_\phi \hat{\phi}$ and assume no dependence upon the z-coordinate. Then Maxwell's equations reduce to ($j\omega t$ time dependence assumed and suppressed)

$$j\omega\epsilon E_\phi = -\frac{\partial H_z}{\partial r} \ , \qquad j\omega\mu r H_z = -\frac{\partial(rE_\phi)}{\partial r} \ . \tag{B.1}$$

The solution in terms of the Hankel functions is:

$$\left. \begin{array}{l} H_z = AH_0^{(1)}(kr) + BH_0^{(2)}(kr) \\[2ex] E_\phi = -j\eta\left[AH_1^{(1)}(kr) + BH_1^{(2)}(kr)\right] \end{array} \right\} \ . \tag{B.2}$$

Let

and

$$\left. \begin{array}{l} H_n^{(1)}(x) = H_n(x)e^{j\theta_n(x)} \\[2ex] H_n^{(2)}(x) = H_n(x)e^{-j\theta_n(x)} \end{array} \right\} \tag{B.3}$$

where

$$\left. \begin{array}{l} H_n(x) = \left[J_n^{(2)}(x) + Y_n^2(x)\right]^{1/2} \\[2ex] \theta_n = \tan^{-1}\left[Y_n(x)/J_n(x)\right] \ . \end{array} \right\} \tag{B.4}$$

Then Eq. (B.2) can be written:

$$\left. \begin{array}{l} H_z = H_0(kr)\left[Ae^{j\theta_0(kr)} + Be^{-j\theta_0(kr)}\right] \\[2ex] E_\phi = -j\eta H_1(kr)\left[Ae^{j\theta_1(kr)} + Be^{-j\theta_1(kr)}\right] \ . \end{array} \right\} \tag{B.5}$$
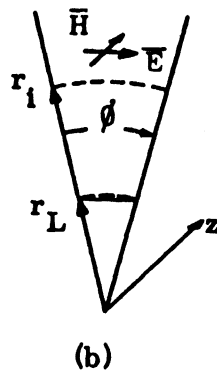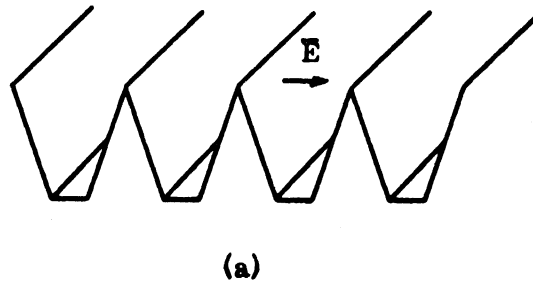
FIG. B-1: CORRUGATIONS WITH TAPERED TRENCHES.

The impedance of the line, looking towards the apex, is defined as

$$Z_i = -E_\phi / H_z \Big|_{r=r_i} \quad .$$

(B. 6)

Let also

$$Z_L = -E_\phi / H_z \Big|_{r=r_L} \quad .$$

(B. 7)

Substituting Eqs. (B. 5) and (B. 7) into (B. 6) one finally obtains the expression

$$Z_i(r_i) = Z_0(kr_i) \cdot \frac{Z_0(kr_L)\sin\left[\theta_1(kr_L) - \theta_1(kr_i)\right] + jZ_L\sin\left[\theta_0(kr_L) - \theta_1(kr_i)\right]}{Z_L\sin\left[\theta_0(kr_L) - \theta_0(kr_i)\right] - jZ_0(kr_L)\sin\left[\theta_1(kr_L) - \theta_0(kr_i)\right]}$$

(B. 8)

where

$$Z_0(kr) = \eta \frac{H_1(kr)}{H_0(kr)} \quad .$$

(B. 9)

For $Z_L = 0$ (short at $r = r_L$) Eq. (B. 8) reduces to

$$Z_i(r_i) = j Z_0(kr_i) \frac{\sin\left[\theta_1(kr_i) - \theta_1(kr_L)\right]}{\sin\left[\theta_0(kr_i) - \theta_1(kr_L)\right]} \quad .$$

(B. 10)

Assuming that the line is narrow enough so that the high order modes are attenuated rapidly one may still use (B. 10) to predict the input impedance of a tapered trench whose walls terminate at $r = r_i$. Then for a series of parallel trenches as shown in Fig. B-1(a) considerations similar to the ones used to derive Eq. (4. 3) yield for the surface reactance

$$X_s(r_i) = \frac{w}{s} Z_0(kr_i) \cdot \frac{\sin\left[\theta_1(kr_i) - \theta_1(kr_L)\right]}{\sin\left[\theta_0(kr_i) - \theta_1(kr_L)\right]}$$

(B. 11)

where w and s have the same meaning as in Eq. (4. 3) and are measured at the aperture. From (B. 11) it is seen that the reactance changes from positive to negative when

$$\theta_0(kr_i) - \theta_1(kr_L) = m\pi \quad ; \quad m = 1, 2, \ldots \quad .$$

(B. 12)

The solution of (B. 12) with $k=2\pi/\lambda_0$ is plotted in Fig. B-2. It is seen that this solution tends asymptotically to the corresponding solution of Eq. (4. 2) as expected. With the help of Fig. B-2 one can determine r_i once r_L and λ_0 have been chosen.

When $r_L=0$, it is seen from Eq. (B. 11) that X_s will become positive when $f=1.6 f_0$. Here f_0 is used to denote the frequency at which the trench depth, $d=r_i-r_L$, is equal to one quarter of the free space wavelength. In general, for $0 \leq r_L \leq \infty$ the crossover point, i. e., the point where X_s becomes inductive, will be at some frequency f, such that

$$1.6 f_0 \leq f \leq 2 f_0 . \tag{B. 13}$$

Thus, the tapering of the trench width restricts somewhat the frequency range over which the corrugations offer a capacitive surface impedance and thereby reduce the antenna radiation along the ground plane.

The more accurate determination of stop bands and pass bands for a periodic transmission system formed by corrugations with tapered walls can be easily performed by means of space harmonics exactly as in the case of corrugations with parallel walls (Watkins, 1958). The only difference is that Eq. (B. 10) now replaces Eq. (4. 2) .
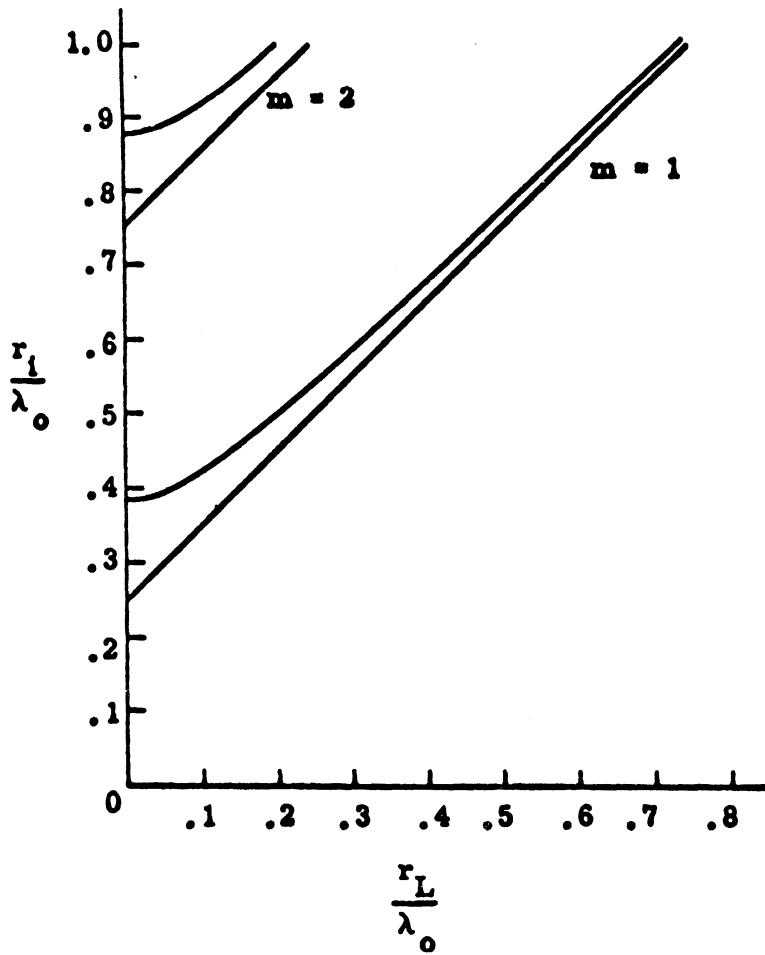
FIG. B-2: SOLUTION OF $\theta_o(2\pi r_i/\lambda_o) = \theta_1(2\pi r_L/\lambda_o) + m\pi$ AND ASYMPTOTE $r_i - r_L = (2m - 1)\lambda_o/4$.

DOCUMENT CONTROL DATA - R & D

(Security classification of title, body of abstract and indexing annotation must be entered when the overall report is classified)

1. ORIGINATING ACTIVITY (Corporate author)	2a. REPORT SECURITY CLASSIFICATION
The University of Michigan Radiation Laboratory 2216 Space Research Bldg., North Campus Ann Arbor, Michigan 48105	UNCLASSIFIED
	2b. GROUP

3. REPORT TITLE

Antenna Sidelobe And Coupling Reduction by Means of Reactive Loading of the Ground Plane

4. DESCRIPTIVE NOTES (Type of report and inclusive dates)

Fifth Interim, Technical

5. AUTHOR(S) (First name, middle initial, last name)

Constantine John Digenis

6. REPORT DATE	7a. TOTAL NO. OF PAGES	7b. NO. OF REFS
April, 1971	146	53

8a. CONTRACT OR GRANT NO.	9a. ORIGINATOR'S REPORT NUMBER(S)
F33615-68-C-1381	
b. PROJECT NO. 6278	01770-5-T
c. Task 627801	9b. OTHER REPORT NO(S) (Any other numbers that may be assigned this report)
d.	AFAL-TR-71-61

10. DISTRIBUTION STATEMENT

This document is subject to special export controls and each transmittal to foreign governments or foreign nationals may be made only with prior approval of AFAL (WRE), Wright-Patterson AFB, Ohio 45433.

11. SUPPLEMENTARY NOTES	12. SPONSORING MILITARY ACTIVITY
	Air Force Avionics Laboratory Air Force Systems Command Wright-Patterson AFB, Ohio 45433

13. ABSTRACT

In this report the loading of the ground plane by a capacitive impedance is described as a method of reducing the sidelobes of one antenna and the coupling between adjacent antennas. Although in the analysis no restrictions are placed upon the frequency, practical considerations regarding the loading make this method particularly suitable for antennas operating in the microwave region of the spectrum.

Explicit expressions are derived for the directivity and radiation resistance of a monopole placed over an infinite sheet characterized by a capacitive surface impedance. Also the problem of a short monopole over an infinite screen which is perfectly conducting throughout except for an annulus of capacitive surface impedance is considered and closed form expressions are obtained for the far zone field by an approximate method. Numerical results show that there is an optimum position for an annulus of a given radial extent in order to achieve maximum antenna gain and minimum radiation along the ground plane. By using annular loading the radiation resistance of the monopole is not reduced considerably in contrast to the loading of the entire ground plane. Experiments conducted using corrugations to create a capacitive reactance show good agreement with theory. The monopole input impedance and near field coupling were also measured.

The study concludes with an experimental investigation of the radiation properties of the slot, horn and spiral antennas in the presence of the capacitive reactance loading. Sidelobe reduction of apprximately 10dB and gain increase of up to 5dB have been measured over a 40 percent bandwidth using loading of approximately one wavelength radial extent.

DD FORM 1473 (NOV 65)

14. KEY WORDS	LINK A		LINK B		LINK C	
	ROLE	WT	ROLE	WT	ROLE	WT
Capacitive Corrugations						
Recuction of Sidelobes						
Coupling Recuction						
Low Sidelobe Elements						